CHAPTER 3

RADIATIVE PROPERTIES OF REAL SURFACES

3.1 INTRODUCTION

Ideally, electromagnetic wave theory may be used to predict all radiative properties of any material (reflectivity and transmissivity at an interface, absorption and emission within a medium). For a variety of reasons, however, the usefulness of the electromagnetic wave theory is extremely limited in practice. For one, the theory incorporates a large number of assumptions that are not necessarily good for all materials. Most importantly, electromagnetic wave theory neglects the effects of surface conditions on the radiative properties of these surfaces, instead assuming optically smooth interfaces of precisely the same (homogeneous) material as the bulk material—conditions that are very rarely met in practice. In the real world surfaces of materials are generally coated to varying degree with contaminants, oxide layers, and the like, and they usually have a certain degree of roughness (which is rarely even known on a quantitative basis). Thus, the greatest usefulness of the electromagnetic wave theory is that it provides the engineer with a tool to augment sparse experimental data through intelligent interpolation and extrapolation. Still, it is important to realize that radiative properties of opaque materials depend exclusively on the makeup of a very thin surface layer and, thus, may, for the same material, change from batch to batch and, indeed, overnight. This behavior is in contrast to most other thermophysical properties, such as thermal conductivity, which are bulk properties and as such are insensitive to surface contamination, roughness, and so on. The National Institute of Standards and Technology (NIST, formerly NBS) has recommended to reserve the ending "-ivity" for radiative properties of pure, perfectly smooth materials (the ones discussed in the previous chapter), and "-ance" for rough and contaminated surfaces. Most real surfaces fall into the latter category, discussed in the present chapter. Consequently, we will use the ending "-ance" for the definitions in the following section, and for most surface properties throughout this chapter (and the remainder of this book), unless the surface in question is optically smooth and the property is obtained from electromagnetic wave theory. Note that there will be occasions when either term could be used ("almost smooth" surfaces, comparing experimental data with electromagnetic wave theory, etc.).

In the present chapter we shall first develop definitions of all radiative properties that are relevant for real opaque surfaces. We then apply electromagnetic wave theory to predict trends of radiative properties for metals and for dielectrics (electrical nonconductors). These theoretical results are compared with a limited number of experimental data. This is followed by a brief

discussion of phenomena that cannot be predicted by electromagnetic wave theory, such as the effects of surface roughness, of surface oxidation and contamination, and of the preparation of "special surfaces" (i.e., surfaces whose properties are customized through surface coatings and/or controlled roughness).

Most experimental data available today were taken in the 1950s and 1960s during NASA's "Golden Age," when considerable resources were directed toward sending a man to the moon. Interest waned, together with NASA's funding, during the 1970s and early 1980s. More recently, because of the development of high-temperature ceramics and high-temperature applications, there has been renewed interest in the measurement of radiative surface properties.

No attempt is made here to present a complete set of experimental data for radiative surface properties. Extensive data sets of such properties have been collected in a number of references, such as [1–8], although all of these surveys are somewhat outdated.

3.2 DEFINITIONS

Emittance

The most basic radiative property for emission from an opaque surface is its *spectral, directional emittance*, defined as

$$\epsilon'_\lambda(T, \lambda, \hat{\mathbf{s}}_o) \equiv \frac{I_\lambda(T, \lambda, \hat{\mathbf{s}}_o) \cos\theta_o \, d\Omega_o}{I_{b\lambda}(T, \lambda) \cos\theta_o \, d\Omega_o} = \frac{I_\lambda(T, \lambda, \hat{\mathbf{s}}_o)}{I_{b\lambda}(T, \lambda)}, \tag{3.1}$$

which compares the actual spectral, directional emissive power with that of a black surface at the same conditions. We have added a prime to the letter ϵ to distinguish the directional emittance from the hemispherical (i.e., directionally averaged) value, and the subscript λ to distinguish the spectral emittance from the total (i.e., spectrally averaged) value. The direction vector is denoted by $\hat{\mathbf{s}}_o$ to emphasize that, for emission, we are considering directions *away* from a surface (outgoing). Finally, we have chosen wavelength λ as the spectral variable, since this is the preferred variable by most authors in the field of surface radiation phenomena. Expressions identical to equation (3.1) hold if frequency ν or wavenumber η are employed.

Some typical trends for experimentally determined directional emittances for actual materials are shown in Fig. 3-1*a*,*b*, as given by Schmidt and Eckert [9] (all emittances in these figures have been averaged over the entire spectrum; see the definition of the *total, directional emittance* below). For nonmetals the directional emittance varies little over a large range of polar angles but decreases rapidly at grazing angles until a value of zero is reached at $\theta = \pi/2$. Similar trends hold for metals, except that, at grazing angles, the emittance first increases sharply before dropping back to zero (not shown). Note that emittance levels are considerably higher for nonmetals.

A spectral surface whose emittance is the same for *all* directions is called a *diffuse emitter*, or a *Lambert surface* [since it obeys Lambert's law, equation (1.35)]. No real surface can be a diffuse emitter since *electromagnetic wave theory* predicts a zero emittance at $\theta = \pi/2$ for all materials. However, little energy is emitted into grazing directions, as seen from equation (1.31), so that the assumption of diffuse emission is often a good one.

The *spectral, hemispherical emittance*, defined as

$$\epsilon_\lambda(T, \lambda) \equiv \frac{E_\lambda(T, \lambda)}{E_{b\lambda}(T, \lambda)}, \tag{3.2}$$

compares the actual *spectral emissive power* (i.e., emission into all directions above the surface) with that of a black surface. The spectral, hemispherical emittance may be related to the

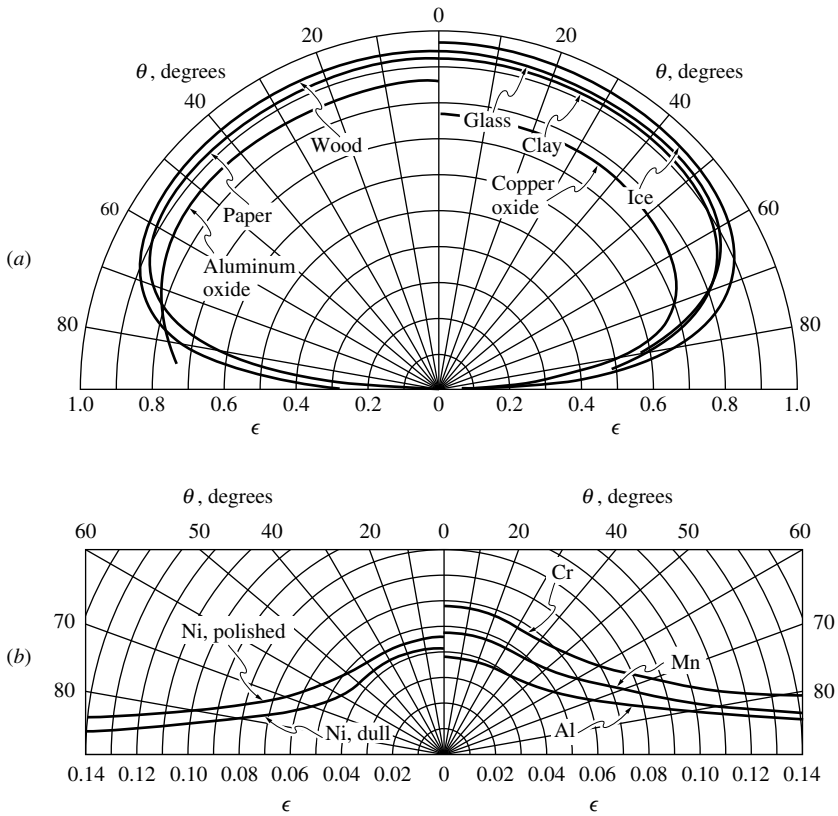

FIGURE 3-1
Directional variation of surface emittances (*a*) for several nonmetals and (*b*) for several metals [9].

directional one through equations (1.31) and (1.33),

$$\begin{aligned}\epsilon_\lambda(T,\lambda) &= \frac{\int_0^{2\pi}\int_0^{\pi/2} I_\lambda(T,\lambda,\theta,\psi)\cos\theta\,\sin\theta\,d\theta\,d\psi}{\pi\, I_{b\lambda}(T,\lambda)} \\ &= \frac{\int_0^{2\pi}\int_0^{\pi/2} \epsilon'_\lambda(T,\lambda,\theta,\psi) I_{b\lambda}(T,\lambda)\cos\theta\,\sin\theta\,d\theta\,d\psi}{\pi\, I_{b\lambda}(T,\lambda)},\end{aligned} \tag{3.3}$$

which may be simplified to

$$\epsilon_\lambda(T,\lambda) = \frac{1}{\pi}\int_0^{2\pi}\int_0^{\pi/2} \epsilon'_\lambda(T,\lambda,\theta,\psi)\cos\theta\,\sin\theta\,d\theta\,d\psi, \tag{3.4}$$

since $I_{b\lambda}$ does not depend on direction. For an *isotropic surface*, i.e., a surface that has no different structure, composition, or behavior for different directions on the surface (azimuthal angle), equation (3.4) reduces to

$$\epsilon_\lambda(T,\lambda) = 2\int_0^{\pi/2} \epsilon'_\lambda(T,\lambda,\theta)\cos\theta\,\sin\theta\,d\theta. \tag{3.5}$$

We note that the hemispherical emittance is an average over all solid angles subject to the weight factor $\cos\theta$ (arising from the directional variation of emissive power). For a *diffuse* surface, ϵ'_λ does not depend on direction and we find

$$\epsilon_\lambda(T,\lambda) = \epsilon'_\lambda(T,\lambda). \tag{3.6}$$

The *total, directional emittance* is a spectral average of ϵ'_λ, defined by

$$\epsilon'(T,\hat{\mathbf{s}}) = \frac{I(T,\hat{\mathbf{s}})\cos\theta\, d\Omega}{I_b(T)\cos\theta\, d\Omega} = \frac{I(T,\hat{\mathbf{s}})}{I_b(T)}, \tag{3.7}$$

or, from equations (1.30) and (1.34),

$$\epsilon'(T,\hat{\mathbf{s}}) = \frac{1}{I_b}\int_0^\infty I_\lambda\, d\lambda = \frac{1}{I_b}\int_0^\infty \epsilon'_\lambda I_{b\lambda}\, d\lambda = \frac{1}{n^2\sigma T^4}\int_0^\infty \epsilon'_\lambda(T,\lambda,\hat{\mathbf{s}})\, E_{b\lambda}(T,\lambda)\, d\lambda. \tag{3.8}$$

Finally, the *total, hemispherical emittance* is defined as

$$\epsilon(T) = \frac{E(T)}{E_b(T)}, \tag{3.9}$$

and may be related to the spectral, hemispherical emittance through

$$\epsilon(T) = \frac{\int_0^\infty E_\lambda(T,\lambda)\, d\lambda}{E_b(T)} = \frac{1}{n^2\sigma T^4}\int_0^\infty \epsilon_\lambda(T,\lambda)\, E_{b\lambda}(T,\lambda)\, d\lambda. \tag{3.10}$$

It is apparent that the total emittance is a spectral average with the spectral emissive power as a weight factor. If the spectral emittance is the same for all wavelengths then equation (3.10) reduces to

$$\epsilon(T) = \epsilon_\lambda(T). \tag{3.11}$$

Such surfaces are termed *gray*. If we have the very special case of a *gray, diffuse surface*, this implies

$$\epsilon(T) = \epsilon_\lambda = \epsilon' = \epsilon'_\lambda. \tag{3.12}$$

While no real surface is truly gray, it often happens that ϵ_λ is relatively constant over that part of the spectrum where $E_{b\lambda}$ is substantial, making the simplifying assumption of a gray surface warranted.

Example 3.1. A certain surface material has the following spectral, directional emittance when exposed to air:

$$\epsilon'_\lambda(\lambda,\theta) = \begin{cases} 0.9\cos\theta, & 0 < \lambda < 2\,\mu\text{m}, \\ 0.3, & 2\,\mu\text{m} < \lambda < \infty. \end{cases}$$

Determine the total hemispherical emittance for a surface temperature of $T = 500\,\text{K}$.

Solution

We first determine the hemispherical, spectral emittance from equation (3.5) as

$$\epsilon_\lambda(\lambda) = \begin{cases} 2\times 0.9\int_0^{\pi/2}\cos^2\theta\,\sin\theta\, d\theta = 0.6, & 0 < \lambda < 2\,\mu\text{m}, \\ 2\times 0.3\int_0^{\pi/2}\cos\theta\,\sin\theta\, d\theta = 0.3, & 2\,\mu\text{m} < \lambda < \infty. \end{cases}$$

The total, hemispherical emittance follows from equation (3.10) as

$$\begin{aligned} \epsilon(T) &= \frac{1}{n^2\sigma T^4}\left(0.6\int_0^{2\mu\text{m}} E_{b\lambda}\, d\lambda + 0.3\int_{2\mu\text{m}}^\infty E_{b\lambda}\, d\lambda\right) = 0.3 + \frac{0.6-0.3}{n^2\sigma T^4}\int_0^{2\mu\text{m}} E_{b\lambda}\, d\lambda \\ &= 0.3\left[1 + f(1\times 2\,\mu\text{m}\times 500\,\text{K})\right] = 0.3\times(1+0.00032) \simeq 0.3, \end{aligned}$$

where the fractional blackbody emissive power $f(n\lambda T)$ is as defined in equation (1.23). For a temperature of 500 K the spectrum below 2 μm is unimportant, and the surface is essentially gray and diffuse.

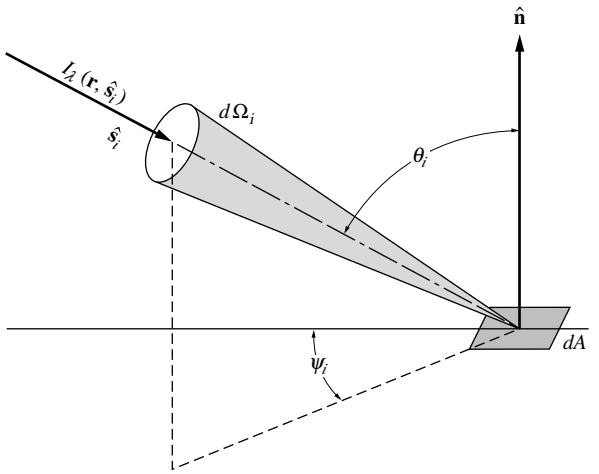

FIGURE 3-2
Directional irradiation onto a surface.

Absorptance

Unlike emittance, absorptance (as well as reflectance and transmittance) is not truly a surface property, since it depends on the external radiation field, as seen from its definition, equation (1.51). As for emittance we distinguish between directional and hemispherical, as well as spectral and total absorptances.

The radiative heat transfer rate per unit wavelength impinging onto an infinitesimal area dA, from the direction of $\hat{\mathbf{s}}_i$ over a solid angle of $d\Omega_i$ is, as depicted in Fig. 3-2,

$$I_\lambda(\mathbf{r}, \lambda, \hat{\mathbf{s}}_i)(\cos\theta_i\, dA)\, d\Omega_i,$$

where we have used the definition of intensity as radiative heat transfer rate per unit area normal to the rays, and per unit solid angle. I_λ is the local radiative intensity at location $\mathbf{r}$ (just above the surface). This incoming heat transfer rate, when evaluated per unit surface area dA and per unit incoming solid angle $d\Omega_i$, is known as *spectral, directional irradiation*,

$$H'_\lambda(\mathbf{r}, \lambda, \hat{\mathbf{s}}_i) = I_\lambda(\mathbf{r}, \lambda, \hat{\mathbf{s}}_i)\cos\theta_i. \tag{3.13}$$

Irradiation is a heat flux *always* pointing *into* the surface. Thus, there is no need to attach a sign to its value, and it is evaluated as an absolute value (in contrast to the definition of net heat flux in Chapter 1). The *spectral, directional absorptance* at surface location $\mathbf{r}$ is then defined as

$$\alpha'_\lambda(\mathbf{r}, \lambda, \hat{\mathbf{s}}_i) \equiv \frac{H'_{\lambda,\text{abs}}}{H'_\lambda}, \tag{3.14}$$

where $H'_{\lambda,\text{abs}}$ is that part of H'_λ that is absorbed by dA. If local thermodynamic equilibrium prevails, the fraction α'_λ will not change if H'_λ increases or decreases. Under this condition we find that the spectral, directional absorptance does not depend on the external radiation field and is a surface property that depends on local temperature, wavelength, and incoming direction. To determine its magnitude, we consider an isothermal spherical enclosure shown in Fig. 3-3, similar to the one used in Section 1.6 to establish the directional isotropy of blackbody intensity. The enclosure coating is again perfectly reflecting except for a small area dA_s, which is also perfectly reflecting except over the wavelength interval between λ and $\lambda + d\lambda$, over which it is black. However, the small surface dA suspended at the center is now nonblack. Following the same arguments as for the development of equation (1.32), augmenting the emitted flux by ϵ'_λ and the absorbed flux by α'_λ, we find immediately

$$\alpha'_\lambda(T, \lambda, \theta, \psi) = \epsilon'_\lambda(T, \lambda, \theta, \psi). \tag{3.15}$$

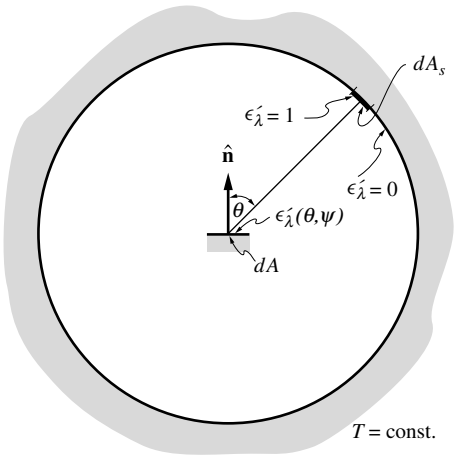

FIGURE 3-3
Kirchhoff's law for the spectral, directional absorptance.

Therefore, if local thermodynamic equilibrium prevails, the spectral, directional absorptance is a true surface property and is equal to the spectral, directional emittance.

The spectral radiative heat flux incident on a surface per unit wavelength from all directions, i.e., from the hemisphere above dA, is

$$H_\lambda(\mathbf{r},\lambda) = \int_{2\pi} H'_\lambda(\mathbf{r},\lambda,\hat{\mathbf{s}}_i)\,d\Omega_i = \int_{2\pi} I_\lambda(\mathbf{r},\lambda,\hat{\mathbf{s}}_i)\cos\theta_i\,d\Omega_i. \tag{3.16}$$

Of this the amount absorbed is, from equation (3.14),

$$\int_{2\pi} \alpha'_\lambda(T,\lambda,\hat{\mathbf{s}}_i) I_\lambda(\mathbf{r},\lambda,\hat{\mathbf{s}}_i)\cos\theta_i\,d\Omega_i.$$

Thus, we define the *spectral, hemispherical absorptance* as

$$\alpha_\lambda(\mathbf{r},\lambda) \equiv \frac{H_{\lambda,\text{abs}}}{H_\lambda} = \frac{\int_{2\pi} \alpha'_\lambda(T,\lambda,\hat{\mathbf{s}}_i) I_\lambda(\mathbf{r},\lambda,\hat{\mathbf{s}}_i)\cos\theta_i\,d\Omega_i}{\int_{2\pi} I_\lambda(\mathbf{r},\lambda,\hat{\mathbf{s}}_i)\cos\theta_i\,d\Omega_i}. \tag{3.17}$$

Since the incoming radiation, I_λ, depends on the radiation field of the surrounding enclosure, the spectral, hemispherical absorptance normally depends on the entire temperature field and is not a surface property. However, if the incoming radiation is approximately diffuse (i.e., if I_λ is independent of $\hat{\mathbf{s}}_i$), then the I_λ may be moved outside the integrals in equation (3.17) and cancelled. Then

$$\alpha_\lambda(T,\lambda) = \frac{1}{\pi}\int_0^{2\pi}\int_0^{\pi/2} \alpha'_\lambda(T,\lambda,\theta_i,\psi_i)\cos\theta_i\sin\theta_i\,d\theta_i\,d\psi_i, \tag{3.18}$$

or, using equations (3.4) and (3.15),

$$\alpha_\lambda(T,\lambda) = \epsilon_\lambda(T,\lambda) \quad \text{(diffuse irradiation)}. \tag{3.19}$$

This equality also holds if $\alpha'_\lambda = \epsilon'_\lambda$ are independent of direction, in which case α'_λ can be removed from the integral. Therefore, spectral hemispherical absorptances and emittances are equal if (and only if) either the irradiation and/or the spectral, directional absorptance are *diffuse* (i.e., do not depend on incoming direction).

On the other hand, energy incident from a single distant source results in (near-) parallel rays from a unique direction $\hat{\mathbf{s}}_i$, such as irradiation from the sun or from a laser. This is known as *collimated irradiation*, and leads to

$$H_\lambda(\mathbf{r},\lambda) = H'_\lambda(\mathbf{r},\lambda,\hat{\mathbf{s}}_i)\,\delta\Omega_i = I_\lambda(\mathbf{r},\lambda,\hat{\mathbf{s}}_i)\cos\theta_i\,\delta\Omega_i \tag{3.20}$$

and

$$\alpha_\lambda(T,\lambda) = \alpha'_\lambda(T,\lambda,\hat{\mathbf{s}}_i) = \epsilon'_\lambda(T,\lambda,\hat{\mathbf{s}}_i) \quad \text{(collimated irradiation)}. \tag{3.21}$$

Thus, for collimated irradiation there is no difference between directional and hemispherical absorptances.

The total irradiation per unit area and per unit solid angle, but over all wavelengths, is

$$H'(\mathbf{r}) = \int_0^\infty I_\lambda(\mathbf{r},\lambda,\hat{\mathbf{s}}_i)\cos\theta_i\, d\lambda. \tag{3.22}$$

Thus, we may define a *total, directional absorptance* as

$$\alpha'(\mathbf{r},\hat{\mathbf{s}}_i) \equiv \frac{\int_0^\infty \alpha'_\lambda(T,\lambda,\hat{\mathbf{s}}_i) I_\lambda(\mathbf{r},\hat{\mathbf{s}}_i)\, d\lambda}{\int_0^\infty I_\lambda(\mathbf{r},\hat{\mathbf{s}}_i)\, d\lambda}, \tag{3.23}$$

where the factor $\cos\theta_i$ has cancelled out since it does not depend on wavelength. Again, α' is not normally a surface property but depends on the entire radiation field. However, if the irradiation may be written as

$$I_\lambda(\mathbf{r},\lambda,\hat{\mathbf{s}}_i) = C(\hat{\mathbf{s}}_i) I_{b\lambda}(T,\lambda), \tag{3.24}$$

where $C(\hat{\mathbf{s}})$ is an otherwise arbitrary function that does not depend on wavelength, i.e., if the incoming radiation is gray (based on the local surface temperature T), then, from equations (3.8) and (3.15),

$$\alpha'(T,\theta,\psi) = \epsilon'(T,\theta,\psi). \tag{3.25}$$

Of course, this relation also holds if the surface is gray (i.e., $\alpha'_\lambda = \epsilon'_\lambda$ do not depend on wavelength).

Finally, the total irradiation per unit area from all directions and over the entire spectrum is

$$H(\mathbf{r}) = \int_0^\infty \int_{2\pi} I_\lambda(\mathbf{r},\lambda,\hat{\mathbf{s}}_i)\cos\theta_i\, d\Omega_i\, d\lambda. \tag{3.26}$$

Therefore, the *total, hemispherical absorptance* is defined as

$$\alpha(\mathbf{r}) \equiv \frac{H_{\text{abs}}}{H} = \frac{\int_0^\infty \alpha_\lambda(\mathbf{r},\lambda) H_\lambda(\mathbf{r},\lambda)\, d\lambda}{\int_0^\infty H_\lambda(\mathbf{r},\lambda)\, d\lambda} = \frac{\int_0^\infty \int_{2\pi} \alpha'_\lambda(T,\lambda,\hat{\mathbf{s}}_i) I_\lambda(\mathbf{r},\lambda,\hat{\mathbf{s}}_i)\cos\theta_i\, d\Omega_i\, d\lambda}{\int_0^\infty \int_{2\pi} I_\lambda(\mathbf{r},\lambda,\hat{\mathbf{s}}_i)\cos\theta_i\, d\Omega_i\, d\lambda}. \tag{3.27}$$

This absorptance is related to the total hemispherical emittance only for the very special cases of a gray, diffuse surface, equation (3.12), and/or *diffuse and gray irradiation*, i.e., if

$$I_\lambda(\mathbf{r},\lambda,\hat{\mathbf{s}}_i) = C I_{b\lambda}(T,\lambda), \tag{3.28}$$

where T is the temperature of the surface and C is a constant. Under those conditions we find, again using equation (3.15),

$$\alpha(T) = \epsilon(T). \tag{3.29}$$

Example 3.2. Let the surface considered in the previous example be irradiated by the sun from a 30° off-normal direction (i.e., a vector pointing to the sun from the surface forms a 30° angle with the outward surface normal). Determine the relevant surface absorptance.

Solution

Since the sun irradiates the surface from only one direction, but over the entire spectrum, we need to find the *total, directional absorptance*. From the last example, with $\theta_i = 30°$, we have

$$\alpha'_\lambda\left(\lambda, \theta_i = \frac{\pi}{6}\right) = \begin{cases} 0.45\sqrt{3}, & 0 < \lambda < 2\,\mu\text{m}, \\ 0.3, & 2\,\mu\text{m} < \lambda < \infty. \end{cases}$$

Since we know that the sun behaves like a blackbody at a temperature of $T_{\text{sun}} = 5777\,\text{K}$, we also know the spectral behavior of the sunshine falling onto our surface, or

$$I_\lambda(\lambda, \theta_i) = C I_{b\lambda}(T_{\text{sun}}, \lambda), \tag{3.30}$$

where C is a proportionality constant independent of wavelength.[1] Substituting this into equation (3.23) leads to

$$\begin{aligned} \alpha'\left(\theta_i = \frac{\pi}{6}\right) &= \frac{\int_0^\infty \epsilon'_\lambda(\lambda, \theta_i) I_{b\lambda}(T_{\text{sun}}, \lambda)\, d\lambda}{\int_0^\infty I_{b\lambda}(T_{\text{sun}}, \lambda)\, d\lambda} \\ &= \frac{1}{n^2 \sigma T_{\text{sun}}^4}\left[0.45\sqrt{3}\int_0^{2\mu\text{m}} E_{b\lambda}(T_{\text{sun}}, \lambda)\, d\lambda + 0.3\int_{2\mu\text{m}}^\infty E_{b\lambda}(T_{\text{sun}}, \lambda)\, d\lambda\right] \\ &= 0.3 + (0.45\sqrt{3} - 0.3) f(1{\times}2{\times}5777) = 0.3 + (0.779 - 0.3) \times 0.93962 = 0.750. \end{aligned}$$

In contrast to the previous example we find that at a temperature of 5777 K the spectrum *above* 2 μm is of very little importance, and the surface is again essentially gray.

We realize from this example that *(i)* if a surface is irradiated from a gray source at temperature T_{source}, and *(ii)* if the spectral, directional emittance of the surface is independent of temperature (as it is for most surfaces with good degree of accuracy), then the total absorptance is equal to its total emittance evaluated at the source temperature, or

$$\alpha = \epsilon(T_{\text{source}}). \tag{3.31}$$

This relation holds on a directional basis, and also for hemispherical values if the irradiation is diffuse.

Reflectance

The reflectance of a surface depends on *two* directions: the direction of the incoming radiation, $\hat{\mathbf{s}}_i$, and the direction into which the reflected energy travels, $\hat{\mathbf{s}}_r$. Therefore, we distinguish between total and spectral values, and between a number of directional reflectances. The heat flux per unit wavelength impinging on an area dA from a direction of $\hat{\mathbf{s}}_i$ over a solid angle of $d\Omega_i$ was given by equation (3.13) as

$$H'_\lambda\, d\Omega_i = I_\lambda(\mathbf{r}, \lambda, \hat{\mathbf{s}}_i) \cos\theta_i\, d\Omega_i. \tag{3.32}$$

Of this, the finite fraction α'_λ will be absorbed by the surface (assuming it to be opaque), and the rest will be reflected into all possible directions (total solid angle 2π). Therefore, in general, only an infinitesimal fraction will be reflected into an infinitesimal cone of solid angle $d\Omega_r$ around direction $\hat{\mathbf{s}}_r$, as shown in Fig. 3-4. Denoting this fraction by $\rho''_\lambda(\mathbf{r}, \lambda, \hat{\mathbf{s}}_i, \hat{\mathbf{s}}_r)\, d\Omega_r$ we obtain the reflected energy within the cone $d\Omega_r$ as

$$dI_\lambda(\mathbf{r}, \lambda, \hat{\mathbf{s}}_i, \hat{\mathbf{s}}_r)\, d\Omega_r = (H'_\lambda\, d\Omega_i)\rho''_\lambda(\mathbf{r}, \lambda, \hat{\mathbf{s}}_i, \hat{\mathbf{s}}_r)\, d\Omega_r. \tag{3.33}$$

The *spectral, bidirectional reflection function*[2] $\rho''_\lambda(\mathbf{r}, \lambda, \hat{\mathbf{s}}_i, \hat{\mathbf{s}}_r)$ is directly proportional to the magnitude of reflected light that travels into the direction of $\hat{\mathbf{s}}_r$,

$$\rho''_\lambda(\mathbf{r}, \lambda, \hat{\mathbf{s}}_i, \hat{\mathbf{s}}_r) = \frac{dI_\lambda(\mathbf{r}, \lambda, \hat{\mathbf{s}}_i, \hat{\mathbf{s}}_r)}{I_\lambda(\mathbf{r}, \lambda, \hat{\mathbf{s}}_i) \cos\theta_i\, d\Omega_i}. \tag{3.34}$$

[1] As we have seen in Section 1.7, this constant is equal to unity.

[2] ρ''_λ is sometimes referred to as a *bidirectional reflectance*; we avoid this nomenclature since the bidirectional reflectance function is not a fraction (i.e., constrained to values between 0 and 1), but may be larger than unity.

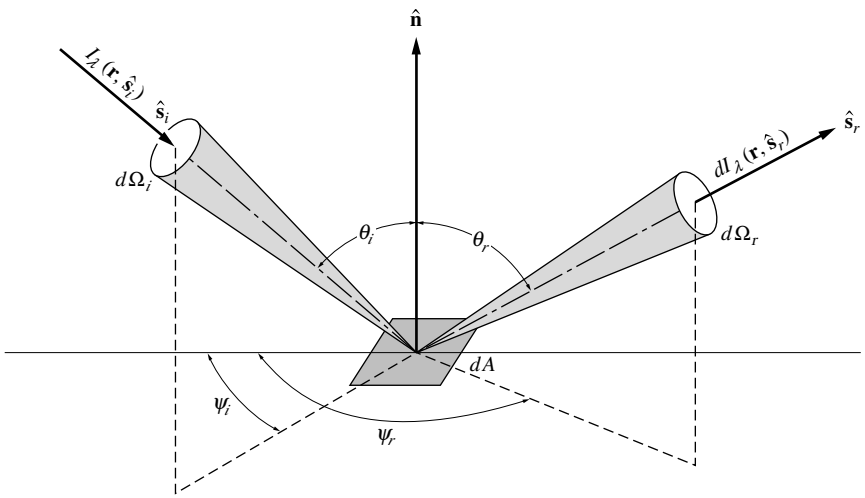

FIGURE 3-4
The bidirectional reflection function.

Equation (3.34) is the most basic of all radiation properties: All other radiation properties of an opaque surface can be related to it. However, experimental determination of this function for all materials, temperatures, wavelengths, incoming directions, and outgoing directions would be a truly Herculean task, limiting its practicality.

One may readily show that the *law of reciprocity* holds for the spectral, bidirectional reflection function (cf. McNicholas [10] or Siegel and Howell [11]),

$$\rho''_\lambda(\mathbf{r}, \lambda, \hat{\mathbf{s}}_i, \hat{\mathbf{s}}_r) = \rho''_\lambda(\mathbf{r}, \lambda, -\hat{\mathbf{s}}_r, -\hat{\mathbf{s}}_i), \tag{3.35a}$$

or

$$\rho''_\lambda(\mathbf{r}, \lambda, \theta_i, \psi_i, \theta_r, \psi_r) = \rho''_\lambda(\mathbf{r}, \lambda, \theta_r, \psi_r, \theta_i, \psi_i). \tag{3.35b}$$

This is done with another variation of *Kirchhoff's law* by placing a surface element into an isothermal black enclosure and evaluating the net heat transfer rate—which must be zero—between two arbitrary, infinitesimal surface elements on the enclosure wall. The sign change on the right-hand side of equation (3.35) emphasizes that $\hat{\mathbf{s}}_i$ points *into* the surface, while $\hat{\mathbf{s}}_r$ points away from it. Examination of equation (3.34) shows that $0 \le \rho''_\lambda < \infty$. Reaching the limit of $\rho''_\lambda \to \infty$ implies that a *finite* fraction of H'_λ is reflected into an *infinitesimal* cone of solid angle $d\Omega_r$. Such ideal behavior is achieved by an *optically smooth surface*, resulting in *specular reflection* (perfect mirror). For a specular reflector we have $\rho''_\lambda = 0$ for all $\hat{\mathbf{s}}_r$ except the specular direction $\theta_r = \theta_i, \psi_r = \psi_i + \pi$, for which $\rho''_\lambda \to \infty$ (see Fig. 3-4).

Some measurements by Torrance and Sparrow [12] for the bidirectional reflection function are shown in Fig. 3-5 for magnesium oxide, a material widely used in radiation experiments because of its diffuse reflectance, as defined in equation (3.38) below, in the near infrared (discussed in the last part of this chapter). The data in Fig. 3-5 are for an average surface roughness of 1 μm and are normalized with respect to the value in the specular direction. It is apparent that the material reflects rather diffusely at shorter wavelengths, but displays strong specular peaks for $\lambda > 2\,\mu$m.

A property of greater practical importance is the *spectral, directional–hemispherical reflectance*, which is defined as the total reflected heat flux leaving dA into all directions due to the spectral, directional irradiation H'_λ. With the reflected intensity (i.e., reflected energy per unit area normal to $\hat{\mathbf{s}}_r$) given by equation (3.33), we have, after multiplying with $\cos\theta_r$,

$$\rho'^{\frown}_\lambda(\mathbf{r}, \lambda, \hat{\mathbf{s}}_i) \equiv \frac{\int_{2\pi} dI_\lambda(\mathbf{r}, \lambda, \hat{\mathbf{s}}_i, \hat{\mathbf{s}}_r) \cos\theta_r \, d\Omega_r}{H'_\lambda(\mathbf{r}, \lambda, \hat{\mathbf{s}}_i)\, d\Omega_i}, \tag{3.36}$$

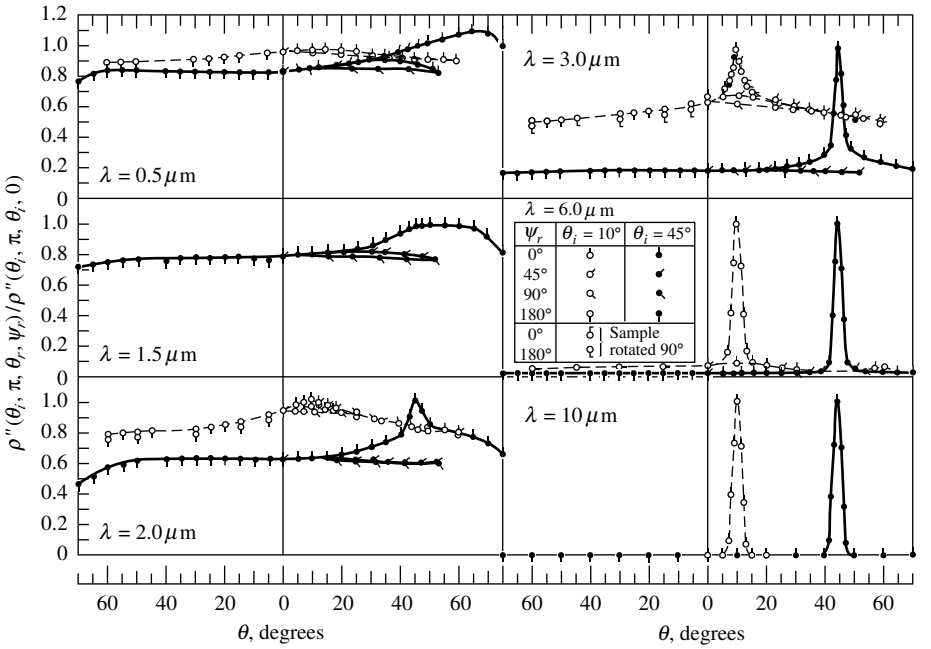

FIGURE 3-5
Normalized bidirectional reflection function for magnesium oxide [12].

or

$$\rho'^{\frown}_{\lambda}(\mathbf{r}, \lambda, \hat{\mathbf{s}}_i) = \int_{2\pi} \rho''_{\lambda}(\mathbf{r}, \lambda, \hat{\mathbf{s}}_i, \hat{\mathbf{s}}_r) \cos\theta_r \, d\Omega_r, \tag{3.37}$$

where the $(H'_{\lambda}\, d\Omega_i)$ cancels out since it does not depend on outgoing direction $\hat{\mathbf{s}}_r$. Here we have temporarily added the superscript "$\frown$" to distinguish the directional–hemispherical reflectance ($\rho'^{\frown}$) from the hemispherical–directional reflectance ($\rho^{\frown}{}'$, defined below). If the reflection function is independent of both $\hat{\mathbf{s}}_i$ and $\hat{\mathbf{s}}_r$, then the surface reflects equal amounts into all directions, regardless of incoming direction, and

$$\rho'^{\frown}_{\lambda}(\mathbf{r}, \lambda) = \pi \rho''_{\lambda}(\mathbf{r}, \lambda). \tag{3.38}$$

Such a surface is called a *diffuse reflector.*

Comparing the definition of the *spectral, directional–hemispherical reflectance* with that of the *spectral, directional absorptance*, equation (3.14), we also find, for an opaque surface,

$$\rho'^{\frown}_{\lambda}(\mathbf{r}, \lambda, \hat{\mathbf{s}}_i) = 1 - \alpha'_{\lambda}(\mathbf{r}, \lambda, \hat{\mathbf{s}}_i). \tag{3.39}$$

Sometimes it is of interest to determine the amount of energy reflected into a certain direction, coming from all possible incoming directions. Equation (3.33) gives the reflected intensity due to a single incoming direction. Integrating this expression over the entire hemisphere of incoming directions leads to

$$\begin{aligned} I_{\lambda}(\mathbf{r}, \lambda, \hat{\mathbf{s}}_r) &= \int_{2\pi} \rho''_{\lambda}(\mathbf{r}, \lambda, \hat{\mathbf{s}}_i, \hat{\mathbf{s}}_r)\, H'_{\lambda}(\mathbf{r}, \lambda, \hat{\mathbf{s}}_i)\, d\Omega_i \\ &= \int_{2\pi} \rho''_{\lambda}(\mathbf{r}, \lambda, \hat{\mathbf{s}}_i, \hat{\mathbf{s}}_r)\, I_{\lambda}(\mathbf{r}, \lambda, \hat{\mathbf{s}}_i) \cos\theta_i \, d\Omega_i. \end{aligned} \tag{3.40}$$

On the other hand, the spectral, hemispherical irradiation is

$$H_{\lambda}(\mathbf{r}, \lambda) = \int_{2\pi} I_{\lambda}(\mathbf{r}, \lambda, \hat{\mathbf{s}}_i) \cos\theta_i \, d\Omega_i. \tag{3.41}$$

If the surface were a perfect reflector, it would reflect all of H_λ, and it would reflect it equally into all outgoing directions. Thus, for the ideal case, the outgoing intensity would be, from equation (1.34), H_λ/π. Consequently, the *spectral, hemispherical–directional reflectance* is defined as

$$\rho_\lambda^{\frown\prime}(\mathbf{r},\lambda,\hat{\mathbf{s}}_r) \equiv \frac{I_\lambda(\mathbf{r},\lambda,\hat{\mathbf{s}}_r)}{H_\lambda(\mathbf{r},\lambda)/\pi} = \frac{\int_{2\pi}\rho_\lambda''(\mathbf{r},\lambda,\hat{\mathbf{s}}_i,\hat{\mathbf{s}}_r)\,I_\lambda(\mathbf{r},\lambda,\hat{\mathbf{s}}_i)\cos\theta_i\,d\Omega_i}{\frac{1}{\pi}\int_{2\pi} I_\lambda(\mathbf{r},\lambda,\hat{\mathbf{s}}_i)\cos\theta_i\,d\Omega_i}. \tag{3.42}$$

For the special case of *diffuse irradiation* (i.e., the incoming intensity does not depend on $\hat{\mathbf{s}}_i$) equation (3.42) reduces to

$$\rho_\lambda^{\frown\prime}(\mathbf{r},\lambda,\hat{\mathbf{s}}_r) = \int_{2\pi}\rho_\lambda''(\mathbf{r},\lambda,\hat{\mathbf{s}}_i,\hat{\mathbf{s}}_r)\cos\theta_i\,d\Omega_i, \tag{3.43}$$

which is identical to equation (3.37) if the reciprocity of the bidirectional reflection function, equation (3.35), is invoked. Thus, for diffuse irradiation,

$$\rho_\lambda^{\frown\prime}(\mathbf{r},\lambda,\hat{\mathbf{s}}_r) \;=\; \rho_\lambda'^{\frown}(\mathbf{r},\lambda,\hat{\mathbf{s}}_i), \quad \hat{\mathbf{s}}_i = -\hat{\mathbf{s}}_r, \tag{3.44a}$$

or

$$\rho_\lambda^{\frown\prime}(\mathbf{r},\lambda,\theta_r,\psi_r) \;=\; \rho_\lambda'^{\frown}(\mathbf{r},\lambda,\theta_i=\theta_r,\psi_i=\psi_r), \tag{3.44b}$$

that is, reciprocity exists between the spectral directional–hemispherical and hemispherical–directional reflectances for any given irradiation/reflection direction. Use of this fact is often made in experimental measurements: While the directional–hemispherical reflectance is of great practical importance, it is very difficult to measure; the hemispherical–directional reflectance, on the other hand, is not very important but readily measured (see Section 3.10).

Finally, we define a *spectral, hemispherical reflectance* as the fraction of the total irradiation from all directions reflected into all directions. From equation (3.36) we have the heat flux reflected into all directions for a single direction of incidence, $\hat{\mathbf{s}}_i$, as

$$\rho_\lambda'^{\frown}(\mathbf{r},\lambda,\hat{\mathbf{s}}_i)\,H_\lambda'(\mathbf{r},\lambda,\hat{\mathbf{s}}_i)\,d\Omega_i.$$

Integrating this expression as well as H_λ' itself over all incidence angles gives

$$\rho_\lambda(\mathbf{r},\lambda) = \frac{\int_{2\pi}\rho_\lambda'^{\frown}(\mathbf{r},\lambda,\hat{\mathbf{s}}_i)\,H_\lambda'(\mathbf{r},\lambda,\hat{\mathbf{s}}_i)\,d\Omega_i}{\int_{2\pi}H_\lambda'(\mathbf{r},\lambda,\hat{\mathbf{s}}_i)\,d\Omega_i} = \frac{\int_{2\pi}\rho_\lambda'^{\frown}(\mathbf{r},\lambda,\hat{\mathbf{s}}_i)\,I_\lambda(\mathbf{r},\lambda,\hat{\mathbf{s}}_i)\cos\theta_i\,d\Omega_i}{\int_{2\pi}I_\lambda(\mathbf{r},\lambda,\hat{\mathbf{s}}_i)\cos\theta_i\,d\Omega_i}. \tag{3.45}$$

If the incident intensity is independent of direction (diffuse irradiation), then equation (3.45) may be simplified again, and

$$\rho_\lambda(\mathbf{r},\lambda) = \frac{1}{\pi}\int_{2\pi}\rho_\lambda'^{\frown}(\mathbf{r},\lambda,\hat{\mathbf{s}}_i)\cos\theta_i\,d\Omega_i. \tag{3.46}$$

Also, comparing the definitions of spectral, hemispherical absorptance and reflectance, we obtain, for an opaque surface,

$$\rho_\lambda(\mathbf{r},\lambda) = 1 - \alpha_\lambda(\mathbf{r},\lambda). \tag{3.47}$$

Finally, as for emittance and absorptance we need to introduce spectrally-integrated or "total" reflectances. This is done by integrating numerator and denominator independently over the full spectrum for each of the spectral reflectances, leading to the following relations:
Total, bidirectional reflection function

$$\rho''(\mathbf{r},\hat{\mathbf{s}}_i,\hat{\mathbf{s}}_r) = \frac{\int_0^\infty \rho_\lambda''(\mathbf{r},\lambda,\hat{\mathbf{s}}_i,\hat{\mathbf{s}}_r)\,I_\lambda(\mathbf{r},\lambda,\hat{\mathbf{s}}_i)\,d\lambda}{\int_0^\infty I_\lambda(\mathbf{r},\lambda,\hat{\mathbf{s}}_i)\,d\lambda}; \tag{3.48}$$

TABLE 3.1
Summary of definitions for radiative properties of surfaces.

Property	Symbol	Equation	Comments
Emittance			
Spectral, directional	$\epsilon'_\lambda(T,\lambda,\theta,\psi)$	(3.1)	
hemispherical	$\epsilon_\lambda(T,\lambda)$	(3.4)	directional average of ϵ'_λ (over outgoing directions)
Total, directional	$\epsilon'(T,\theta,\psi)$	(3.8)	spectral average of ϵ'_λ (with $I_{b\lambda}$ as weight factor)
hemispherical	$\epsilon(T)$	(3.10)	directional and spectral average of ϵ'_λ
Absorptance			depends on incoming intensity I_{in}
Spectral, directional	$\alpha'_\lambda(T,\lambda,\theta,\psi)$	(3.14)	
hemispherical	$\alpha_\lambda(I_{\lambda,\text{in}},T,\lambda)$	(3.17)	directional average of α'_λ (over incoming directions)
Total, directional	$\alpha'(I_{\text{in}},T,\theta,\psi)$	(3.23)	spectral average of α'_λ (with $I_{\lambda,\text{in}}$ as weight factor)
hemispherical	$\alpha(I_{\text{in}},T)$	(3.27)	directional and spectral average of α'_λ
Reflectance			depends on incoming intensity I_{in}
Spectral, bidirectional	$\rho''_\lambda(T,\lambda,\theta_i,\psi_i,\theta_r,\psi_r)$	(3.34)	reflection function, $0 \le \rho''_\lambda \le \infty$
directional–hemispherical	$\rho'^{\frown}_\lambda(I_{\lambda,\text{in}},T,\lambda,\theta_i,\psi_i)$	(3.37)	integral of ρ''_λ over outgoing directions
hemispherical–directional	$\rho^{\frown\prime}_\lambda(I_{\lambda,\text{in}},T,\lambda,\theta_r,\psi_r)$	(3.42)	directional average of ρ''_λ over incoming directions
hemispherical	$\rho_\lambda(I_{\lambda,\text{in}},T,\lambda)$	(3.45)	directional average of ρ'_λ (incoming and outgoing directions)
Total, bidirectional	$\rho''(I_{\text{in}},T,\theta_i,\psi_i,\theta_r,\psi_r)$	(3.48)	spectral average of ρ''_λ (with $I_{\lambda,\text{in}}$ as weight factor)
directional–hemispherical	$\rho'^{\frown}(I_{\text{in}},T,\theta_i,\psi_i)$	(3.49)	integral of ρ'' over outgoing directions
hemispherical–directional	$\rho^{\frown\prime}(I_{\text{in}},T,\theta_r,\psi_r)$	(3.50)	directional average of ρ'' over incoming directions
hemispherical	$\rho(I_{\text{in}},T)$	(3.51)	directional and spectral average of $\rho'^{\frown}_\lambda$

Total, directional–hemispherical reflectance

$$\rho'^{\frown}(\mathbf{r},\hat{\mathbf{s}}_i) = \frac{\int_0^\infty \rho'^{\frown}_\lambda(\mathbf{r},\lambda,\hat{\mathbf{s}}_i)\, I_\lambda(\mathbf{r},\lambda,\hat{\mathbf{s}}_i)\, d\lambda}{\int_0^\infty I_\lambda(\mathbf{r},\lambda,\hat{\mathbf{s}}_i)\, d\lambda}; \tag{3.49}$$

Total, hemispherical–directional reflectance

$$\rho^{\frown\prime}(\mathbf{r},\hat{\mathbf{s}}_r) = \frac{\int_0^\infty \rho^{\frown\prime}_\lambda(\mathbf{r},\lambda,\hat{\mathbf{s}}_r) \int_{2\pi} I_\lambda(\mathbf{r},\lambda,\hat{\mathbf{s}}_i)\cos\theta_i\, d\Omega_i\, d\lambda}{\int_0^\infty \int_{2\pi} I_\lambda(\mathbf{r},\lambda,\hat{\mathbf{s}}_i)\cos\theta_i\, d\Omega_i\, d\lambda}; \tag{3.50}$$

Total, hemispherical reflectance

$$\rho(\mathbf{r}) = \frac{\int_0^\infty \rho_\lambda(\mathbf{r},\lambda) \int_{2\pi} I_\lambda(\mathbf{r},\lambda,\hat{\mathbf{s}}_i)\cos\theta_i\, d\Omega_i\, d\lambda}{\int_0^\infty \int_{2\pi} I_\lambda(\mathbf{r},\lambda,\hat{\mathbf{s}}_i)\cos\theta_i\, d\Omega_i\, d\lambda}. \tag{3.51}$$

The reciprocity relations in equations (3.35) and (3.44) also hold for total reflectances (subject to the same restrictions), as do the relations between reflectance and absorptance, equations (3.39) and (3.47).

The rather confusing array of radiative property definitions and their interrelationships have been summarized in Table 3.1 (property definitions) and Table 3.2 (property interrelations).

TABLE 3.2
Summary of relations between radiative properties of surfaces.

Property	Relation	Restrictions
Spectral, directional	$\alpha'_\lambda(T,\lambda,\theta,\psi) = 1 - \rho'^{\frown}_\lambda(T,\lambda,\theta,\psi)$	opaque surfaces (θ,ψ = incoming directions)
	$= \epsilon'_\lambda(T,\lambda,\theta,\psi)$	none (θ,ψ = outgoing directions)
Spectral, hemispherical	$\alpha_\lambda(T,\lambda) = 1 - \rho_\lambda(T,\lambda)$	opaque surfaces (values depend on directional distribution of source)
	$= \epsilon_\lambda(T,\lambda)$	irradiation and/or ϵ'_λ independent of direction (diffuse)
Total, directional	$\alpha'(T,\theta,\psi) = 1 - \rho'^{\frown}(T,\theta,\psi)$	opaque surfaces (values depend on spectral distribution of source)
	$= \epsilon'(T,\theta,\psi)$	ϵ'_λ independent of wavelength (gray)
	$\alpha'(T_s,T,\theta,\psi) = \epsilon'(T_s,\theta,\psi)$	source is gray with source temperature T_s, and ϵ'_λ is independent of T, or $T_s = T$
Total, hemispherical	$\alpha(T) = 1 - \rho(T)$	opaque surfaces (values depend on spectral and directional distribution of source)
	$= \epsilon(T)$	ϵ'_λ independent of wavelength and direction (gray and diffuse)
	$\alpha(T_s,T) = \epsilon(T_s)$	source is gray and diffuse with source temperature T_s, and ϵ'_λ is independent of T, or $T_s = T$

3.3 PREDICTIONS FROM ELECTROMAGNETIC WAVE THEORY

In Chapter 2 we developed in some detail how the spectral, directional–hemispherical reflectivity of an optically smooth interface (specular reflector) can be predicted by the *electromagnetic wave* and *dispersion theories*. Before comparing such predictions with experimental data, we shall briefly summarize the results of Chapter 2.

Consider an electromagnetic wave traveling through air (refractive index = 1), hitting the surface of a *conducting medium* (complex index of refraction $m = n - ik$) at an angle of θ_1 with the surface normal (cf. Fig. 3-6). *Fresnel's relations* predict the reflectivities for parallel- and perpendicular-polarized light from equations (2.107) through (2.113)[3] as

$$\rho_\parallel = \frac{(p - \sin\theta_1 \tan\theta_1)^2 + q^2}{(p + \sin\theta_1 \tan\theta_1)^2 + q^2}\rho_\perp, \tag{3.52}$$

$$\rho_\perp = \frac{(\cos\theta_1 - p)^2 + q^2}{(\cos\theta_1 + p)^2 + q^2}, \tag{3.53}$$

where

$$p^2 = \frac{1}{2}\left[\sqrt{(n^2 - k^2 - \sin^2\theta_1)^2 + 4n^2k^2} + (n^2 - k^2 - \sin^2\theta_1)\right], \tag{3.54}$$

$$q^2 = \frac{1}{2}\left[\sqrt{(n^2 - k^2 - \sin^2\theta_1)^2 + 4n^2k^2} - (n^2 - k^2 - \sin^2\theta_1)\right]. \tag{3.55}$$

Nonreflected light is refracted into the medium, traveling on at an angle of θ_2 with the surface normal, as predicted by the *generalized Snell's law*, from equation (2.108),

$$p \tan\theta_2 = \sin\theta_1. \tag{3.56}$$

[3]For simplicity of notation we shall drop the superscripts $'^{\frown}$ for the directional–hemispherical reflectivity whenever there is no possibility of confusion.

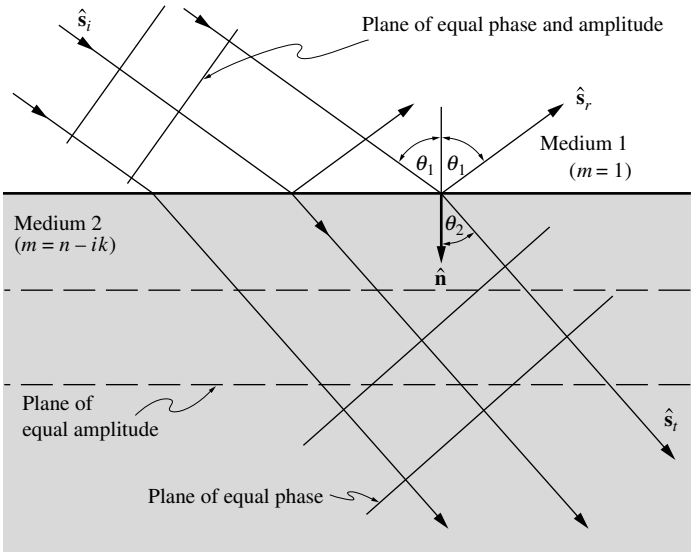

FIGURE 3-6
Transmission and reflection at an interface between air and an absorbing medium.

For normal incidence $\theta_1 = \theta_2 = 0$, and equations (3.52) through (3.55) simplify to $p = n$, $q = k$, and

$$\rho_{n\lambda} = \rho_{\parallel} = \rho_{\perp} = \frac{(n-1)^2 + k^2}{(n+1)^2 + k^2}. \tag{3.57}$$

If the incident radiation is *unpolarized*, the reflectivity may be calculated as an average, i.e.,

$$\rho = \tfrac{1}{2}(\rho_{\parallel} + \rho_{\perp}). \tag{3.58}$$

For a *dielectric medium* ($k = 0$), $p^2 = n^2 - \sin^2\theta_1$, and Snell's law becomes

$$n \sin\theta_2 = \sin\theta_1. \tag{3.59}$$

Therefore, $p = n\cos\theta_2$ and, with $q = 0$, Fresnel's relations reduce to

$$\rho_{\parallel} = \left(\frac{\cos\theta_2 - n\cos\theta_1}{\cos\theta_2 + n\cos\theta_1}\right)^2, \tag{3.60a}$$

$$\rho_{\perp} = \left(\frac{\cos\theta_1 - n\cos\theta_2}{\cos\theta_1 + n\cos\theta_2}\right)^2. \tag{3.60b}$$

Except for the section on semitransparent sheets, in this chapter we shall be dealing with opaque media. For such media $\rho + \alpha = 1$ and, from Kirchhoff's law,

$$\epsilon'_{\lambda} = \alpha'_{\lambda} = 1 - \rho'_{\lambda}. \tag{3.61}$$

To predict radiative properties from electromagnetic wave theory, the complex index of refraction, m, must be known, either from direct measurements or from dispersion theory predictions. In the dispersion theory the complex dielectric function, $\varepsilon = \varepsilon' - i\varepsilon''$, is predicted by assuming that the surface material consists of harmonic oscillators interacting with electromagnetic waves. The complex dielectric function is related to the complex index of refraction by $\varepsilon = m^2$, or

$$n^2 = \tfrac{1}{2}\left(\varepsilon' + \sqrt{\varepsilon'^2 + \varepsilon''^2}\right), \tag{3.62a}$$

$$k^2 = \tfrac{1}{2}\left(-\varepsilon' + \sqrt{\varepsilon'^2 + \varepsilon''^2}\right), \tag{3.62b}$$

where

$$\varepsilon' = \frac{\epsilon}{\epsilon_0}, \quad \varepsilon'' = \frac{\sigma_e}{2\pi\nu\epsilon_0};$$

ϵ is the electrical permittivity, ϵ_0 is its value in vacuum, and σ_e is the medium's electrical conductivity. Both ϵ and σ_e are functions of the frequency of the electromagnetic wave ν. For an isolated oscillator (nonoverlapping band) ε is predicted by the Lorentz model, equation (2.139), as

$$\varepsilon' = \varepsilon_0 + \frac{\nu_{pi}^2(\nu_i^2 - \nu^2)}{(\nu_i^2 - \nu^2)^2 + \gamma_i^2\nu^2}, \tag{3.63a}$$

$$\varepsilon'' = \frac{\nu_{pi}^2\gamma_i\nu}{(\nu_i^2 - \nu^2)^2 + \gamma_i^2\nu^2}, \tag{3.63b}$$

where ε_0 is the contribution to ε' from bands at shorter wavelengths, ν_i is the resonance frequency, ν_{pi} is called the plasma frequency, and γ_i is an oscillation damping factor. If these three constants can be determined or measured, then n and k can be predicted for all frequencies (or wavelengths) from equation (3.62), and the radiative properties can be calculated for all frequencies (or wavelengths) and all directions from equations (3.52) through (3.55).

3.4 RADIATIVE PROPERTIES OF METALS

In this section we shall briefly discuss how the radiative properties of clean and smooth metallic surfaces (i.e., electrical conductors) can be predicted from electromagnetic wave theory and dispersion theory, and how these predictions compare with experimental data. The variation of the spectral, normal reflectance with wavelength and total, normal properties will be examined, followed by a discussion of the directional dependence of radiative properties and the evaluation of hemispherical reflectances (and emittances). Finally, we will look at the temperature dependence of spectral as well as total properties.

Wavelength Dependence of Spectral, Normal Properties

Metals are in general excellent electrical conductors because of an abundance of free electrons. Drude [13] developed an early theory to predict the dielectric function for free electrons that is essentially a special case of the Lorentz model: Since free electrons do not oscillate but propagate freely, they may be modeled as a "spring" with a vanishing spring constant leading to a resonance frequency of $\nu_i = 0$. Thus the *Drude theory* for the dielectric function for free electrons follows from equation (3.63) as

$$\varepsilon'(\nu) = \varepsilon_0 - \frac{\nu_p^2}{\nu^2 + \gamma^2}, \tag{3.64a}$$

$$\varepsilon''(\nu) = \frac{\nu_p^2\gamma}{\nu(\nu^2 + \gamma^2)}. \tag{3.64b}$$

Figure 3-7 shows the spectral, normal reflectivity of three metals—aluminum, copper, and silver. The theoretical lines are from Ehrenreich and coworkers [14] (aluminum) and Ehrenreich and Phillip [15] (copper and silver), who semiempirically determined the values of the unknowns ε_0, ν_p, and γ in equation (3.64). The experimental reflectance data are taken from Shiles and coworkers [16] (aluminum) and Hagemann and coworkers [17] (copper and silver). The agreement between experiment and theory in the infrared is very good. For wavelengths

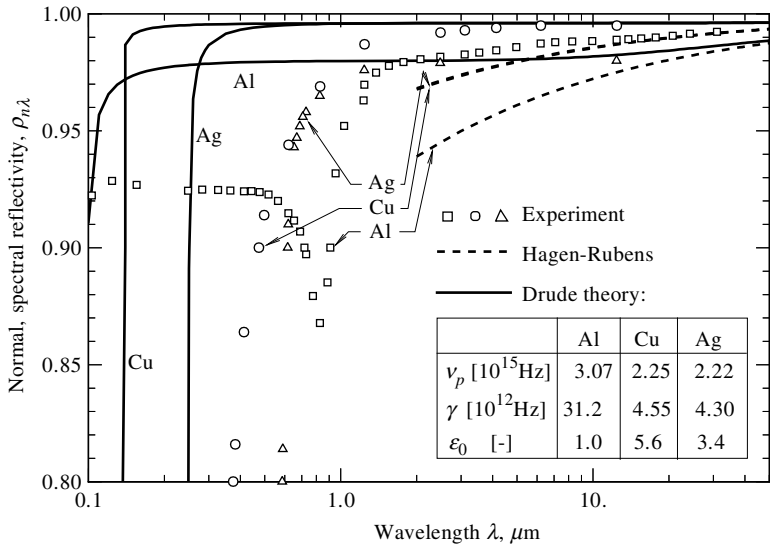

FIGURE 3-7
Spectral, normal reflectivity at room temperature for aluminum, copper, and silver.

$\lambda > 1\,\mu$m the Drude theory has been shown to represent the reflectivity of many metals accurately, if samples are prepared with great care. Discrepancies are due to surface preparation methods and the limits of experimental accuracy. Aluminum has a dip in reflectivity centered at $\sim 0.8\,\mu$m; this is due to bound electron transitions that are not considered by the Drude model. Since $\gamma \ll \nu_p$ always, there exists for each metal a frequency in the vicinity of the plasma frequency, $\nu \simeq \nu_p$, where $\varepsilon' = 1$ and $\varepsilon'' \ll 1$ or $n \simeq 1, k \ll 1$: This fact implies that many metals neither reflect nor absorb radiation in the ultraviolet near ν_p, but are highly transparent!

For extremely long wavelengths (very small frequency ν), we find from equations (3.64) and (2.134) that

$$\varepsilon'' = \frac{\nu_p^2}{\nu\gamma} = \frac{\sigma_e}{2\pi\nu\epsilon_0}, \qquad \nu \ll \gamma, \tag{3.65}$$

where σ_e is the (in general, frequency-dependent) electrical conductivity, and

$$\sigma_e = 2\pi\epsilon_0\nu_p^2/\gamma = \text{const} = \sigma_{\text{dc}}. \tag{3.66}$$

Note that at the long-wavelength limit the electrical conductivity becomes independent of wavelength and is known as the *dc-conductivity*. Since the *dc-conductivity* is easily measured it is advantageous to recast equation (3.64) as

$$\varepsilon(\nu) = \varepsilon_0 - \frac{\sigma_{\text{dc}}\gamma/2\pi\epsilon_0}{\nu(\nu + i\gamma)}, \tag{3.67a}$$

$$\varepsilon' = \varepsilon_0 - \frac{\sigma_{\text{dc}}\gamma/2\pi\epsilon_0}{\nu^2 + \gamma^2}, \tag{3.67b}$$

$$\varepsilon'' = \frac{\sigma_{\text{dc}}\gamma^2/2\pi\epsilon_0}{\nu(\nu^2 + \gamma^2)}. \tag{3.67c}$$

Room temperature values for electrical resistivity, $1/\sigma_{\text{dc}}$, and for electron relaxation time, $1/2\pi\gamma$, have been given by Parker and Abbott [18] for a number of metals. They have been converted and are reproduced in Table 3.3. Note that these values differ appreciably from those given in Fig. 3-7. No values for ε_0 are given; however, the influence of ε_0 is generally negligible in the

TABLE 3.3
Inverse relaxation times and dc electrical conductivities for various metals at room temperature [18].

Metal	γ, Hz	$\sigma_{dc}, \Omega^{-1}\text{cm}^{-1}$	$\nu_p^2 = \sigma_{dc}\gamma/2\pi\epsilon_0, \text{Hz}^2$
Lithium	1.85×10^{13}	1.09×10^5	3.62×10^{30}
Sodium	5.13×10^{12}	2.13×10^5	1.96×10^{30}
Potassium	3.62×10^{12}	1.52×10^5	9.88×10^{29}
Cesium	7.56×10^{12}	0.50×10^5	6.78×10^{29}
Copper	5.89×10^{12}	5.81×10^5	6.14×10^{30}
Silver	3.88×10^{12}	6.29×10^5	4.38×10^{30}
Gold	5.49×10^{12}	4.10×10^5	4.04×10^{30}
Nickel	1.62×10^{13}	1.28×10^5	3.72×10^{30}
Cobalt	1.73×10^{13}	1.02×10^5	3.17×10^{30}
Iron	6.63×10^{12}	1.00×10^5	1.19×10^{30}
Palladium	1.73×10^{13}	0.91×10^5	2.83×10^{30}
Platinum	1.77×10^{13}	1.00×10^5	3.18×10^{30}

infrared. Extensive sets of spectral data for a large number of metals have been collected by Ordal and coworkers [19] (for a smaller number of metals they also give the Drude parameters, which are also conflicting somewhat with the data of Table 3.3), while a listing of spectral values of the complex index of refraction for a large numbers of metals and semiconductors has been given in a number of handbooks [20–23].

For long wavelengths equation (3.62) may be simplified considerably, since for such case, $\varepsilon'' \gg |\varepsilon'|$, and it follows that

$$n^2 \approx k^2 \approx \varepsilon''/2 = \frac{\sigma_{dc}}{4\pi\nu\epsilon_0} = \frac{\sigma_{dc}\lambda_0}{4\pi c_0\epsilon_0} \gg 1, \tag{3.68}$$

where λ_0 is the wavelength in vacuum. Substituting values for the universal constants c_0 and ϵ_0, equation (3.68) becomes

$$n \simeq k \simeq \sqrt{30\lambda_0\sigma_{dc}}, \quad \lambda_0 \text{ in cm}, \quad \sigma_{dc} \text{ in } \Omega^{-1}\text{cm}^{-1}, \tag{3.69}$$

which is known as the *Hagen–Rubens relation* [24]. For comparison, results from equation (3.69) are also included in Fig. 3-7. It is commonly assumed that the Hagen–Rubens relation may be used for $\lambda_0 > 6\,\mu$m, although this assumption can lead to serious errors, in particular as far as evaluation of the index of refraction is concerned. While equation (3.69) is valid for the metal being adjacent to an arbitrary material, we will—for notational simplicity—assume for the rest of this discussion that the adjacent material has a refractive index of unity (vacuum or gas), that is, $\lambda_0 = \lambda$. Substituting equation (3.69) into equation (3.57) leads to

$$\rho_{n\lambda} = \frac{2n^2 - 2n + 1}{2n^2 + 2n + 1}, \tag{3.70}$$

$$\epsilon_{n\lambda} = 1 - \rho_{n\lambda} = \frac{4n}{2n^2 + 2n + 1}. \tag{3.71}$$

Since $n \gg 1$ equation (3.71) may be further simplified to

$$\epsilon_{n\lambda} = \frac{2}{n} - \frac{2}{n^2} + \cdots, \tag{3.72a}$$

and, with equation (3.69), to

$$\epsilon_{n\lambda} \simeq \frac{2}{\sqrt{30\lambda\,\sigma_{dc}}} - \frac{1}{15\lambda\,\sigma_{dc}}, \quad \lambda \text{ in cm}, \quad \sigma_{dc} \text{ in } \Omega^{-1}\,\text{cm}^{-1}. \tag{3.72b}$$

This $1/\sqrt{\lambda}$ dependence is not predicted by the Drude theory (except for the far infrared), nor is it observed with optically smooth surfaces. However, it often approximates the behavior of polished (i.e., not entirely smooth) surfaces.

Example 3.3. Using the constants given in Fig. 3-7 calculate the complex index of refraction and the normal, spectral reflectivity of silver at $\lambda = 6.2\,\mu$m, using *(a)* the Drude theory, and *(b)* the Hagen–Rubens relation.

Solution
(a) From Fig. 3-7 we have for silver $\varepsilon_0 = 3.4$, $\nu_p = 2.22 \times 10^{15}$ Hz, and $\gamma = 4.30 \times 10^{12}$ Hz. Substituting these into equation (3.64) with $\nu = c_0/\lambda = 2.998 \times 10^8$ m/s $\times$ $(10^6\,\mu\text{m/m})/6.2\,\mu\text{m} = 4.84 \times 10^{13}$ Hz, we obtain

$$\begin{aligned} \varepsilon' &= 3.4 - \frac{(2.22 \times 10^{15})^2}{(4.84 \times 10^{13})^2 + (4.30 \times 10^{12})^2} = 3.4 - 2087 = -2084, \\ \varepsilon'' &= 2087 \times 4.30 \times 10^{12} \Big/ 4.84 \times 10^{13} = 185.1. \end{aligned}$$

The complex index of refraction follows from equation (3.62) as

$$\begin{aligned} n^2 &= \frac{1}{2}\left(-2084 + \sqrt{2084^2 + 185.1^2}\right) = 4.102, \\ k^2 &= \frac{1}{2}\left(2084 + \sqrt{2084^2 + 185.1^2}\right) = 2088, \end{aligned}$$

or $n = 2.03$ and $k = 45.7$. Finally, the normal reflectivity follows from equation (3.57) as

$$\rho_{n\lambda} = \frac{(1 - 2.03)^2 + 45.7^2}{(1 + 2.03)^2 + 45.7^2} = 0.996.$$

(b) Using the Hagen–Rubens relation we find, from equation (3.66), that

$$\begin{aligned} \sigma_{\text{dc}} &= 2\pi \times 8.8542 \times 10^{-12} \frac{\text{C}^2}{\text{N m}^2} \times \left(2.22 \times 10^{15}\,\text{Hz}\right)^2 \Big/ 4.30 \times 10^{12}\,\text{Hz} \\ &= 6.376{\times}10^7 \frac{\text{C}^2}{\text{N m}^2\,\text{s}} = 6.376{\times}10^7\,\Omega^{-1}\text{m}^{-1} = 6.376{\times}10^5\,\Omega^{-1}\text{cm}^{-1}. \end{aligned}$$

Substituting this value into equation (3.69) yields

$$n = k = \sqrt{30 \times 6.2 \times 10^{-4} \times 6.376 \times 10^5} = 108.9,$$

and

$$\rho_{n\lambda} = 1 - \epsilon_{n\lambda} = 1 - \frac{2}{n} + \frac{2}{n^2} = 1 - \frac{2}{108.9} + \frac{2}{108.9^2} = 0.982.$$

The two sets of results may be compared with experimental results of $n = 2.84$, $k = 45.7$ and $\rho_{n\lambda} = 0.995$ [17]. At first glance the Hagen–Rubens prediction for $\rho_{n\lambda}$ appears very good because, for any $k \gg 1$, $\rho_{n\lambda} \approx 1$. The values for n and k show that the Hagen–Rubens relation is in serious error even at a relatively long wavelength of $\lambda = 6.2\,\mu$m.

Total Properties for Normal Incidence

The total, normal reflectance and emittance may be evaluated from equation (3.8), with spectral, normal properties evaluated from the Drude theory or from the simple Hagen–Rubens relation. While the Hagen–Rubens relation is not very accurate, it does predict the emittance *trends* correctly in the infrared, and it does allow an explicit evaluation of total, normal emittance. Substituting equation (3.72) into equation (3.8) leads to an integral that may be evaluated in a similar fashion as for the total emissive power, equation (1.19), and, retaining the first three terms of the series expansion

$$\epsilon_n = 0.578\,(T/\sigma_{\text{dc}})^{1/2} - 0.178\,(T/\sigma_{\text{dc}}) + 0.0584\,(T/\sigma_{\text{dc}})^{3/2}, \quad T \text{ in K, } \sigma_{\text{dc}} \text{ in } \Omega^{-1}\text{cm}^{-1}. \tag{3.73}$$

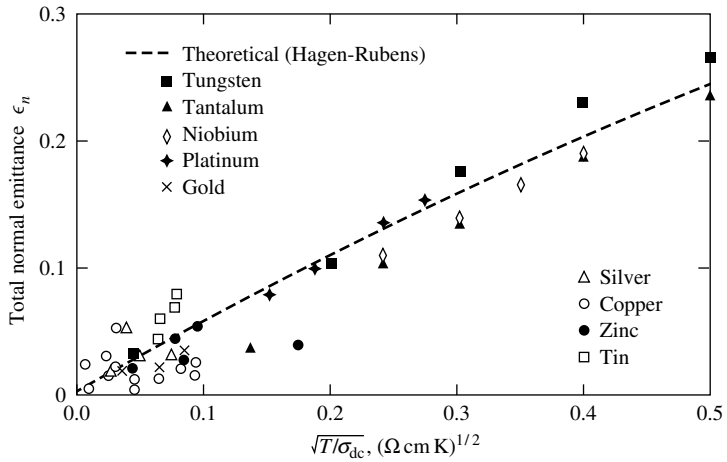

FIGURE 3-8
Total, normal emittance of various polished metals as a function of temperature [18].

Of course, equation (3.73) is only valid for small values of (T/σ_{dc}), i.e., the temperature of the surface must be such that only a small fraction of the blackbody emissive power comes from short wavelengths (where the Hagen–Rubens relation is not applicable). For pure metals, to a good approximation, the dc-conductivity is inversely proportional to absolute temperature, or

$$\sigma_{dc} = \sigma_{ref}\frac{T_{ref}}{T}. \tag{3.74}$$

Therefore, for low enough temperatures, the total, normal emittance of a pure metal should be approximately linearly proportional to temperature. Comparison with experiment (Fig. 3-8) shows that this nearly linear relationship holds for many metals up to surprisingly high temperatures; for example, for platinum $(T/\sigma_{dc})^{1/2} = 0.5$ corresponds to a temperature of 2700 K. It is interesting to note that spectral integration of the Drude model results in 30% to 70% lower total emissivities for all metals and, thus, fails to follow experimental trends. Such integration was carried out by Parker and Abbott [18] in an approximate fashion. They attributed the discrepancy to imperfections in the molecular lattice induced by surface preparation and to the *anomalous skin effect* [25], both of which lower the electrical conductivity in the surface layer.

Directional Dependence of Radiative Properties

The spectral, directional reflectivity at the interface between an absorber and a nonabsorber is given by Fresnel's relations, (3.52) through (3.55). Since, in the infrared, n and k are generally fairly large for metals one may with little error neglect the $\sin^2\theta_1$ in equations (3.54) and (3.55), leading to $p \simeq n$ and $q \simeq k$. Then, from equations (3.52) and (3.53) the reflectivities for parallel- and perpendicular-polarized light are evaluated from[4]

$$\rho_{\parallel} = \frac{(n\cos\theta - 1)^2 + (k\cos\theta)^2}{(n\cos\theta + 1)^2 + (k\cos\theta)^2}, \tag{3.75a}$$

$$\rho_{\perp} = \frac{(n - \cos\theta)^2 + k^2}{(n + \cos\theta)^2 + k^2}. \tag{3.75b}$$

The directional, spectral emissivity (unpolarized) follows as

[4]The simple form for $\rho_{\parallel}$ used here is best obtained from the reflection coefficient given by equation (2.111) by neglecting $\sin^2\theta_1$ and canceling $m = n - ik$ from both numerator and denominator.

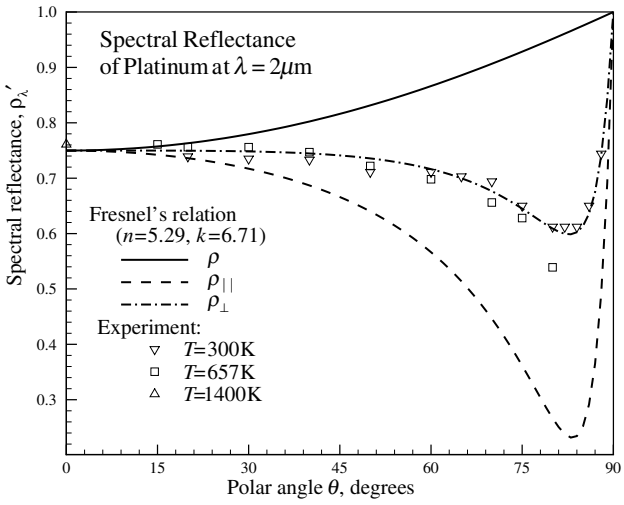

FIGURE 3-9
Spectral, directional reflectance of platinum at $\lambda = 2\,\mu$m.

$$\epsilon'_\lambda = 1 - \tfrac{1}{2}(\rho_\parallel + \rho_\perp), \tag{3.76}$$

and is shown (as reflectance) in Fig. 3-9 for platinum at $\lambda = 2\,\mu$m. The theoretical line for room temperature has been calculated with $n = 5.29$, $k = 6.71$ from [23]. Comparison with experimental emittances of Brandenberg [26], Brandenberg and Clausen [27], and Price [28] demonstrates the validity of Fresnel's relations.[5]

Equation (3.75) may be integrated analytically over all directions to obtain the spectral, hemispherical emissivity from equation (3.5). This was done by Dunkle [29] for the two different polarizations, resulting in

$$\epsilon_\parallel = \frac{8n}{n^2+k^2}\left(1 - \frac{n}{n^2+k^2}\ln\left[(n+1)^2+k^2\right] + \frac{(n^2-k^2)}{k(n^2+k^2)}\tan^{-1}\frac{k}{n+1}\right), \tag{3.77a}$$

$$\epsilon_\perp = 8n\left(1 - n\ln\frac{(n+1)^2+k^2}{n^2+k^2} + \frac{(n^2-k^2)}{k}\tan^{-1}\frac{k}{n(n+1)+k^2}\right), \tag{3.77b}$$

$$\epsilon_\lambda = \frac{1}{2}(\epsilon_\parallel + \epsilon_\perp). \tag{3.77c}$$

Figure 3-10, from Dunkle [30], is a plot of the ratio of the hemispherical and normal emissivities, $\epsilon_\lambda/\epsilon_{n\lambda}$. For the case of $k/n = 1$ the dashed line represents results from equation (3.77), while the solid lines were obtained by numerically integrating equations (3.52) through (3.55). For $k/n > 1$ the two lines become indistinguishable. Hering and Smith [31] reported that equation (3.77) is accurate to within 1–2% for values of $n^2 + k^2$ larger than 40 and 3.25, respectively. In view of the large values that n and, in particular, k assume for metals, equation (3.77) is virtually always accurate to better than 2% for metals in the visible and infrared wavelengths. For the reader's convenience the function `emmet` is included in Appendix F for the evaluation of equation (3.77).

Example 3.4. Determine the spectral, hemispherical emissivity for room-temperature nickel at a wavelength of $\lambda = 10\,\mu$m, using *(a)* the Drude theory, and *(b)* the Hagen–Rubens relation.

Solution
We first need to determine the optical constants n and k from either theory, then calculate the hemispherical emissivity from equation (3.77) or read it from Fig. 3-10.

[5] In the original figure of Brandenberg and Clausen [27] older values for n and k were used that gave considerably worse agreement with experiment.

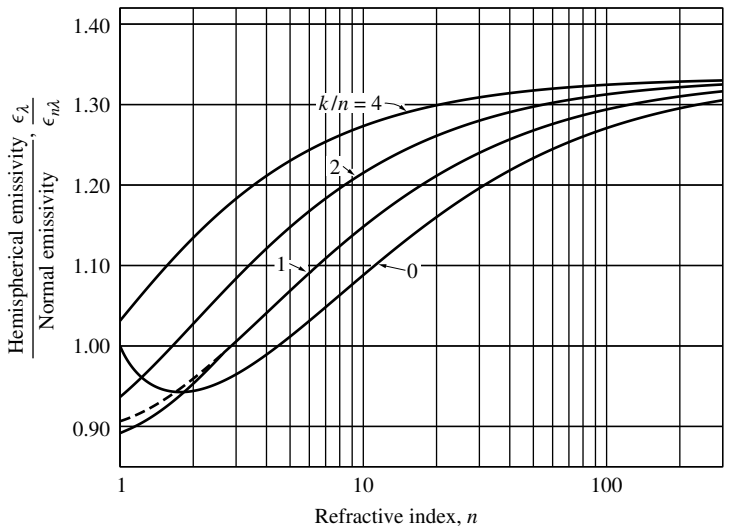

FIGURE 3-10
Ratio of hemispherical and normal spectral emissivity for electrical conductors as a function of n and k [30].

(a) Using values for nickel from Table 3.3 in equation (3.64), we find with $\nu = c_0/\lambda = 2.998 \times 10^8\ \text{m/s}/10^{-5}\ \text{m} = 2.998 \times 10^{13}\ \text{Hz}$,

$$\varepsilon' = 1.0 - 3.72 \times 10^{30} \Big/ \left[(2.998 \times 10^{13})^2 + (1.62 \times 10^{13})^2\right] = 1 - 3204 = -3203,$$

$$\varepsilon'' = 3204 \times 1.62 \times 10^{13} \Big/ 2.998 \times 10^{13} = 1731,$$

$$n^2 = 0.5 \times \left(-3208 + \sqrt{3208^2 + 1731^2}\right) = 219,$$

$$k^2 = 0.5 \times \left(3208 + \sqrt{3208^2 + 1731^2}\right) = 3422,$$

and

$$n = 14.8, \quad k = 58.5, \quad k/n = 58.5/14.8 = 3.95.$$

To use Fig. 3-10 we first determine $\rho_{n\lambda}$ as

$$\rho_{n\lambda} = \frac{13.8^2 + 58.5^2}{15.8^2 + 58.5^2} = 0.984,$$

and

$$\epsilon_{n\lambda} = 1 - \rho_{n\lambda} = 0.016.$$

From Fig. 3-10 $\epsilon_\lambda/\epsilon_{n\lambda} \simeq 1.29$ and, therefore, $\epsilon_\lambda \simeq 0.021$.

(b) Using the Hagen–Rubens relation we find, from equation (3.72),

$$\epsilon_{n\lambda} = \frac{2}{\sqrt{30 \times 10^{-3} \times 1.28 \times 10^5}} - \frac{1}{15 \times 10^{-3} \times 1.28 \times 10^5} = 0.032.$$

Further, with $n \simeq k \simeq \sqrt{30 \times 10^{-3} \times 1.28 \times 10^5} = 62.0$, we obtain from Fig. 3-10 $\epsilon_\lambda/\epsilon_{n\lambda} \simeq 1.275$ and $\epsilon_\lambda \simeq 0.041$.

The answers from both models differ by a factor of ~2. This agrees with the trends shown in Fig. 3-7.

Theoretical values for total, directional emissivities are obtained by (numerical) integration of equations (3.75) and (3.76) over the entire spectrum. The directional behavior of total emissivities is similar to that of spectral emissivities, as shown by the early measurements of Schmidt and Eckert [9], as depicted in Fig. 3-1*b* in a polar diagram (as opposed to the Cartesian representation of Fig. 3-9). The emittances were determined from total radiation measurements from samples heated to a few hundred degrees Celsius.

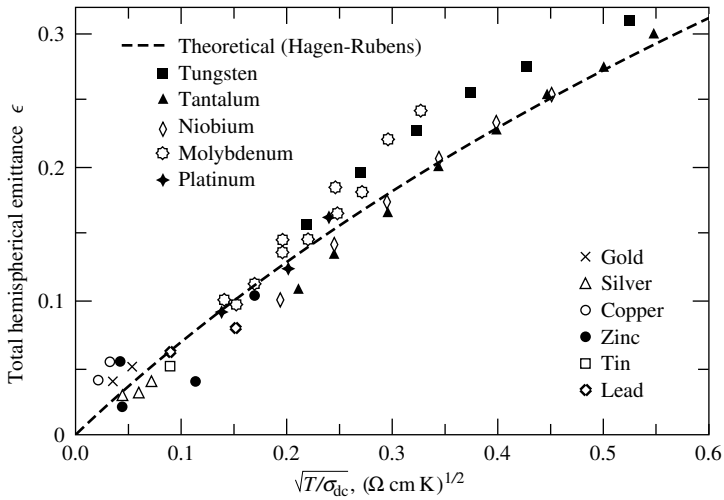

FIGURE 3-11
Total, hemispherical emittance of various polished metals as a function of temperature [18].

Total, Hemispherical Emittance

Equation (3.77) may be integrated over the spectrum using equation (3.10), to obtain the total, hemispherical emittance of a metal. Several approximate relations, using the Hagen–Rubens limit, have been proposed, notably the ones by Davisson and Weeks [32] and by Schmidt and Eckert [9]. Expanding equation (3.77) into a series of powers of $1/n$ (with $n = k \gg 1$), Parker and Abbott [18] were able to integrate equation (3.77) analytically, leading to

$$\epsilon(T) = 0.766(T/\sigma_{dc})^{1/2} - [0.309 - 0.0889\ln(T/\sigma_{dc})]\,(T/\sigma_{dc}) - 0.0175(T/\sigma_{dc})^{3/2}, \quad T \text{ in K}, \quad \sigma_{dc} \text{ in } \Omega^{-1}\text{cm}^{-1}. \tag{3.78}$$

As for the total, normal emittance the total, hemispherical emittance is seen to be approximately linearly proportional to temperature (since $\sigma_{dc} \propto 1/T$) as long as the surface temperature is relatively low (so that only long wavelengths are of importance, for which the Hagen–Rubens relation gives reasonable results). Emittances calculated from equation (3.78) are compared with experimental data in Fig. 3-11. Parker and Abbott also integrated the series expansion of equation (3.77) with n and k evaluated from the Drude theory. As for normal emissivities, the Drude model predicts values 30–70% lower than the Hagen–Rubens relations, contrary to experimental evidence shown in Fig. 3-11. Again, the discrepancy was attributed to lattice imperfections and to the anomalous skin effect.

Effects of Surface Temperature

The Hagen–Rubens relation, equation (3.72), predicts that the spectral, normal emittance of a metal should be proportional to $1/\sqrt{\sigma_{dc}}$. Since the electrical conductivity is approximately inversely proportional to temperature, the spectral emittance should, therefore, be proportional to the square root of absolute temperature for long enough wavelengths. This trend should also hold for the spectral, hemispherical emittance. Experiments have shown that this is indeed true for many metals. A typical example is given in Fig. 3-12, showing the spectral dependence of the hemispherical emittance for tungsten for a number of temperatures [33]. Note that the emittance for tungsten tends to increase with temperature beyond a *crossover wavelength* of approximately 1.3 μm, while the temperature dependence is reversed for shorter wavelengths. Similar trends of a single crossover wavelength have been observed for many metals.

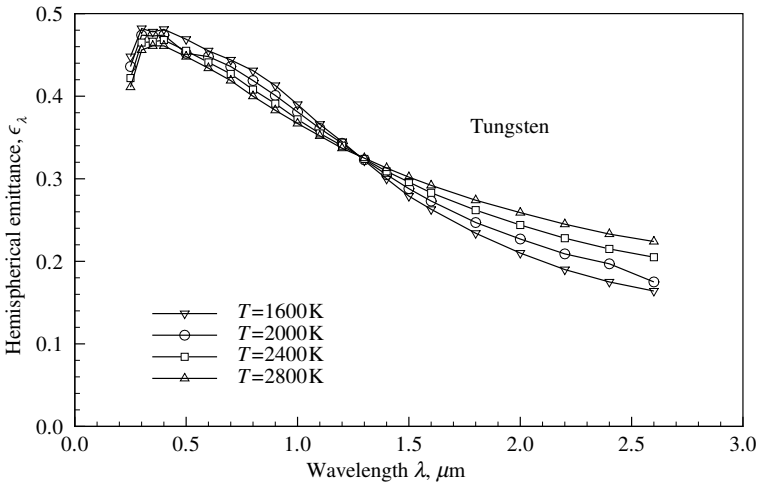

FIGURE 3-12
Temperature dependence of the spectral, hemispherical emittance of tungsten [33].

The total, normal or hemispherical emittances are calculated by integrating spectral values over all wavelengths, with the blackbody emissive power as weight function. Since the peak of the blackbody emissive power shifts toward shorter wavelengths with increasing temperature, we infer that hotter surfaces emit a higher fraction of energy at shorter wavelengths, where the spectral emittance is higher, resulting in an increase in total emittance as demonstrated in Figs. 3-8 and 3-11. Since the crossover wavelength is fairly short for many metals, the Hagen–Rubens temperature relation often holds for surprisingly high temperatures.

3.5 RADIATIVE PROPERTIES OF NONCONDUCTORS

Electrical nonconductors have few free electrons and, thus, do not display the high reflectance and opaqueness behavior across the infrared as do metals. Semiconductors, as their title suggests, have some free electrons and are usually discussed together with nonconductors; however, they display some of the characteristics of a metal. The radiative properties of pure nonconductors are dominated in the infrared by photon–phonon interaction, i.e., by the photon excitation of the vibrational energy levels of the solid's crystal lattice. Outside the spectral region of strong absorption by vibrational transitions there is generally a region of fairly high transparency (and low reflectance), where absorption is dominated by impurities and imperfections in the crystal lattice. As such, these spectral regions often show irregular and erratic behavior.

Wavelength Dependence of Spectral, Normal Properties

The spectral behavior of pure, crystalline nonconductors is often well described by the single oscillator Lorentz model of equation (3.63). One such material is the semiconductor α-SiC (silicon carbide), a high-temperature ceramic of ever increasing importance. The spectral, normal reflectivity of pure, smooth α-SiC at room temperature is shown in Fig. 3-13, as given by Spitzer and coworkers [34]. The theoretical reflectivity in Fig. 3-13 is evaluated from equations (3.63), (3.62) and (3.57) with $\varepsilon_0 = 6.7$, $\nu_{pi} = 4.327 \times 10^{13}$ Hz, $\nu_i = 2.380 \times 10^{13}$ Hz, $\gamma_i = 1.428 \times 10^{11}$ Hz. Agreement between theory and experiment is superb for the entire range between $2\,\mu$m and $22\,\mu$m. Inspection of equations (3.63) and (3.62) shows that outside the spectral range $10\,\mu\text{m} < \lambda < 13\,\mu\text{m}$ (or 2.5×10^{13} Hz $> \nu > 1.9 \times 10^{13}$ Hz), α-SiC is essentially transparent

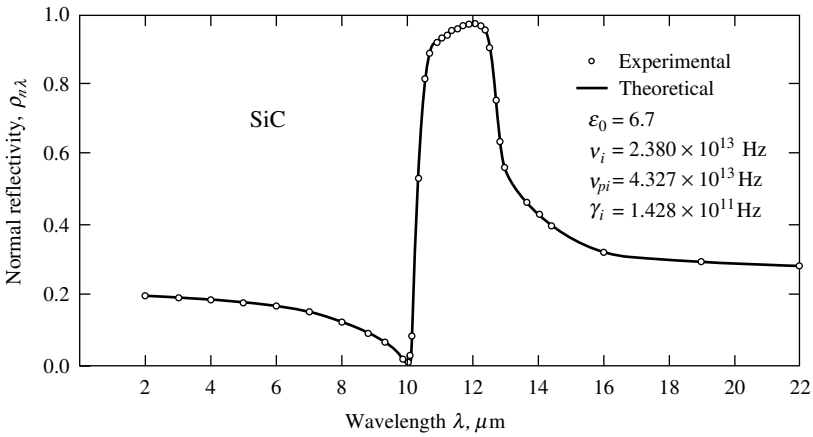

FIGURE 3-13
Spectral, normal reflectivity of α-SiC at room temperature [34].

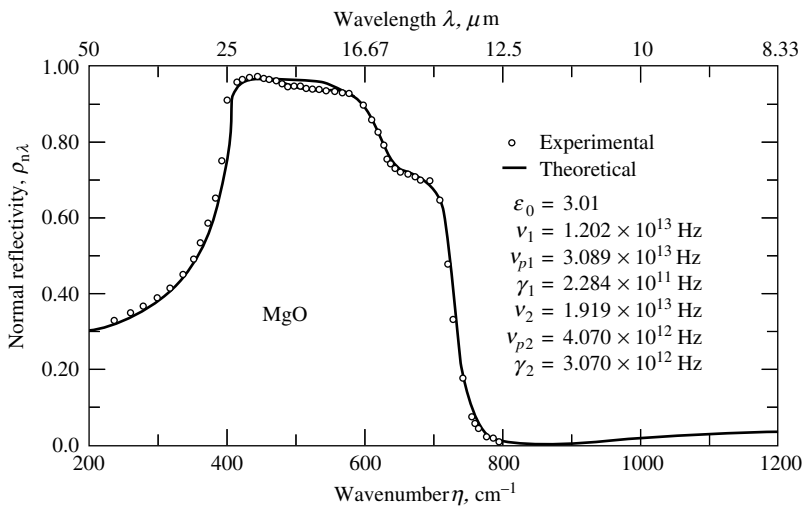

FIGURE 3-14
Spectral, normal reflectivity of MgO at room temperature [36].

(absorptive index $k \ll 1$) and weakly reflecting. Within the range of $10\,\mu\text{m} < \lambda < 13\,\mu\text{m}$ α-SiC is not only highly reflecting but also opaque (i.e., any radiation not reflected is absorbed within a very thin surface layer, since $k > 1$). The reflectivity drops off sharply on both sides of the absorption band. For this reason materials such as α-SiC are sometimes used as *bandpass filters*: If electromagnetic radiation is reflected several times by an α-SiC mirror, the emerging light will nearly exclusively lie in the spectral band $10\,\mu\text{m} < \lambda < 13\,\mu\text{m}$. This effect has led to the term *Reststrahlen band* (German for "remaining rays") for absorption bands due to crystal vibrational transitions. Bao and Ruan [35] have demonstrated that the dielectric function for semiconductors can be calculated through density functional theory, resulting in good agreement with experiment for GaAs.

Not all crystals are well described by the single oscillator model since two or more different vibrational transitions may be possible and can result in overlapping bands. Magnesium oxide (MgO) is an example of material that can be described by a two-oscillator model (two overlapping bands), as Jasperse and coworkers [36] have shown (Fig. 3-14). The theoretical reflectivities are obtained with the parameters for the evaluation of equation (3.63) given in the figure. Note that for the calculation of ε' and ε'', equation (3.63) needs to be summed over both

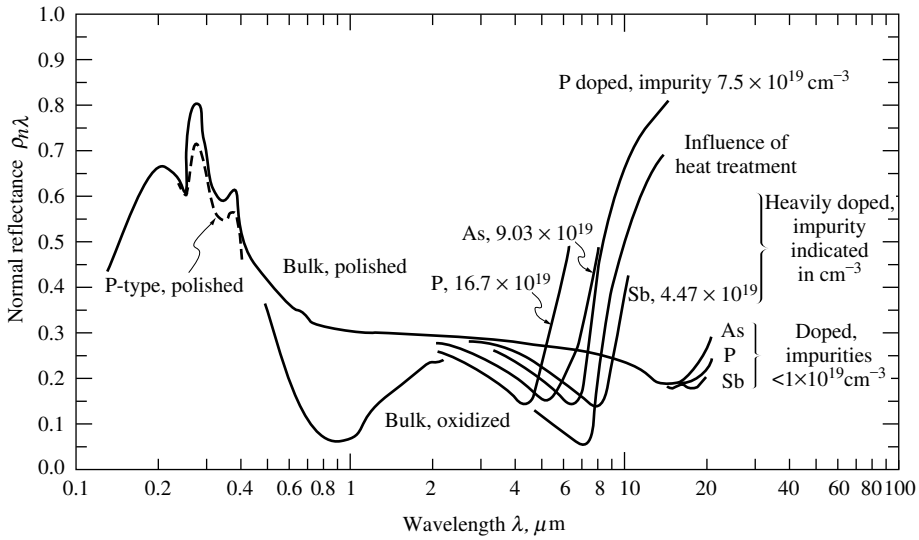

FIGURE 3-15
Spectral, normal reflectance of silicon at room temperature [7].

bands, $i = 1$ and 2. From a quantum viewpoint, the second, weaker oscillator is interpreted as the excitation of two phonons by a single photon [37].

Since the radiative properties outside a Reststrahlen band depend strongly on defects and impurities they may vary appreciably from specimen to specimen and even between different points on the same sample. For example, the spectral, normal reflectance of silicon at room temperature is shown in Fig. 3-15 (redrawn from data collected by Touloukian and DeWitt [7]). Strong influence of different types and levels of impurities is clearly evident. Therefore, looking up properties for a given material in published tables is problematical unless a detailed description of surface and material preparation is given.

Equation (3.63) demonstrates that—outside a Reststrahlen band—ε'' and, therefore, the absorptive index k of a nonconductor are very small; typically $k < 10^{-6}$ for a pure substance. While impurities and lattice defects can increase the value of k, it is very unlikely to find values of $k > 10^{-2}$ for a nonconductor outside Reststrahlen bands. At first glance it might appear, therefore, that all nonconductors must be highly transparent in the near infrared (and the visible). That this is not the case is readily seen from equation (1.55), which relates transmissivity to absorption coefficient. This, in turn, is related to the absorptive index through equation (2.42):

$$\tau = e^{-\kappa s} = e^{-4\pi k s/\lambda_0}. \tag{3.79}$$

For a 1 mm thick layer of a material with $k = 10^{-3}$ at a wavelength (in vacuum) of $\lambda_0 = 2\,\mu$m, equation (3.79) translates into a transmissivity of $\tau = \exp(-4\pi \times 10^{-3} \times 1/2 \times 10^{-3}) = 0.002$, i.e., the layer is essentially opaque. Still, the low values of k allow us to simplify Fresnel's relations considerably for the reflectivity of an interface. With $k^2 \ll (n-1)^2$ the nonconductor essentially behaves like a perfect dielectric and, from equation (3.57), the spectral, normal reflectivity may be evaluated as

$$\rho_{n\lambda} = \left(\frac{n-1}{n+1}\right)^2, \qquad k^2 \ll n^2. \tag{3.80}$$

Therefore, for optically smooth nonconductors the radiative properties may be calculated from refractive index data. Refractive indices for a number of semitransparent materials at room temperature are displayed in Fig. 3-16 as a function of wavelength [20]. All these crystalline materials show similar spectral behavior: The refractive index drops rapidly in the visible

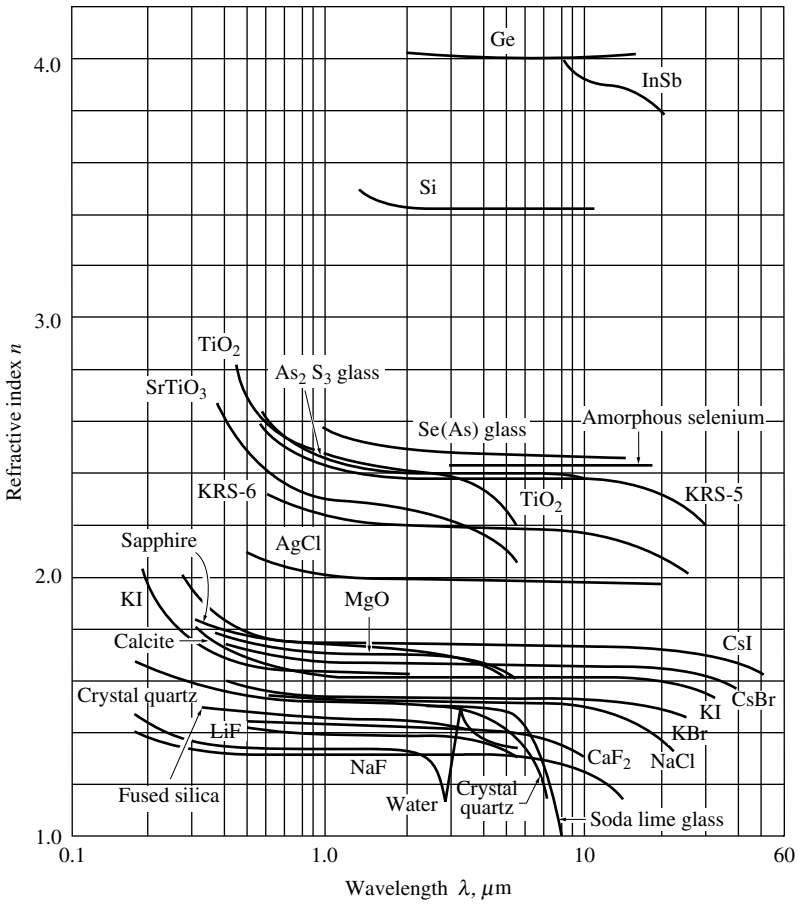

FIGURE 3-16
Refractive indices for various semitransparent materials [20].

region, then is nearly constant (declining very gradually) until the midinfrared, where n again starts to drop rapidly. This behavior is explained by the fact that crystalline solids tend to have an absorption band, due to electronic transitions, near the visible, and a Reststrahlen band in the infrared: The first drop in n is due to the tail end of the electronic band, as illustrated in Fig. 2-15*b*;[6] the second drop in the midinfrared is due to the beginning of a Reststrahlen band. Listings of refractive indices for various glasses, water, inorganic liquids, and air are also available [23].

Directional Dependence of Radiative Properties

For optically smooth nonconductors experiment has been found to follow Fresnel's relations of electromagnetic wave theory closely. Figure 3-17 shows a comparison between theory and experiment for the directional reflectivity of glass (blackened on one side to avoid multiple reflections) for polarized, monochromatic irradiation [26]. Because $k^2 \ll n^2$, the absorptive index may be eliminated from equations (3.52) and (3.53), and the relations for a perfect dielectric become valid. Thus, for unpolarized light incident from vacuum (or a gas), from equations (3.59)

[6]Note that the abscissa in Fig. 2-15*b* is frequency ν, i.e., wavelength increases to the left.

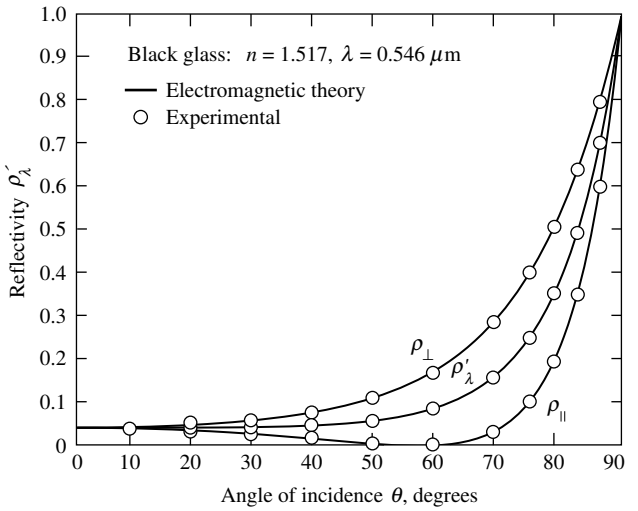

FIGURE 3-17
Spectral, directional reflectivity of glass at room temperature, for polarized light [26].

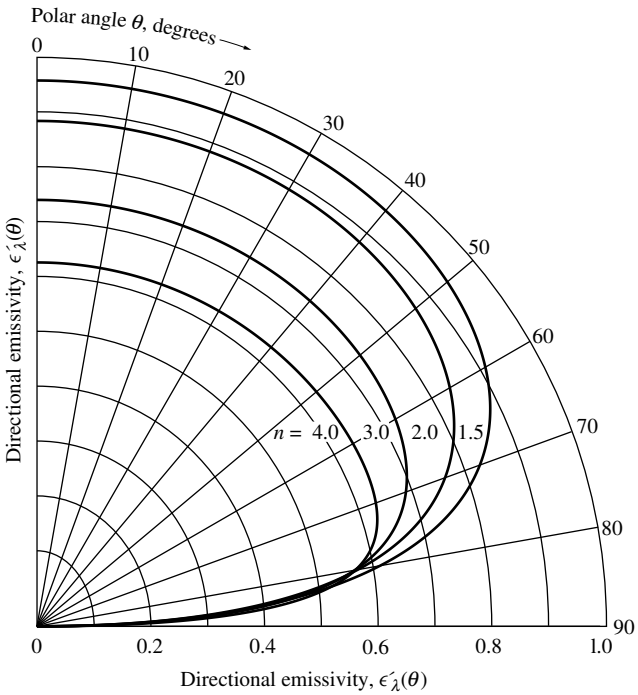

FIGURE 3-18
Directional emissivities of nonconductors as predicted by electromagnetic wave theory.

and (3.60)

$$\epsilon'_\lambda = 1 - \frac{1}{2}(\rho_\parallel + \rho_\perp) = 1 - \frac{1}{2}\left[\left(\frac{n^2\cos\theta - \sqrt{n^2 - \sin^2\theta}}{n^2\cos\theta + \sqrt{n^2 - \sin^2\theta}}\right)^2 + \left(\frac{\cos\theta - \sqrt{n^2 - \sin^2\theta}}{\cos\theta + \sqrt{n^2 - \sin^2\theta}}\right)^2\right]. \qquad (3.81)$$

Of course, the spectral, directional reflectivity for a dielectric can also be calculated from subroutine `fresnel` in Appendix F by setting k equal to zero. The directional variation of the spectral emissivity of dielectrics is shown in Fig. 3-18. Comparison with Fig. 3-1 demonstrates that experiment agrees well with electromagnetic wave theory for a large number of nonconductors, even for total (rather than spectral) directional emittances.

The spectral, hemispherical emissivity of a nonconductor may be obtained by integrating

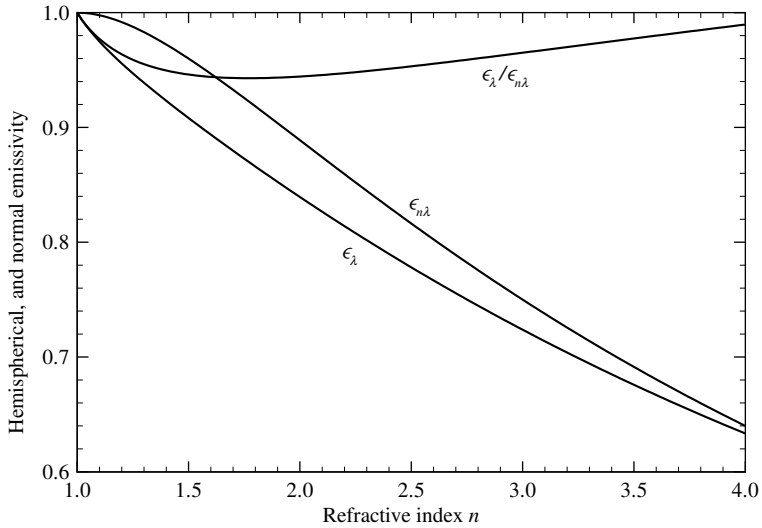

FIGURE 3-19
Normal and hemispherical emissivities for nonconductors as a function of refractive index.

equation (3.81) with equation (3.5). While tedious, such an integration is possible, as shown by Dunkle [30]:

$$\epsilon_\parallel = \frac{4(2n+1)}{3(n+1)^2}, \tag{3.82a}$$

$$\epsilon_\perp = \frac{4n^3(n^2+2n-1)}{(n^2+1)(n^4-1)} + \frac{2n^2(n^2-1)^2}{(n^2+1)^3}\ln\left(\frac{n+1}{n-1}\right) - \frac{16n^4(n^4+1)\ln n}{(n^2+1)(n^4-1)^2}, \tag{3.82b}$$

$$\epsilon_\lambda = \frac{1}{2}(\epsilon_\parallel + \epsilon_\perp). \tag{3.82c}$$

The variation of normal and hemispherical emissivities with refractive index may be calculated with functions `emdiel` (ϵ_λ) and `emdielr` ($\epsilon_\lambda/\epsilon_{n\lambda}$) from Appendix F and is shown in Fig. 3-19. While for metals the hemispherical emittance is generally larger than the normal emittance (cf. Fig. 3-10), the opposite is true for nonconductors. The reason for this behavior is obvious from Fig. 3-1: Metals have a relatively low emittance over most directions, but display a sharp increase for grazing angles before dropping back to zero. Nonconductors, on the other hand, have a (relatively high) emittance for most directions, which gradually drops to zero at grazing angles (without a peak).

Example 3.5. The directional reflectance of silicon carbide at $\lambda = 2\ \mu$m and an incidence angle of $\theta = 10°$ has been measured as $\rho'_\lambda = 0.20$ (cf. Fig. 3-13). What is the hemispherical emittance of SiC at 2 μm?

Solution
Since at $\theta = 10°$ the directional reflectance does not deviate substantially from the normal reflectance (cf. Fig. 3-18), we have $\epsilon_{n\lambda} = 1 - \rho_{n\lambda} \simeq 1 - 0.20 = 0.80$. Then, from Fig. 3-19, $n \simeq 2.6$ and $\epsilon_\lambda \simeq 0.76$.

Effects of Surface Temperature

The temperature dependence of the radiative properties of nonconductors is considerably more difficult to quantify than for metals. Infrared absorption bands in ionic solids due to excitation of lattice vibrations (*Reststrahlen bands*) generally increase in width and decrease in strength with temperature, and the wavelength of peak reflection/absorption shifts toward higher values. Figure 3-20 shows the behavior of the MgO Reststrahlen band [36]; similar results have been

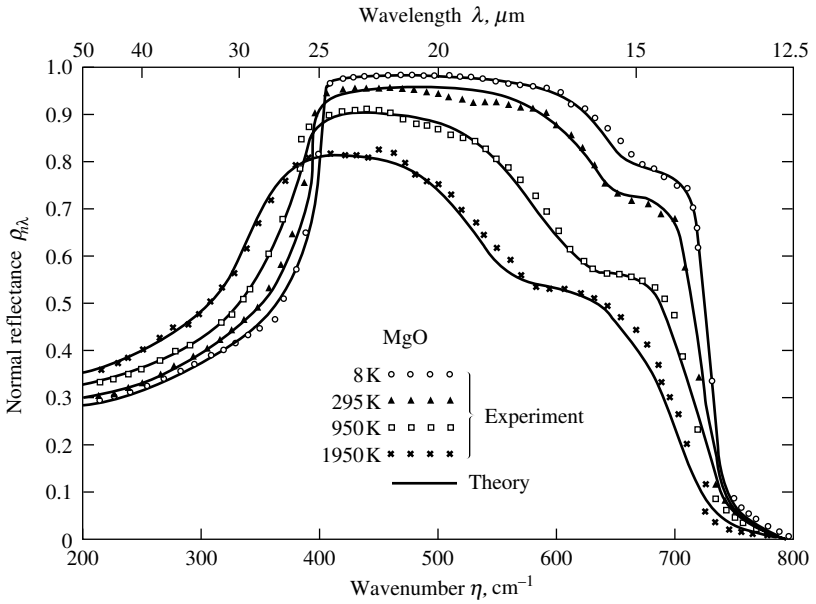

FIGURE 3-20
Variation of the spectral, normal reflectance of MgO with temperature [36].

obtained for SiC [38]. The reflectance for shorter wavelengths largely depends on the material's impurities. Often the behavior is similar to that of metals, i.e., the emittance increases with temperature for the near infrared, while it decreases with shorter wavelengths. As an example, Fig. 3-21 shows the normal emittance for zirconium carbide [39]. On the other hand, the emittance of amorphous solids (i.e., solids without a crystal lattice) tends to be independent of temperature [40].

3.6 EFFECTS OF SURFACE ROUGHNESS

Up to this point, our discussion of radiative properties has assumed that the material surfaces are optically smooth, i.e., that the average length scale of *surface roughness* is much less than the wavelength of the electromagnetic wave. Therefore, a surface that appears rough in visible light ($\lambda \simeq 0.5\,\mu$m) may well be optically smooth in the intermediate infrared ($\lambda \simeq 50\,\mu$m). This difference is the primary reason why the electromagnetic wave theory ceases to be valid for very short wavelengths.

In this section we shall very briefly discuss some fundamental aspects of how surface roughness affects the radiative properties of opaque surfaces. Detailed discussions have been given in the books by Beckmann and Spizzichino [41] and Bass and Fuks [42], and in a review article by Ogilvy [43]

The character of roughness may be very different from surface to surface, depending on the material, method of manufacture, surface preparation, and so on, and classification of this character is difficult. A common measure of surface roughness is given by the *root-mean-square roughness* σ_h, defined as (cf. Fig. 3-22)

$$\sigma_h = \left[\left\langle (z - z_m)^2 \right\rangle\right]^{1/2} = \left[\frac{1}{A}\int_A (z - z_m)^2\, dA\right]^{1/2}, \tag{3.83}$$

where A is the surface to be examined, and $|z - z_m|$ is the local height deviation from the mean. The root-mean-square roughness can be readily measured with a *profilometer* (a sharp

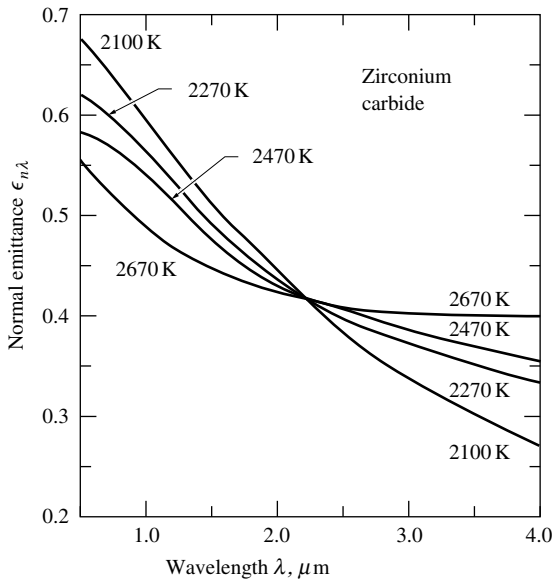

FIGURE 3-21
Temperature dependence of the spectral, normal emittance of zirconium carbide [39].

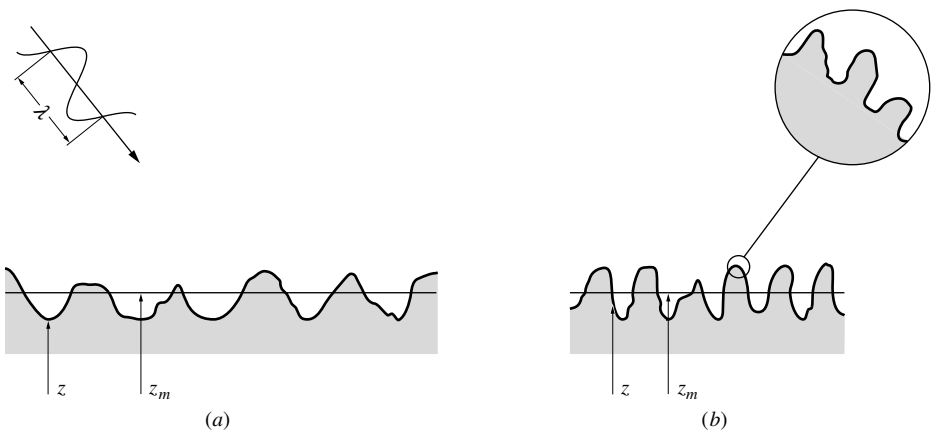

FIGURE 3-22
Topography of a rough surface: *(a)* roughness with gradual slopes, *(b)* roughness with steep slopes. Both surfaces have similar root-mean-square roughness.

stylus that traverses the surface, recording the height fluctuations). Unfortunately, σ_h alone is woefully inadequate to describe the roughness of a surface as seen by comparing Fig. 3-22*a* and *b*. Surfaces of identical σ_h may have vastly different frequencies of roughness peaks, resulting in different average slopes along the rough surface; in addition, σ_h gives no information on second order (or higher) roughness superimposed onto the fundamental roughness.

A first published attempt at modeling was made by Davies [44], who applied diffraction theory to a perfectly reflecting surface with roughness distributed according to a Gaussian probability distribution. The method neglects shading from adjacent peaks and, therefore, does poorly for grazing angles and for roughness with steep slopes (Fig. 3-22*b*). Comparison with experiments of Bennett [45] shows that, for small incidence angles, Davies' model predicts the decay of specular peaks rather well (e.g., Fig. 3-14 for MgO).

Davies' model predicts a sharp peak in the bidirectional reflection function, ρ''_λ, for the specular reflection direction, as has been found to be true experimentally for most cases as long

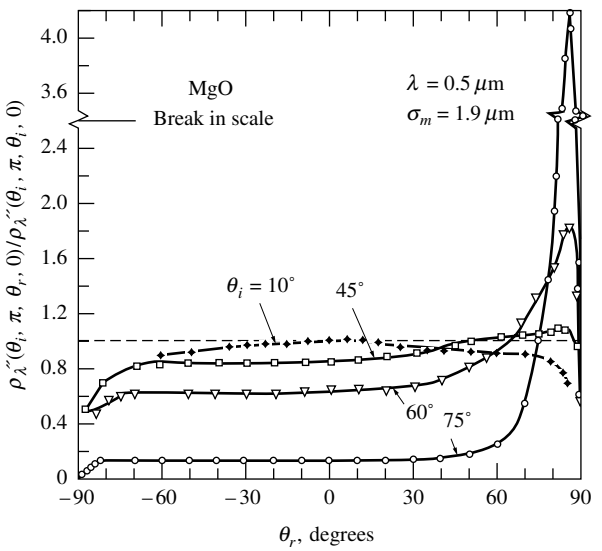

FIGURE 3-23
Normalized bidirectional reflection function (in plane of incidence) for magnesium oxide ceramic; $\sigma_h = 1.9\,\mu$m, $\lambda = 0.5\,\mu$m [47].

as the incidence angle was not too large (e.g., Fig. 3-5). For large off-normal angles of incidence, experiment has shown that the bidirectional reflectance function has its peak at polar angles greater than the specular direction. An example is given in Fig. 3-23 for magnesium oxide with a roughness of $\sigma_h = 1.9\,\mu$m, illuminated by radiation with a wavelength of $\lambda = 0.5\,\mu$m. Shown is the bidirectional reflection function (normalized with its value in the specular direction) for the plane of incidence (the plane formed by the surface normal and the direction of the incoming radiation). We see that for small incidence angles ($\theta_i = 10^\circ$) the reflection function is relatively diffuse, with a small peak in the specular direction. For comparison, diffuse reflection with a direction-independent reflection function is indicated by the dashed line. For larger incidence angles the reflection function displays stronger and stronger *off-specular peaks*. For example, for an incidence angle of $\theta_i = 45^\circ$, the off-specular peak lies in the region of $\theta = 80^\circ$ to 85°. Apparently, these off-specular peaks are due to *shadowing* of parts of the surface by adjacent peaks. The effects of shadowing have been incorporated into the model by Beckmann [46] and Torrance and Sparrow [47]. With the appropriate choice for two unknown constants, Torrance and Sparrow found their model agreed very well with their experimental data (Fig. 3-23).

The above models assumed that the surfaces have a certain root-mean-square roughness, but that they were otherwise random—no attempt was made to classify roughness slopes, secondary roughness, etc. Berry and coworkers [48,49] considered diffraction of radiation from *fractal surfaces*. The behavior of fractal surfaces is such that the enlarged images appear very similar to the original surface when the surface roughness is repeatedly magnified (Fig. 3-22*b*). Majumdar and colleagues [50,51] carried out roughness measurements on a variety of surfaces and found that both processed and unprocessed surfaces are generally fractal. Majumdar and Tien [52] extended Davies' theory to include fractal surfaces, resulting in good agreement for experiments with different types of metallic surfaces [53,54]. However, since shadowing effects have not been considered, the model is again limited to near-normal incidence.

Buckius and coworkers [55–58] have investigated various one-dimensionally rough surfaces (i.e., where surface height is a function of one coordinate only, $z = z(x)$ in Fig. 3-23), including the effects of roughness peak frequency (or slopes). For a randomly rough surface peak-to-peak spacing is usually characterized by a correlation length σ_l in a Gaussian correlation function $C(L)$, where L is the length over which the correlation diminishes by a factor of e, or

$$C(L) = \frac{1}{\sigma_h^2}\left\langle \Big(z(x) - z_m\Big)\Big(z(x+L) - z_m\Big)\right\rangle = e^{-(L/\sigma_l)^2}. \tag{3.84}$$

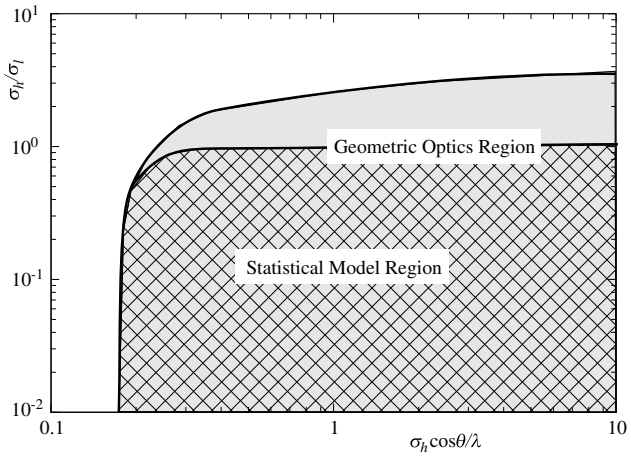

FIGURE 3-24
Domains of validity for the geometric optics and the statistical rough surface reflection models, constructed for incidence angles between −45° and +45° from the surface normal.

They first considered triangular grooves with roughnesses σ_h, σ_l and wavelength λ all of the same order, finding the bidirectional reflectance by solving an integral form of Maxwell's equations. They found that these exact solutions predict the same scattering peaks as found from optical grating theory. They then applied their model to randomly rough surfaces described by equations (3.83) and (3.84), and compared their electromagnetic wave theory results with those from the simple *Kirchhoff approximation* [41]. In the Kirchhoff approximation a simplified set of electromagnetic wave equations is considered, assuming that at every point on the surface the electromagnetic field is equal to the field that would exist on a local tangent plane, and multiple reflections between local peaks are neglected. This approximation has been applied by a number of researchers to one- and two-dimensionally rough surfaces, and domains of validity have been constructed [56, 59–61]. It is generally understood that the Kirchhoff approximation gives satisfactory results when surface geometric parameters (σ_h, σ_l) are less than or comparable to the wavelength and the slope of the roughness is small ($\sigma_h/\sigma_l \lesssim 0.3$). In more recent work Buckius and coworkers have concentrated on geometric optics (i.e., assuming Fresnel's relations to hold at every point on the surface), noting that Kirchhoff's approximation results in considerably larger numerical effort without significant improvement over the specular approximation. They considered one- and two-dimensionally uncoated rough surfaces [58, 62, 63], and surfaces coated with a thin film [64] (together with thin film theory). A map was constructed, shown in Fig. 3-24, depicting under what conditions geometric optics gives satisfactory results as compared to exact electromagnetic wave theory calculations, using the criterion

$$E_d = \left| \int_{-\pi/2}^{\pi/2} (I_e - I_a) \cos\theta \, d\theta \right| \Big/ \int_{-\pi/2}^{\pi/2} I_e \cos\theta \, d\theta < 0.2, \tag{3.85}$$

where I_e and I_a are exact and approximate reflected intensities, respectively. In general, geometric optics requires generation of statistical surfaces together with ray tracing, a relatively time-consuming task. Along the same line Zhang and coworkers investigated scattering from rough silicon surfaces and wafers [65–67]. Surface topographic data obtained with an atomic force microscope showed the surface roughness to be significantly non-Gaussian and anisotropic. Nevertheless, the use of two-dimensional slope distributions and statistical ray tracing recovered experimental bidirectional reflection very accurately. Tang and Buckius [68] also introduced a statistical geometric optics model that does not require ray tracing. The resulting closed-form expressions were found to be satisfactory for $\sigma_h/\sigma_l \lesssim 1$, as also indicated in Fig. 3-24. Comparison of geometric optics calculations with experiment (Al_2O_3 film on aluminum) showed good agreement, corroborating the applicability of their model [64]. Figure 3-24 was further confirmed (and augmented somewhat) by Fu and Hsu [69], who compared statistical ray tracing results with numerical solutions of Maxwell's equations.

Carminati and colleagues [70] used Kirchhoff's approximation to provide an expression for the spectral, directional emittance (polarized or unpolarized) of a one-dimensionally randomly rough surface as

$$\epsilon'_\lambda(\theta) = \int_{-\infty}^{\infty} \left[1 - \rho_\lambda(\theta - \tan^{-1} p)\right] \left|1 - p \tan\theta\right| P(p)\, dp, \tag{3.86}$$

where $\rho_\lambda(\theta)$ is the reflectivity as given by Fresnel's relations, equations (3.52) through (3.55), and $P(p)$ is a slope probability derived from the correlation function as

$$P(p) = \frac{\sigma_l}{\sigma_h \sqrt{4\pi}}\, e^{-(p\sigma_l/2\sigma_h)^2}. \tag{3.87}$$

Calling this a "small slope emission model" (since, similar to the conclusions of Fig. 3-24, its validity—in particular for parallel polarization—is limited to $\sigma_h/\lambda \lesssim 0.3$), they extended this formula to a "large slope emission model," using Ishimaru and Chen's [71] shadowing function and assuming secondary reflection fields to be isotropic.

3.7 EFFECTS OF SURFACE DAMAGE AND OXIDE FILMS

Even optically smooth surfaces have a surface structure that is different from the bulk material, due to either surface damage or the presence of thin layers of foreign materials. Surface damage is usually caused by the machining process, particularly for metals and semiconductors, which distorts or damages the crystal lattice near the surface. Thin foreign coats may be formed by chemical reaction (mostly oxidation), adsorption (e.g., coats of grease or water), or electrostatics (e.g., dust particles). All of these effects may have a severe impact on the radiation properties of metals, and may cause considerable changes in the properties of semiconductors. Other materials are usually less affected, because metals have large absorptive indices, k, and thus high reflectances. A thin, nonmetallic layer with small k can significantly decrease the composite's reflectance (and raise its emittance). Dielectric materials, on the other hand, have small k's and their relatively strong emission and absorption take place over a very thick surface layer. The addition of a thin, different dielectric layer cannot significantly alter their radiative properties.

A minimum amount of surface damage is introduced during sample preparation if *(i)* the technique of electropolishing is used [45], *(ii)* the surface is evaporated onto a substrate within an ultra-high vacuum environment [72], or *(iii)* the metal is evaporated onto a smooth sheet of transparent material and the reflectance is measured at the transparent medium–metal interface [73]. Figure 3-25 shows the spectral, normal emittance of aluminum for a surface prepared by the ultra-high vacuum method [72], and for several other aluminum surface finishes [74]. While ultra-high vacuum aluminum follows the Drude theory for $\lambda > 1\,\mu$m (cf. Fig. 3-7), polished aluminum (clean and optically smooth for large wavelengths) has a much higher emittance over the entire spectrum. Still, the overall level of emittance remains very low, and the reflectance remains rather specular. Similar results have been obtained by Bennett [45], who compared electropolished and mechanically polished copper samples. As Fig. 3-25 shows, the emittance is much larger still when off-the-shelf commercial aluminum is tested, probably due to a combination of roughness, contamination, and slight atmospheric oxidation. Bennett and colleagues [75] have shown that deposition of a thin oxide layer on aluminum (up to 100 Å) appreciably increases the emittance only for wavelengths less than $1.5\,\mu$m. This statement clearly is not true for thick oxide layers, as evidenced by Fig. 3-25: Anodized aluminum (i.e., electrolytically oxidized material with a thick layer of alumina, Al_2O_3) no longer displays the typical trends of a metal, but rather shows the behavior of the dielectric alumina. The effects of thin and thick oxide layers have been measured for many metals, with similar results. A good collection of such measurements has been given by Wood and coworkers [3]. As a rule of thumb, clean metal exposed to air at room temperature grows oxide films so thin that infrared

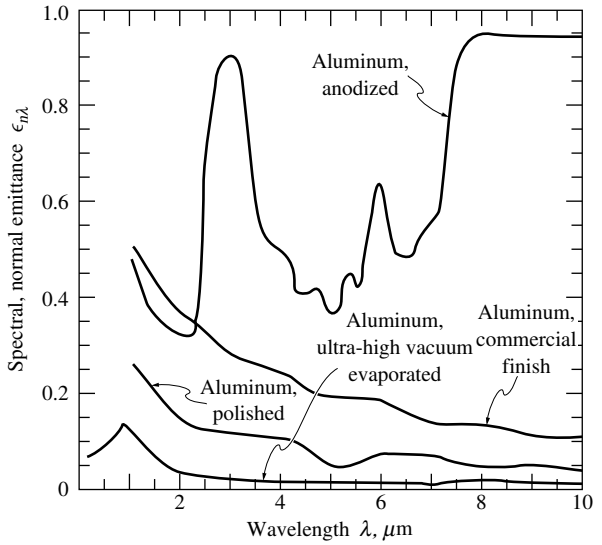

FIGURE 3-25
Spectral, normal emittance for aluminum with different surface finishes [72, 74].

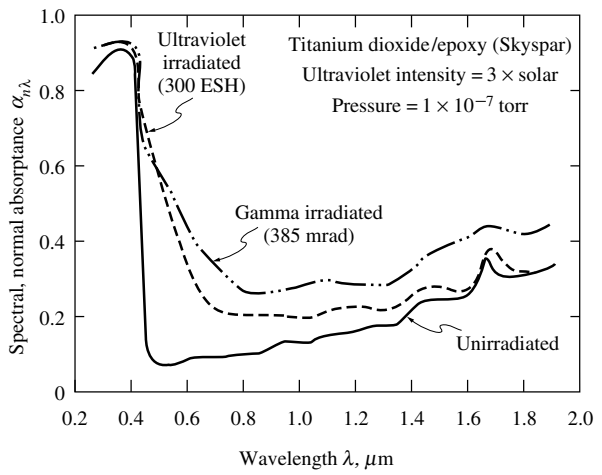

FIGURE 3-26
Effects of ultraviolet and gamma ray irradiation on a titanium dioxide/epoxy coating [78].

emittances are not affected appreciably. On the other hand, metal surfaces exposed to high-temperature oxidizing environments (furnaces, etc.) generally have radiative properties similar to those of their oxide layer.

While most severe for metallic surfaces the problem of surface modification is not unknown for nonmetals. For example, it is well known that silicon carbide (SiC), when exposed to air at high temperature, forms a silica (SiO_2) layer on its surface, resulting in a reflection band around 9 μm [76]. Nonoxidizing chemical reactions can also significantly change the radiative properties of dielectrics. For example, the strong ultraviolet radiation in outer space (from the sun) as well as gamma rays (from inside the Earth's van Allen belt) can damage the surface of spacecraft protective coatings like white acrylic paint [77] or titanium dioxide/epoxy coating [78], as shown in Fig. 3-26.

In summary, radiative properties for opaque surfaces, when obtained from figures in this chapter, from the tables given in Appendix B, or from other tabulations and figures of [1–8,79,80], should be taken with a grain of salt. Unless detailed descriptions of surface purity, preparation, treatment, etc., are available, the data may not give any more than an order-of-magnitude estimate. One should also keep in mind that the properties of a surface may change during a process or overnight (by oxidation and/or contamination).

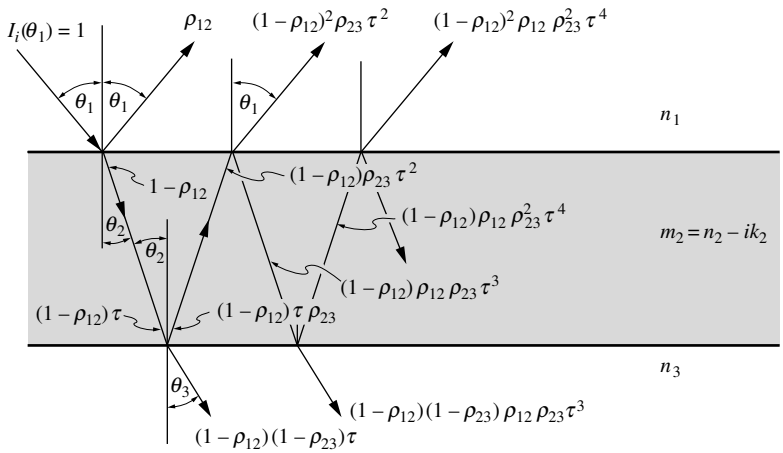

FIGURE 3-27
Reflectivity and transmissivity of a thick semitransparent sheet.

3.8 RADIATIVE PROPERTIES OF SEMITRANSPARENT SHEETS

The properties of radiatively participating media will be discussed in Chapters 11 through 13; i.e., semitransparent media that absorb and emit in depth and whose temperature distribution is, thus, strongly affected by thermal radiation. There are, however, important applications where thermal radiation enters an enclosure through semitransparent sheets, and where the temperature distribution within the sheet is unimportant or not significantly affected by thermal radiation. Applications include solar collector cover plates, windows in connection with light level calculations within interior spaces, and so forth. We shall, therefore, briefly present here the radiative properties of window glass, for single and multiple pane windows with and without surface coatings. Glass and other amorphous solids tend to have extremely smooth surfaces, allowing for accurate predictions of interface reflectivities from electromagnetic wave theory.

Properties of Single Pane Glasses

For an optically smooth window pane of a thickness d substantially larger than the wavelength of incident light, $d \gg \lambda$, the radiative properties are readily determined through *geometric optics* and *ray tracing*. Consider the sheet of semitransparent material depicted in Fig. 3-27. The sheet has a complex index of refraction $m_2 = n_2 - ik_2$ with $k_2 \ll 1$, so that the transmission through the sheet (not counting surface reflections),

$$\tau = e^{-\kappa_2 d/\cos\theta_2} = e^{-4\pi k_2 d/\lambda_0 \cos\theta_2}, \tag{3.88}$$

is appreciable [cf. equation (2.42)]. Here $\kappa_2 = 4\pi k_2/\lambda_0$ is the absorption coefficient, λ_0 is the wavelength of the incident light in vacuum, and $d/\cos\theta_2$ is the distance a light beam of oblique incidence travels through Medium 2 in a single pass. The semitransparent sheet is surrounded by two dielectric materials with refractive indices n_1 and n_3. To calculate the reflectivity at the interfaces 1–2 and 2–3 it is sufficient to use Fresnel's relations for dielectric media, since $k_2 \ll 1$. Interchanging n_1 and n_2, as well as θ_1 and θ_2, in equation (2.96) shows that the reflectivity at the 1–2 interface is the same, regardless of whether radiation is incident from Medium 1 or Medium 2, i.e., $\rho_{12} = \rho_{21}$ and $\rho_{23} = \rho_{32}$. Now consider radiation of unit strength to be incident upon the sheet from Medium 1 in the direction of θ_1. As indicated in Fig. 3-27 the fraction ρ_{12} is reflected at the first interface, while the fraction $(1 - \rho_{12})$ is refracted into Medium 2, according to Snell's law. After traveling a distance $d/\cos\theta_2$ through Medium 2 the attenuated fraction

$(1-\rho_{12})\tau$ arrives at the 2–3 interface. Here the amount $(1-\rho_{12})\tau\rho_{23}$ is reflected back to the 1–2 interface, while the fraction $(1-\rho_{12})\tau(1-\rho_{23})$ leaves the sheet and penetrates into Medium 3 in a direction of θ_3. The internally reflected fraction keeps bouncing back and forth between the interfaces, as indicated in the figure, until all energy is depleted by reflection back into Medium 1, by absorption within Medium 2, and by transmission into Medium 3. Therefore, the *slab reflectivity*, R_{slab}, may be calculated by summing over all contributions, or

$$R_{\text{slab}} = \rho_{12} + \rho_{23}(1-\rho_{12})^2\tau^2\left[1 + \rho_{12}\rho_{23}\tau^2 + (\rho_{12}\rho_{23}\tau^2)^2 + \cdots\right].$$

Since $\rho_{12}\rho_{23}\tau^2 < 1$ the series is readily evaluated [81], and

$$R_{\text{slab}} = \rho_{12} + \frac{\rho_{23}(1-\rho_{12})^2\tau^2}{1-\rho_{12}\rho_{23}\tau^2} = \frac{\rho_{12} + (1-2\rho_{12})\rho_{23}\tau^2}{1-\rho_{12}\rho_{23}\tau^2}. \tag{3.89}$$

Similarly, the *slab transmissivity*, T_{slab}, follows as

$$\begin{aligned} T_{\text{slab}} &= (1-\rho_{12})(1-\rho_{23})\tau\left[1 + \rho_{12}\rho_{23}\tau^2 + (\rho_{12}\rho_{23}\tau^2)^2 + \cdots\right] \\ &= \frac{(1-\rho_{12})(1-\rho_{23})\tau}{1-\rho_{12}\rho_{23}\tau^2}. \end{aligned} \tag{3.90}$$

These relations are the same as the ones evaluated for thick sheets by the electromagnetic wave theory, equations (2.129) and (2.130). From conservation of energy $A_{\text{slab}} + R_{\text{slab}} + T_{\text{slab}} = 1$, and the *slab absorptivity* follows as

$$A_{\text{slab}} = \frac{(1-\rho_{12})(1+\rho_{23}\tau)(1-\tau)}{1-\rho_{12}\rho_{23}\tau^2}. \tag{3.91}$$

If Media 1 and 3 are identical (say, air), then $\rho_{12} = \rho_{23} = \rho$ and equations (3.89) through (3.91) reduce to

$$R_{\text{slab}} = \rho\left[1 + \frac{(1-\rho)^2\tau^2}{1-\rho^2\tau^2}\right], \tag{3.92}$$

$$T_{\text{slab}} = \frac{(1-\rho)^2\tau}{1-\rho^2\tau^2}, \tag{3.93}$$

$$A_{\text{slab}} = \frac{(1-\rho)(1-\tau)}{1-\rho\tau}. \tag{3.94}$$

Figure 3-28 shows typical slab transmissivities and reflectivities of several different types of glasses for normal incidence and for a pane thickness of 12.7 mm. Most glasses have fairly constant and low slab reflectivity in the spectral range from 0.1 μm up to about 9 μm (relatively constant refractive index n, small absorptive index k). Beyond 9 μm the reflectivity increases because of two Reststrahlen bands [82] (not shown). Glass transmissivity tends to be very high between 0.4 μm and 2.5 μm. Beyond 2.5 μm the transmissivity of window glass diminishes rapidly, making windows opaque to infrared radiation. This gives rise to the so-called "greenhouse" effect: Since the sun behaves much like a blackbody at 5777 K, most of its energy ($\approx 95\%$) falling onto Earth lies in the spectral range of high glass transmissivities. Therefore, solar energy falling onto a window passes readily into the space behind it. The spectral variation of solar irradiation, for extraterrestrial and unity air mass conditions, was given in Fig. 1-3. On the other hand, if the space behind the window is at low to moderate temperatures (300 to 400 K), emission from such surfaces is at fairly long wavelengths, which is absorbed by the glass and, thus, cannot escape.

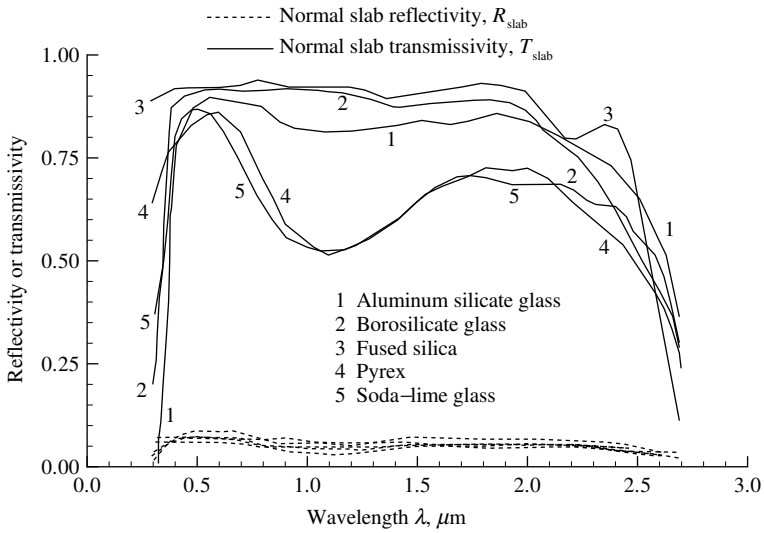

FIGURE 3-28
Spectral, normal slab transmissivity and reflectivity for panes of five different types of glasses at room temperature; data from [7].

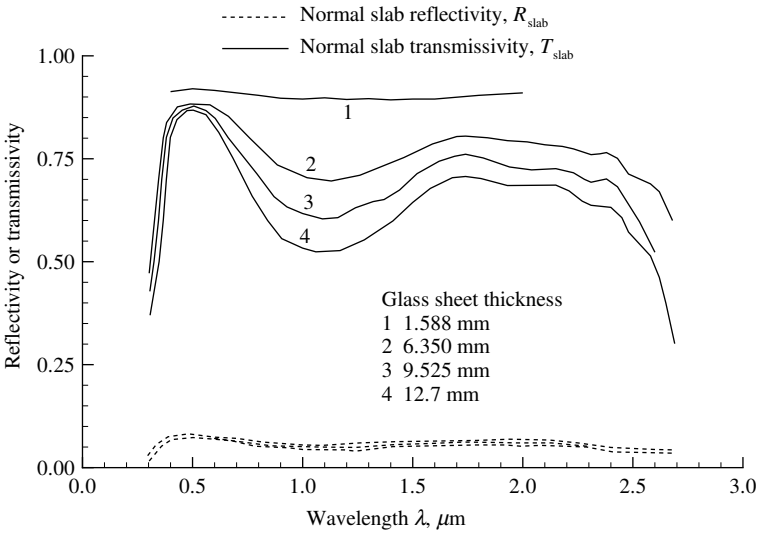

FIGURE 3-29
Spectral, normal slab transmissivity and reflectivity of soda–lime glass at room temperature, for a number of pane thicknesses; data from [7].

The influence of pane thickness on reflectivity and transmissivity is shown in Fig. 3-29 for the case of soda–lime glass (i.e., ordinary window glass). As the pane thickness increases, transmissivity decreases due to the increasing absorption. Since the absorption coefficient is small for $\lambda < 2.7\,\mu$m (see Fig. 1-17), the effect is rather minor (and even less so for the other glasses shown in Fig. 3-28).

In some high-temperature applications the emission from hot glass surfaces becomes important (e.g., in the manufacture of glass). Gardon [83] has calculated the spectral, hemispherical and total, hemispherical emissivity of soda–lime glass sheets at 1000°C based on the data of Neuroth [84]. Spectral emissivities beyond 2.7 μm do not depend strongly on temperature since the absorption coefficient is relatively temperature-independent (see Fig. 1-17). For all but the thinnest glass sheets the material becomes totally opaque, and the hemispherical emissivity is

evaluated as $\epsilon_\lambda = 1 - \rho_\lambda \simeq 0.91$.[7]

Coatings

Glass sheets and other transparent solids often have coatings on them for a variety of reasons: to eliminate transmission of ultraviolet radiation, to decrease or increase transmission over certain spectral regions, and the like. We distinguish between thick coatings ($d \gg \lambda$, no interference effects) and thin film coatings ($d = \mathcal{O}(\lambda)$, with wave interference, as discussed in Chapter 2). The effects of a thick dielectric layer (with refractive index n_2, and absorptive index $k_2 \simeq 0$) on the reflectivity of a thick sheet of glass (n_3 and $k_3 \simeq 0$) is readily analyzed with the two-interface formula given by equation (3.89). With $\tau \simeq 1$ and, for normal incidence,

$$\rho_{12} = \left(\frac{n_1 - n_2}{n_1 + n_2}\right)^2 \quad \text{and} \quad \rho_{23} = \left(\frac{n_2 - n_3}{n_2 + n_3}\right)^2,$$

the coating reflectivity becomes

$$\begin{aligned} R_{\text{coat}} &= \frac{\rho_{12} + \rho_{23} - 2\rho_{12}\rho_{23}}{1 - \rho_{12}\rho_{23}} = 1 - \frac{(1 - \rho_{12})(1 - \rho_{23})}{1 - \rho_{12}\rho_{23}} \\ &= 1 - \frac{(4n_1n_2)(4n_2n_3)}{(n_1 + n_2)^2(n_2 + n_3)^2 - (n_1 - n_2)^2(n_2 - n_3)^2}, \end{aligned}$$

which is readily simplified to

$$R_{\text{coat}} = 1 - \frac{4n_1n_2n_3}{(n_2^2 + n_1n_3)(n_1 + n_3)}. \tag{3.95}$$

If the aim is to minimize the overall reflectivity of the semitransparent sheet, then a value for the refractive index of the coating must be chosen to make R_{coat} a minimum. Thus, setting $dR_{\text{coat}}/dn_2 = 0$ leads to

$$n_{2,\min} = \sqrt{n_1 n_3}. \tag{3.96}$$

Substituting equation (3.96) into (3.95) results in a minimum coated-surface reflectivity of

$$R_{\text{coat,min}} = 1 - \frac{2\sqrt{n_1 n_3}}{n_1 + n_3}. \tag{3.97}$$

The slab reflectivity for a thin dielectric coating on a dielectric substrate, $d = \mathcal{O}(\lambda)$, is subject to wave interference effects and has been evaluated in Chapter 2, from equation (2.124), with $\delta_{12} = \pi$ and $\delta_{23} = 0$ (cf. Example 2.6), as

$$R_{\text{coat}} = \frac{r_{12}^2 + 2r_{12}r_{23}\cos\zeta + r_{23}^2}{1 + 2r_{12}r_{23}\cos\zeta + r_{12}^2r_{23}^2}, \tag{3.98a}$$

$$r_{12} = \frac{n_1 - n_2}{n_1 + n_2}, \quad r_{23} = \frac{n_2 - n_3}{n_2 + n_3}, \quad \zeta = \frac{4\pi n_2 d}{\lambda}. \tag{3.98b}$$

Equation (3.98) has an interference minimum when $\zeta = \pi$ (i.e., if the film thickness is a quarter of the wavelength inside the film, $d = 0.25\lambda/n_2$). For this interference minimum the reflectivity of the coated surface becomes

$$R_{\text{coat}} = \left(\frac{r_{12} - r_{23}}{1 - r_{12}r_{23}}\right)^2. \tag{3.99}$$

[7] The *hemispherical* emissivity is evaluated by first evaluating $\rho_{n\lambda}$: With $n \simeq 1.5$ (for $\lambda > 2.7\,\mu$m), from Fig. 3-16 $\rho_{n\lambda} = 0.04$ and $\epsilon_{n\lambda} = 0.96$; finally, from Fig. 3-19 $\epsilon_\lambda \simeq 0.91$.

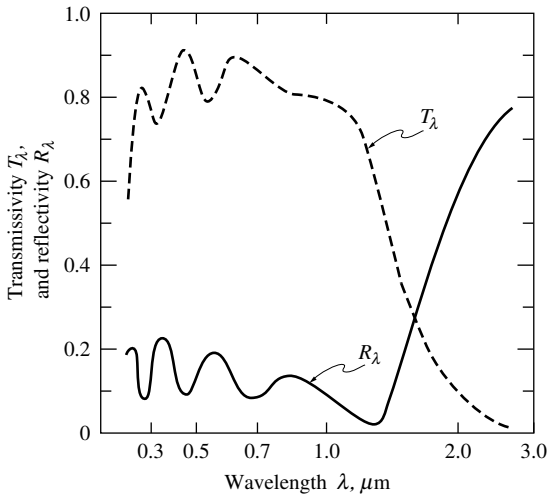

FIGURE 3-30
Spectral, normal reflectivity and transmissivity of a 0.35 μm thick Sn-doped In_2O_3 film deposited on Corning 7059 glass [86].

Clearly, this equation results in a minimum (or zero) reflectivity if $r_{12} = r_{23}$, or $n_{2,\min} = \sqrt{n_1 n_3}$, which is the same as for thick films, equation (3.96). To obtain minimum reflectivities for glass ($n_3 \simeq 1.5$) facing air ($n_1 \simeq 1$) would require a dielectric film with $n_2 \simeq 1.22$. Dielectric films of such low refractive index do not appear possible. However, Yoldas and Partlow [85] showed that a porous film (pore size $\ll \lambda$) can effectively lower the refractive index, and they obtained glass transmissivities greater than 99% throughout the visible.

In other applications a strong reflectivity is desired. An example of experimentally determined reflectivity and transmissivity of a coated dielectric is given in Fig. 3-30 for a 0.35 μm thick layer of Sn-doped In_2O_3 film on glass [86]. The oscillating properties clearly demonstrate the effects of wave interference at shorter wavelengths. At wavelengths $\lambda > 1.5\,\mu$m the material has a strong absorption band, making it highly reflective and opaque. Thus, this coated glass makes a better solar collector cover plate than ordinary glass, since internally emitted infrared radiation is *reflected back* into the collector (rather than being absorbed), keeping the cover glass cool and reducing losses. Similar behavior was obtained by Yoldas and O'Keefe [87], who deposited thin (20 to 50 nm) triple-layer films (titanium dioxide–silver–titanium dioxide) on soda–lime glass. It is also possible to tailor the directional reflection behavior using special, obliquely deposited films [88].

Multiple Parallel Sheets

To minimize convection losses, two or more parallel sheets of windows are often employed, as illustrated in Fig. 3-31*a*. To find the total reflectivity and transmissivity of n layers, we break the system up into a single layer and the remaining $(n-1)$ layers. Then ray tracing (see Fig. 3-31*b*) results in

$$R_n = R_1 + T_1^2 R_{n-1}\left[1 + R_1 R_{n-1} + (R_1 R_{n-1})^2 + \cdots\right] = R_1 + \frac{T_1^2 R_{n-1}}{1 - R_1 R_{n-1}}, \tag{3.100}$$

and, similarly,

$$T_n = \frac{T_1 T_{n-1}}{1 - R_1 R_{n-1}}, \tag{3.101}$$

where R_{n-1} and T_{n-1} are the net reflectivity and transmissivity of $(n-1)$ layers. The net absorptivity of the n layers can be calculated directly either from

$$\begin{aligned} A_n &= A_1 + A_1 T_1 R_{n-1}(1 + R_1 R_{n-1} + \cdots) + A_{n-1} T_1 (1 + R_1 R_{n-1} + \cdots) \\ &= A_1 + \frac{T_1(A_1 R_{n-1} + A_{n-1})}{1 - R_1 R_{n-1}}, \end{aligned} \tag{3.102}$$

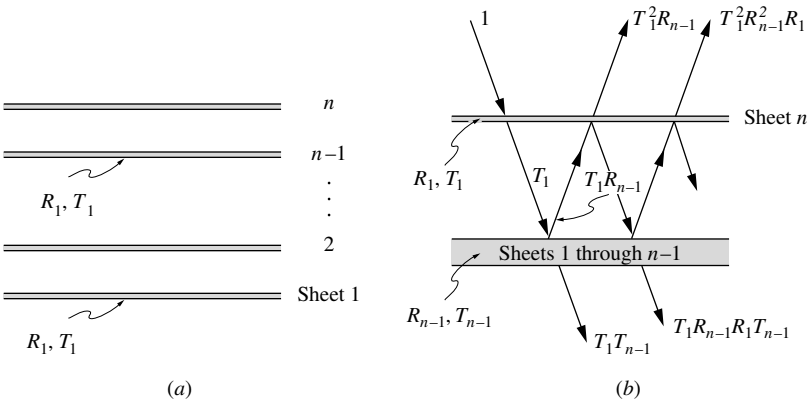

FIGURE 3-31
Reflectivity and transmissivity of multiple sheets: *(a)* geometric arrangement, *(b)* ray tracing for interaction between a single layer and the remainder of the sheets.

or from conservation of energy, i.e., $A_n + R_n + T_n = 1$. In the development of equation (3.100) we have assumed that R_1 is the same for light shining onto the top or the bottom of the sheet ($\rho_{12} = \rho_{23}$), in other words, that equation (3.92) is valid. The above recursion formulae were first derived by Edwards [89] without the restriction of $\rho_{12} = \rho_{23}$. In a later paper Edwards [90] expanded the method to include wave interference effects for stacked thin films. Multiple sheets subject to mixed diffuse and collimated irradiation, but without interference effects, were analyzed by Mitts and Smith [91].

Example 3.6. Determine the normal transmissivity of a triple-glazed window for visible wavelengths. The window panes are thin sheets of soda–lime glass, separated by layers of air.

Solution
The reflectivity R_1 and transmissivity T_1 of a single sheet are readily calculated from equations (3.92) and (3.93). For thin sheets (e.g., curve 1 in Fig. 3-29) we have $\tau \simeq 1$, and with $n \simeq 1.5$ (cf. Fig. 3-16), $\rho = [(1.5 - 1)/(1.5 + 1)]^2 = 0.04$. Therefore,

$$R_1 = \rho\left[1 + \frac{(1-\rho)^2}{1-\rho^2}\right] = \frac{2\rho}{1+\rho} = \frac{2 \times 0.04}{1 + 0.04} = 0.0769,$$

$$T_1 = \frac{(1-\rho)^2}{1-\rho^2} = \frac{1-\rho}{1+\rho} = 1 - R_1 = 0.9231$$

(and $A_1 = 0$, since we assumed $\tau \simeq 1$). For two panes, from equations (3.100) and (3.101) with $n = 2$,

$$R_2 = R_1 + \frac{T_1^2 R_1}{1 - R_1^2} = 0.0769\left(1 + \frac{0.9231^2}{1 - 0.0769^2}\right) = 0.1429,$$

$$T_2 = \frac{T_1^2}{1 - R_1^2} = 0.8571$$

(and, again $A_2 = 0$). Finally, for three panes

$$R_3 = R_1 + \frac{T_1^2 R_2}{1 - R_1 R_2} = 0.0769 + \frac{0.9231^2 \times 0.1429}{1 - 0.0769 \times 0.1429} = 0.2000,$$

$$T_3 = \frac{T_1 T_2}{1 - R_1 R_2} = \frac{0.9231 \times 0.8571}{1 - 0.0769 \times 0.1429} = 0.8000.$$

Assuming negligible absorption within the glass, 80% of visible radiation is transmitted through the triple-pane window (at normal incidence), while 20% is reflected back.

Although they are valid, equations (3.89) and (3.90) are quite cumbersome for oblique incidence, in particular, if absorption cannot be neglected. Some calculations for nonabsorbing

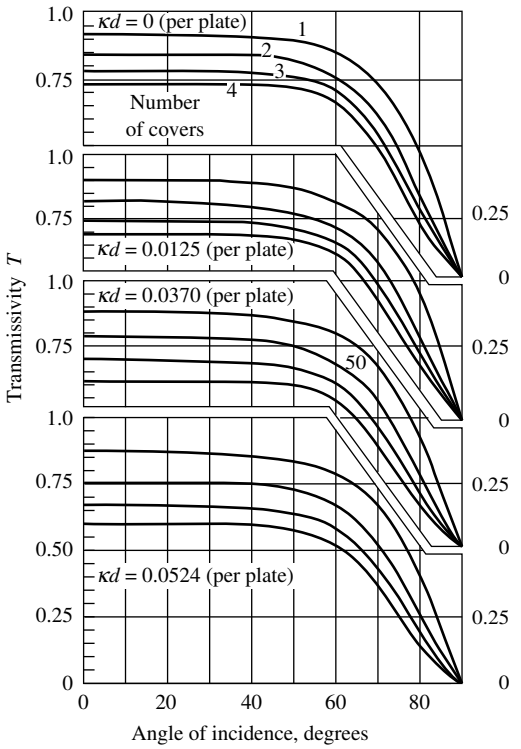

FIGURE 3-32
Transmissivities of 1, 2, 3, and 4 sheets of glass (n = 1.526) for different optical thicknesses per sheet, κd [93].

(for n = 1.5 [92] and for n = 1.526 [93]) and absorbing [93] (n = 1.526) multiple sheets of window glass have been carried out. Note that, for oblique incidence, the overall reflectivity and transmissivity are different for parallel- and perpendicular-polarized light. Even for unpolarized light the polarized components must be determined before averaging, as

$$R_n = \frac{1}{2}(R_{n\perp} + R_{n\parallel}), \quad T_n = \frac{1}{2}(T_{n\perp} + T_{n\parallel}). \tag{3.103}$$

The results of the calculations by Duffie and Beckman [93] are given in graphical form in Fig. 3-32.

3.9 SPECIAL SURFACES

For many engineering applications it would be desirable to have a surface material available with very specific radiative property characteristics. For example, the net radiative heat gain of a solar collector is the difference between absorbed solar energy and radiation losses due to emission by the collector surface. While a black absorber plate would absorb all solar irradiation, it unfortunately would also lose a maximum amount of energy due to surface emission. An ideal solar collector surface has a maximum emittance for those wavelengths and directions over which solar energy falls onto the surface, and a minimum emittance for all other wavelengths and directions. On the other hand, a radiative heat rejector, such as the ones used by the U.S. Space Shuttle to reject excess heat into outer space, should have a high emittance at longer wavelengths, and a high reflectance for those wavelengths and directions with which sunshine falls onto the heat rejector.

To a certain degree the radiative properties of a surface can be tailored toward desired characteristics. Surfaces that absorb and emit strongly over one wavelength range, and reflect strongly over the rest of the spectrum are called *spectrally selective*, while surfaces with tailored directional properties are known as *directionally selective.*

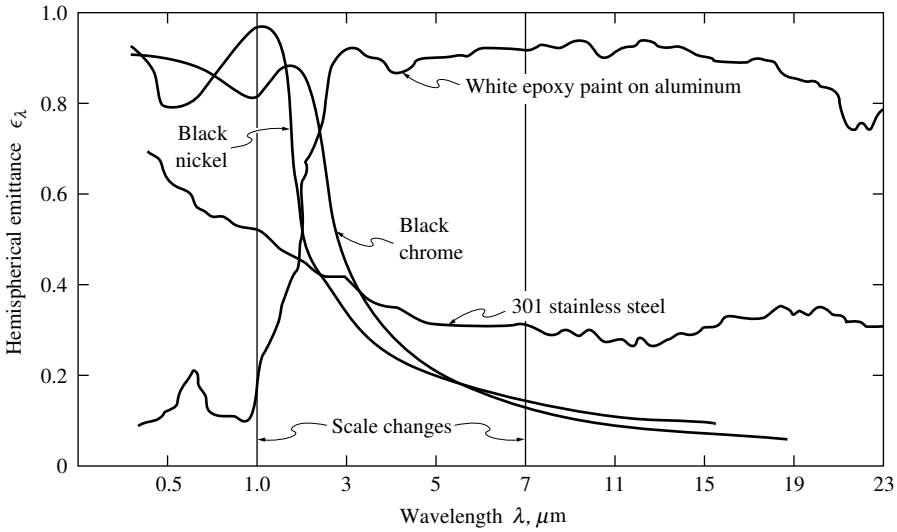

FIGURE 3-33
Spectral, hemispherical reflectances of several spectrally selective surfaces [99].

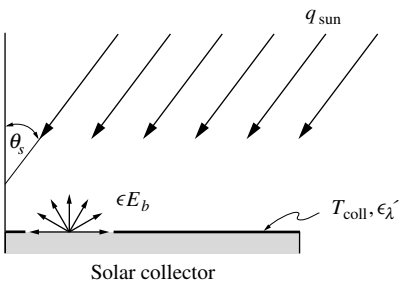

FIGURE 3-34
Solar irradiation on and emission from a solar collector plate.

An ideal, spectrally selective surface would be black ($\alpha_\lambda = \epsilon_\lambda = 1$) over the wavelength range over which maximum absorption (or emission) is *desired*, and would be totally reflective ($\alpha_\lambda = \epsilon_\lambda = 0$) beyond a certain *cutoff wavelength* λ_c, where *undesirable* emission (or absorption) would occur. Of course, in practice such behavior can only be approximated. Such an ideal surface is indicated by the long-dash line in Fig. 3-33.

The performance of a selective surface is usually measured by the "α/ϵ-ratio," where α is the total, directional absorptance of the material for solar irradiation, while ϵ is the total, hemispherical emittance for infrared surface emission. Consider a solar collector plate (Fig. 3-34), irradiated by the sun at an off-normal angle of θ_s. Making an energy balance (per unit area of the collector), we find

$$q_{\text{net}} = \epsilon\sigma T_{\text{coll}}^4 - \alpha q_{\text{sun}} \cos\theta_s, \tag{3.104}$$

where the factor $\cos\theta_s$ appears since q_{sun} is solar heat flux per unit area *normal to the sun's rays.* The total, hemispherical emittance may be related to spectral, hemispherical values through equation (3.10), while the total, directional absorptance is found from equation (3.23). Thus

$$\epsilon = \frac{1}{\sigma T_{\text{coll}}^4} \int_0^\infty \epsilon_\lambda(T_{\text{coll}}, \lambda)\, E_{b\lambda}(T_{\text{coll}}, \lambda)\, d\lambda, \tag{3.105a}$$

$$\alpha = \frac{1}{q_{\text{sun}}} \int_0^\infty \alpha_\lambda(T_{\text{coll}}, \lambda, \theta_s)\, q_{\text{sun},\lambda}\, d\lambda = \frac{1}{\sigma T_{\text{sun}}^4} \int_0^\infty \alpha_\lambda(T_{\text{coll}}, \lambda, \theta_s)\, E_{b\lambda}(T_{\text{sun}}, \lambda)\, d\lambda, \tag{3.105b}$$

where we have made use of the fact that the spectral distribution of q_{sun} is the same as the blackbody emission from the sun's surface. Clearly, for optimum performance of a collector the solar absorptance should be maximum, while the infrared emittance should be minimum. Therefore, a large α/ϵ-ratio indicates a better performance for a solar collector. On the other hand, for radiative heat rejectors a minimum value for α/ϵ is desirable.

Most selective absorbers are manufactured by coating a thin nonmetallic film onto a metal. Over most wavelengths the nonmetallic film is very transmissive and incoming radiation passes straight through to the metal interface with its very high reflectance. However, many nonconductors have spectral regions over which they do absorb appreciably without being strongly reflective (usually due to lattice defects or contaminants). The result is a material that acts like a strongly reflecting metal over most of the spectrum, but like a strongly absorbing nonconductor for selected wavelength ranges. A few examples of such selective surfaces are also given in Fig. 3-33. Black chrome (chrome-oxide coating) and black nickel (nickel-oxide coating) are popular solar collector materials, while epoxy paint may be used as an efficient solar energy rejector. If the coatings are extremely thin, interference effects can also be exploited to improve selectivity. For example, Martin and Bell [94] showed that a three-layer coating of SiO_2–Al–SiO_2 on metallic substrates has a solar absorptance greater than 90%, but an infrared emittance of < 10%. Fan and Bachner [86] produced a coating for glass that raised its reflectance to > 80% for infrared wavelengths, without appreciably affecting solar transmittance (Fig. 3-30).

The advantages of spectrally selective surface properties were first recognized by Hottel and Woertz [95]. With the growing interest in solar energy collection during the 1950s and 1960s, a number of selective coatings were developed, and the subject was discussed by Gier and Dunkle [96], and Tabor and coworkers [97,98]. There are several compilations for radiative properties of selective absorbers [3,8,99]. A somewhat more detailed discussion about spectrally selective surface properties has been given by Duffie and Beckman [93].

Example 3.7. Let us assume that it is possible to manufacture a diffusely absorbing/emitting selective absorber with a spectral emittance $\epsilon_\lambda = \epsilon_s = 0.05$ for $0 < \lambda < \lambda_c$ and $\epsilon_\lambda = \epsilon_c = 0.95$ for $\lambda > \lambda_c$, where the cutoff wavelength can be varied through manufacturing methods. Determine the optimum cutoff wavelength for a solar collector with an absorber plate at 350 K that is exposed to solar irradiation of $q_{\text{sun}} = 1000\,\text{W/m}^2$ at an angle of $\theta_s = 30°$ off-normal. What is the net radiative energy gain for such a collector?

Solution

A simple energy balance on the surface, using equations (3.9) and (3.41) leads to

$$q_{\text{net}} = E - H'_{\text{abs}}(\theta_s) = \epsilon E_b - \alpha'(\theta_s) H'(\theta_s)$$

where $q_{\text{net}} > 0$ if a net amount of energy leaves the surface, and $q_{\text{net}} < 0$ if energy is collected. Total, hemispherical emittance follows from equation (3.10) while total, directional absorptance is determined from equation (3.23). For our diffuse absorber we have $\alpha'_\lambda(\lambda,\theta) = \epsilon_\lambda(\lambda)$ and

$$\epsilon = \frac{1}{\sigma T_{\text{coll}}^4}\left[\epsilon_s \int_0^{\lambda_c} E_{b\lambda}(T_{\text{coll}},\lambda)\,d\lambda + \epsilon_c \int_{\lambda_c}^{\infty} E_{b\lambda}(T_{\text{coll}},\lambda)\,d\lambda\right] = \epsilon_s + \frac{(\epsilon_c - \epsilon_s)}{\sigma T_{\text{coll}}^4}\int_{\lambda_c}^{\infty} E_{b\lambda}(T_{\text{coll}},\lambda)\,d\lambda,$$

$$\alpha = \frac{1}{\sigma T_{\text{sun}}^4}\left[\epsilon_s \int_0^{\lambda_c} E_{b\lambda}(T_{\text{sun}},\lambda)\,d\lambda + \epsilon_c \int_{\lambda_c}^{\infty} E_{b\lambda}(T_{\text{sun}},\lambda)\,d\lambda\right] = \epsilon_s + \frac{(\epsilon_c - \epsilon_s)}{\sigma T_{\text{sun}}^4}\int_{\lambda_c}^{\infty} E_{b\lambda}(T_{\text{sun}},\lambda)\,d\lambda.$$

Substituting these expressions into our energy balance leads to

$$q_{\text{net}} = \epsilon_s(\sigma T_{\text{coll}}^4 - q_{\text{sun}}\cos\theta_s) + (\epsilon_c - \epsilon_s)\int_{\lambda_c}^{\infty}\left[E_{b\lambda}(T_{\text{coll}},\lambda) - \frac{q_{\text{sun}}\cos\theta_s}{\sigma T_{\text{sun}}^4}E_{b\lambda}(T_{\text{sun}},\lambda)\right]d\lambda.$$

Optimizing the value of λ_c implies finding a maximum for q_{net}. Therefore, from *Leibniz's rule* (see, e.g., [81]), which states that

$$\frac{d}{dx}\int_{a(x)}^{b(x)} f(x,y)\,dy = \frac{db}{dx}f(x,b) - \frac{da}{dx}f(x,a) + \int_a^b \frac{df}{dx}(x,y)\,dy, \tag{3.106}$$

we find

$$\frac{dq_{\text{net}}}{d\lambda_c} = -(\epsilon_c - \epsilon_s)\left[E_{b\lambda}(T_{\text{coll}}, \lambda_c) - \frac{q_{\text{sun}} \cos\theta_s}{\sigma T_{\text{sun}}^4} E_{b\lambda}(T_{\text{sun}}, \lambda_c)\right] = 0,$$

or

$$E_{b\lambda}(T_{\text{coll}}, \lambda_c) = \frac{q_{\text{sun}} \cos\theta_s}{\sigma T_{\text{sun}}^4} E_{b\lambda}(T_{\text{sun}}, \lambda_c).$$

Note that the cutoff wavelength does not depend on the values for ϵ_c and ϵ_s. Using Planck's law, equation (1.13), with $n = 1$ (surroundings are air), the last expression reduces to

$$\exp(C_2/\lambda_c T_{\text{coll}}) - 1 = \frac{\sigma T_{\text{sun}}^4}{q_{\text{sun}} \cos\theta_s} \left[\exp(C_2/\lambda_c T_{\text{sun}}) - 1\right].$$

This transcendental equation needs to be solved by iteration. As a first guess one may employ Wien's distribution, equation (1.18) (dropping two '−1' terms),

$$\exp(C_2/\lambda_c T_{\text{coll}}) \simeq \frac{\sigma T_{\text{sun}}^4}{q_{\text{sun}} \cos\theta_s} \exp(C_2/\lambda_c T_{\text{sun}})$$

or

$$\exp\left[\frac{C_2}{\lambda_c}\left(\frac{1}{T_{\text{coll}}} - \frac{1}{T_{\text{sun}}}\right)\right] \simeq \frac{\sigma T_{\text{sun}}^4}{q_{\text{sun}} \cos\theta_s},$$

$$\begin{aligned}
\lambda_c &\simeq C_2\left(\frac{1}{T_{\text{coll}}} - \frac{1}{T_{\text{sun}}}\right) \Big/ \ln \frac{\sigma T_{\text{sun}}^4}{q_{\text{sun}} \cos\theta_s} \\
&= 14{,}388\left(\frac{1}{350} - \frac{1}{5777}\right) \mu\text{m} \Big/ \ln \frac{5.670 \times 10^{-8} \times 5777^4}{1000 \times \cos 30^\circ} = 3.45\,\mu\text{m}.
\end{aligned}$$

Iterating the full Planck's law leads to a cutoff wavelength of $\lambda_c = 3.69\,\mu$m. Substituting these values into the expressions for emittance and absorptance,

$$\begin{aligned}
\epsilon &= \epsilon_s + (\epsilon_c - \epsilon_s)\left[1 - f(\lambda_c T_{\text{coll}})\right] = 0.95 - 0.90 + 0.90 f(3.69 \times 350) \\
&= 0.05 + 0.90 \times 0.00413 = 0.054,
\end{aligned}$$

$$\begin{aligned}
\alpha &= \epsilon_s + (\epsilon_c - \epsilon_s)\left[1 - f(\lambda_c T_{\text{sun}})\right] = 0.05 + 0.90 \times f(3.69 \times 5777) \\
&= 0.05 + 0.90 \times 0.98785 = 0.939.
\end{aligned}$$

The net heat flux follows then as

$$q_{\text{net}} = 0.054 \times 5.760 \times 10^{-8} \times 350^4 - 0.939 \times 1000 \times \cos 30^\circ = -767\,\text{W/m}^2.$$

Actually, neither $f(\lambda_c T_{\text{coll}}) \simeq 0$ nor $f(\lambda_c T_{\text{sun}}) \simeq 1$ is particularly sensitive to the exact value of λ_c, because there is very little spectral overlap between solar radiation (95% of which is in the wavelength range[8] of $\lambda < 2.2\,\mu$m) and blackbody emission at 350 K (95% of which is at $\lambda > 5.4\,\mu$m).

Surfaces can be made directionally selective by mechanically altering the surface finish on a microscale (microgrooves) or macroscale. For example, large V-grooves (large compared with the wavelengths of radiation) tend to reflect incoming radiation several times for near-normal incidence, as indicated in Fig. 3-35 (from Trombe and coworkers [101]) for an opening angle of $\gamma = 30^\circ$, each time absorbing a fraction of the beam. The number of reflections decreases with increasing incidence angle, down to a single reflection for incidence angles $\theta > 90^\circ - \gamma$ (or 60° in the case of Fig. 3-35). Hollands [102] has shown that this type of surface has a significantly higher normal emittance, which is important for collection of solar irradiation, than hemispherical emittance, which governs emission losses. A similarly shaped material, with flat black bottoms, was theoretically analyzed by Perlmutter and Howell [103]. Their analytical values for directional emittance were experimentally confirmed by Brandenberg and Clausen [27], as illustrated in Fig. 3-36.

[8] Based on a blackbody at 5777 K. This number remains essentially unchanged for true, extraterrestrial solar irradiation [100], while the 95% fraction moves to even shorter wavelengths if atmospheric absorption is taken into account (cf. Fig. 1-3).

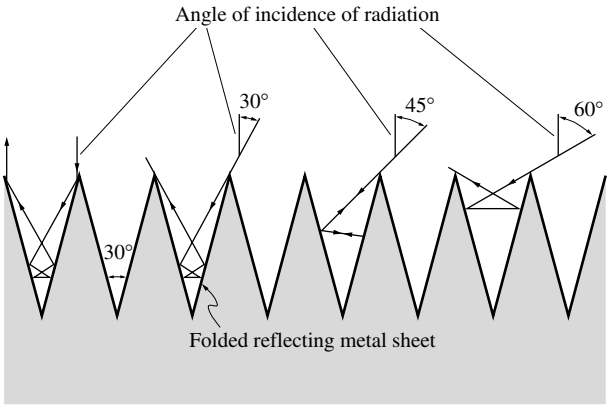

FIGURE 3-35
Directional absorption and reflection of irradiation by a V-grooved surface [101].

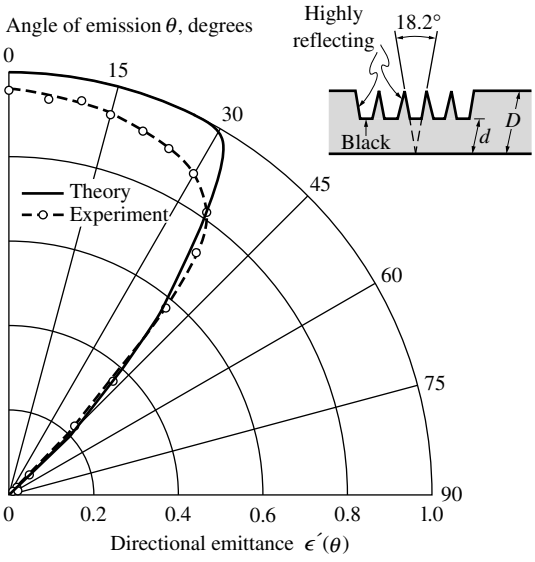

FIGURE 3-36
Directional emittance of a grooved surface with highly reflective, specular sidewalls and near-black base. Results are for plane perpendicular to groove length. Theory ($\rho_{\text{sides}} = \epsilon_{\text{base}} = 1$) from [103], experiment [taken at $\lambda = 8\,\mu$m with aluminum sidewalls and black paint base with $\epsilon_\lambda(8\,\mu\text{m}) = 0.95$] from [27].

3.10 EXPERIMENTAL METHODS

It is quite apparent from the discussion in the preceding sections that, although electromagnetic wave theory can be used to *augment* experimental data, it cannot replace them. While the spectral, bidirectional reflection function, equation (3.34), is the most basic radiation property of an opaque surface, to which all other properties can be related, it is rarely measured. Obtaining the bidirectional reflection function is difficult because of the low achievable signal strength. It is also impractical since it is a function of both incoming and outgoing directions and of wavelength and temperature. A complete description of the surface requires enormous amounts of data. In addition, the use of the bidirectional reflection function complicates the analysis to such a point that it is rarely attempted.

If bidirectional data are not required it is sufficient, for an opaque material, to measure one of the following, from which all other ones may be inferred: absorptance, emittance, directional–hemispherical reflectance, and hemispherical–directional reflectance. Various different measurement techniques have been developed, which may be separated into three loosely-defined groups: *calorimetric emission measurements*, *radiometric emission measurements*, and *reflection measurements*. The interest in experimental methods was at its peak during the 1960s as a result of the advent of the space age. Compilations covering the literature of that period have been

given in two NASA publications [104, 105]. Interest waned during the 1970s and 1980s but has recently picked up again because of the development of better and newer materials operating at higher temperatures. Sacadura [106] has given an updated review of experimental methods.

While measurement techniques vary widely from method to method, most of them employ similar optical components, such as light sources, monochromators, and detectors. Therefore, we shall begin our discussion of experimental methods with a short description of important optical components.

Instrumentation

Radiative property measurements generally require a light source, a monochromator, a detector, and the components of the optical path, such as mirrors, lenses, beam splitters, optical windows, and so on. Depending on the nature of the experiment and/or detector, other accessories, such as optical choppers, may also be necessary.

LIGHT SOURCES. Light sources are required for the measurement of absorption by, or reflection from, an opaque surface, as well as for the alignment of optical components in any spectroscopic system. In addition, light sources are needed for transmission and scattering measurements of absorbing/scattering media, such as gases, particles, and semitransparent solids, and liquids (to be discussed in later chapters). We distinguish between monochromatic and polychromatic light sources.

Monochromatic sources. These types of sources operate through *stimulated emission*, producing light over an extremely narrow wavelength range. Their monochromaticity, low beam divergence, coherence, and high power concentration make *lasers* particularly attractive as light sources. While only invented some 30 years ago, there are today literally dozens of solid-state and gas lasers covering the spectrum between the ultraviolet and the far infrared. Although lasers are generally monochromatic, there are a number of gas lasers that can be tuned over a part of the spectrum by stimulating different transitions. For example, *dye lasers* (using large organic dye molecules as the lasing medium) may be operated at a large number of wavelengths in the range $0.2\,\mu\text{m} < \lambda < 1\,\mu\text{m}$, while the common CO_2 laser (usually operating at $10.6\,\mu\text{m}$) may be equipped with a movable grating, allowing it to lase at a large number of wavelengths in the range $9\,\mu\text{m} < \lambda < 11\,\mu\text{m}$. Even solid-state lasers can be operated at several wavelengths through frequency-doubling. For example, the Nd-YAG laser, the most common solid-state laser, can be used at $1.064\,\mu\text{m}$, $0.532\,\mu\text{m}$, $0.355\,\mu\text{m}$, and $0.266\,\mu\text{m}$. Of particular importance for radiative property measurements is the helium–neon laser because of its low price and small size and because it operates in the visible at $0.633\,\mu\text{m}$ (making it useful for optical alignment).

A different kind of monochromatic source is the *low-pressure gas discharge lamp*, in which a low-density electric current passes through a low-pressure gas. Gas atoms and molecules become ionized and conduct the current. Electrons bound to the gas atoms become excited to higher energy levels, from which they fall again, emitting radiation over a number of narrow spectral lines whose wavelengths are characteristic of the gas used, such as zinc, mercury, and so on.

Polychromatic sources. These usually incandescent light sources emit radiation by *spontaneous emission* due to the thermal excitation of source atoms and molecules, resulting in a continuous spectrum. The spectral distribution and total radiated power depend on the temperature, area, and emittance of the surface. Incandescent sources may be of the filament type (similar to an ordinary light bulb) or of the bare-element type. The *quartz–tungsten–halogen* lamp has a doped tungsten filament inside a quartz envelope, which is filled with a rare gas and a small amount of a halogen. Operating at a filament temperature greater than 3000 K, this lamp produces a near-blackbody spectrum with maximum emission below $1\,\mu\text{m}$. However, because of the transmission characteristics of quartz (which is the same as fused silica, Fig. 3-28), there is no appreciable emission beyond $3\,\mu\text{m}$. Bare-element sources are either rods

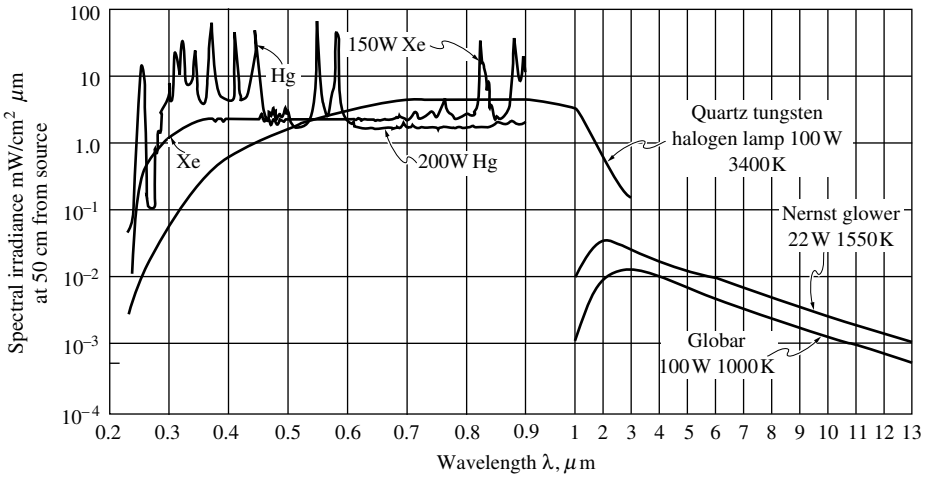

FIGURE 3-37
Spectral irradiation on a distant surface from various incandescent light sources.

of silicon carbide, called *globars*, or heating wires embedded in refractory oxides, called *Nernst glowers*. Globars operate at a temperature of 1000 K and produce an almost-gray spectrum with a maximum around 2.9 μm. Nernst glowers operate at temperatures up to 1500 K, with a somewhat less ideal spectral distribution. The irradiation onto a distant surface from different incandescent sources is shown in Fig. 3-37. None of the light sources shown in Fig. 3-37 has a truly "black" spectral distribution, since their output is influenced by their spectral emittance. In most experiments this is of little importance since, in general, sample and reference signals (coming from the same spectral source) are compared. If a true blackbody source is required (primarily for calibration of instruments) *blackbody cavity sources* are available from a number of manufacturers. In these sources a cylindrical and/or conical cavity, made of a high-temperature, high-emittance material (such as silicon carbide) is heated to a desired temperature. Radiation leaving the cavity, also commonly called *Hohlraum* (German for "hollow space"), is essentially black (cf. Table 5.1).

The brightest conventional source of optical radiation is the *high-pressure gas discharge lamp*, which combines the characteristics of spontaneous and stimulated emission. The lamp is similar to a low-pressure gas discharge source, but with high current density and gas pressure. This configuration results in an arc with highly excited atoms and molecules forming a plasma. While the hot plasma emits as an incandescent source, ionized atoms emit over substantially broadened spectral lines, resulting in a mixed spectrum (Fig. 3-37). Commonly used gases for such arc sources are xenon, mercury, and deuterium.

SPECTRAL SEPARATORS. Spectral radiative properties can be measured over part of the spectrum in one of two ways: *(i)* Measurements are made using a variety of monochromatic light sources, which adequately represent the desired part of the spectrum, or *(ii)* a polychromatic source is used together with a device that allows light of only a few select wavelengths to reach the detector. Such devices may consist of simple *optical filters,* manually driven or motorized *monochromators,* or highly sophisticated *FTIR* (Fourier Transform InfraRed) spectrometers.

Optical filters. These are multilayer thin-film devices that selectively transmit radiation only over desired ranges of wavelengths. *Bandpass filters* transmit light only over a finite, usually narrow, wavelength region, while *edge filters* transmit only above or below certain *cutoff* or *edge wavelengths*. Bandpass filters consist of a series of thin dielectric films that, at each interface, partially reflect and partially transmit radiation (cf. Fig. 2-13). The spacing between layers is such that beams of the desired wavelength are, after multiple reflections within the layers, in phase with the transmitted beam (constructive interference). Other wavelengths are rejected

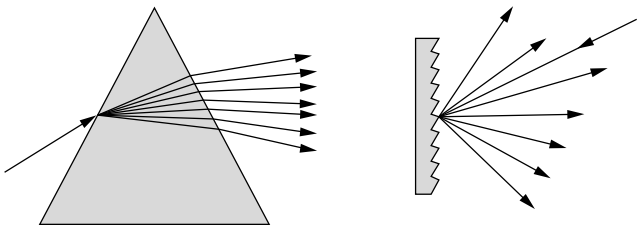

FIGURE 3-38
Schematic of spectral separation with *(a)* a transparent prism, *(b)* a diffraction grating.

because they destructively interfere with one another. Bandpass filters for any conceivable wavelength between the ultraviolet and the midinfrared are routinely manufactured. Edge filters operate on the same principle, but are more complex in design.

Monochromators. These devices separate an incoming polychromatic beam into its spectral components. They generally consist of an entrance slit, a prism or grating that spreads the incoming light according to its wavelengths, and an exit slit, which allows only light of desired wavelengths to escape. If a prism is used, it is made of a highly-transparent material with a refractive index that varies slightly across the spectrum (cf. Fig. 3-16). As shown in Fig. 3-38*a*, the incoming radiant energy is separated into its constituent wavelengths since, by Snell's law, the prism bends different wavelengths (with different refractive index) by different amounts. Rotating the prism around an axis allows different wavelengths to escape through the exit slit. Instead of a prism one can use a *diffraction grating* to separate the wavelengths of incoming light, employing the principle of constructive and destructive interference [107], as schematically indicated in Fig. 3-38*b*. Until a few years ago all monochromators employed salt prisms, while today almost all systems employ diffraction gratings, since they are considerably cheaper and simpler to handle (salt prisms tend to be hygroscopic, i.e., they are attacked by the water vapor in the surrounding air). However, diffraction gratings have the disadvantages that their spectral range is more limited (necessitating devices with multiple gratings), and they may give erroneous readings due to higher-order signals (frequency-doubling).

FTIR spectrometers. These instruments collect the entire radiant energy (i.e., comprising all FTIR spectrometer wavelengths) after reflection from a moving mirror. The measured intensity depends on the position of the moving mirror owing to constructive and destructive interference. This signal is converted by a computer through an inverse *Fast Fourier Transform* into a power *vs.* wavelength plot. The spectral range of FTIRs is limited only by the choice of beam splitters and detectors, and is comparable to that of prism monochromators. However, while monochromators generally require several minutes to collect data over their entire spectral range, the FTIR is able to do this in a fraction of a second. Detailed descriptions of the operation of FTIRs may be found in books on the subject, such as the one by Griffiths and de Haseth [108].

DETECTORS. In a typical spectroscopic experiment the detector measures the intensity of incoming radiation due to transmission through, emission from, or reflection by, a sample. This irradiation may be relatively monochromatic (i.e., covers a very narrow wavelength range after having passed through a filter or monochromator), or may be polychromatic (for total emittance measurements, or if an FTIR is used). In either case, the detector converts the beam's power into an electrical signal, which is amplified and recorded. The performance of detectors is measured by certain criteria, which are generally functions of several operating conditions, such as wavelength, temperature, modulating frequency, bias voltage, and gain of any internal amplifier. The *response time* (τ) is the time for a detector's output to reach $1 - 1/e = 63\%$ of its final value, after suddenly being subjected to constant irradiation. The *linearity range* of a detector is the range of input power over which the output signal is a linear function of the input. The *noise equivalent power (NEP)* is the radiant energy rate in watts that is necessary to give an output signal equal to the *rms* noise output from the detector. More widely used is the

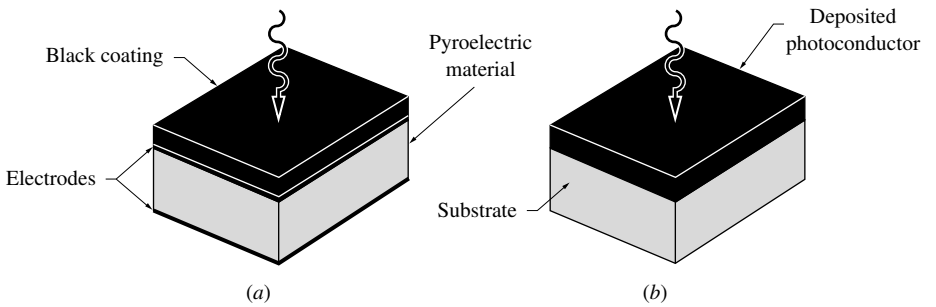

FIGURE 3-39
Schematic of *(a)* a pyroelectric detector, *(b)* a photoconductive detector.

reciprocal of *NEP*, the *detectivity (D)*. The detectivity is known to vary inversely with the square root of the detector area, A_D, while the signal noise is proportional to the square root of the amplifier's noise-equivalent bandwidth Δf (in Hz). Thus, a *normalized detectivity (D*)* is defined to allow comparison between different types of detectors regardless of their detector areas and amplifier bandwidths as

$$D^* = (A_D\,\Delta f)^{1/2}\,D. \tag{3.107}$$

Depending on how the incoming radiation interacts with the detector material, detectors are grouped into *thermal* and *photon* (or *quantum*) *detectors*.

Thermal detectors. These devices convert incident radiation into a temperature rise. This temperature change is measured either through one or more thermocouples, or by using the pyroelectric effect. A single, usually blackened (to increase absorptance) *thermocouple* is the simplest and cheapest of all thermal detectors. However, it suffers from high amplifier noise and, therefore, limited detectivity. One way to increase output voltage and detectivity is to connect a number of thermocouples in series (typically 20 to 120), constituting a *thermopile*. Thermopiles can be manufactured economically through thin-film processes. *Pyroelectric detectors* are made of crystalline materials that have permanent electric polarization. When heated by irradiation, the material expands and changes its polarization, which causes a current to flow in a circuit that connects the detector's top and bottom surfaces, as shown in the schematic of Fig. 3-39*a*. Since the change in temperature produces the current, pyroelectric detectors respond only to pulsed or chopped irradiation. They respond to changes in irradiation much more rapidly than thermocouples and thermopiles, and are not affected by steady background radiation.

Photon detectors. These absorb the energy of incident radiation with their electrons, producing free charge carriers (*photoconductive* and *photovoltaic detectors*) or even ejecting electrons from the material (*photoemissive detectors*). In photoconductive and photovoltaic detectors the production of free electrons increases the electrical conductivity of the material. In the photoconductive mode an applied voltage, or *reverse bias*, causes a current that is proportional to the strength of irradiation to flow, as schematically shown in Fig. 3-39*b*. In the photovoltaic mode no bias is applied and, closing the electric circuit, a current flows as a result of the excitation of electrons (as in the operation of photovoltaic, or solar, cells). Photovoltaic detectors have greater detectivity, while photoconductive detectors exhibit extremely fast response times. For optimum performance each mode requires slightly different design, although a single device may be operated in either mode. Typical semiconductor materials used for photovoltaic and photoconductive detectors are silicon (Si), germanium (Ge), indium antimonide (InSb), mercury cadmium telluride (HgCdTe),[9] lead sulfide and selenide (PbS and PbSe), and cadmium sulfide (CdS). While most semiconductor detectors have a single detector element, many of them today

[9] *M*ercury–*C*admium–*T*elluride detectors are also commonly referred to as *MCT* detectors.

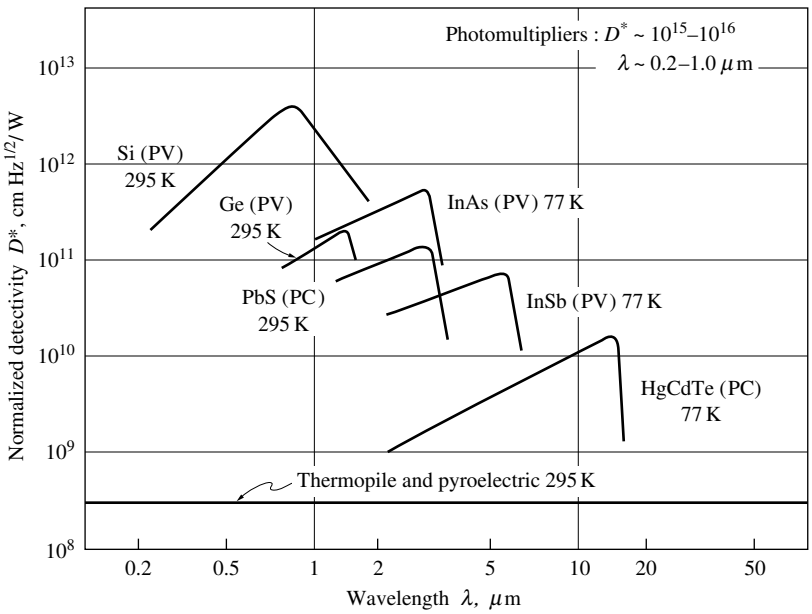

FIGURE 3-40
Typical spectral ranges and normalized detectivities for various detectors.

are also available as linear arrays and surface arrays (up to 512 × 512 elements), which—when combined with a monochromator—allows for ultra-fast data acquisition at many wavelengths.

The most basic photoemissive device is a *photodiode*, in which high-energy photons (ultraviolet to near infrared) cause emission of electrons from photocathode surfaces placed in a vacuum. Applying a voltage causes a current that is proportional to the intensity of incident radiation to flow. The signal of a vacuum photodiode is amplified in a *photomultiplier* by fitting it with a series of anodes (called *dynodes*), which produce secondary emission electrons and a current. The latter is an order-of-magnitude higher than the original photocurrent.

Thermal detectors generally respond evenly across the entire spectrum, while photon detectors have limited spectral response but higher detectivity and faster response times. The normalized detectivity of several detectors is compared in Fig. 3-40. The spectral response of photon detectors can be tailored to a degree by varying the relative amounts of detector material components. The response time of thermal detectors is relatively slow, normally in the order of milliseconds, while the response time of photon detectors ranges from microseconds to a few nanoseconds. The detectivity is often increased by cooling the detector thermoelectrically (to −30°C), with dry ice (195 K), or by attaching it to a liquid-nitrogen Dewar flask (77 K).

OTHER COMPONENTS. In a spectroscopic experiment light from a source and/or sample is guided toward the detector by a number of mirrors and lenses. *Plane mirrors* are employed to bend the beam path while *curved mirrors* are used to focus an otherwise diverging beam onto a sample, the monochromator entrance slit, or the detector. Today's optical mirrors provide extremely high reflectivities (> 99.5%) over the entire spectrum of interest. While focusing mirrors are generally preferable for a number of reasons, sometimes *lenses* need to be used for focusing. The most important drawbacks of lenses are that they tend to have relatively large reflection losses and their spectral range (with high transmissivity) is limited. While antireflection coatings can be applied, these coatings are generally only effective over narrow spectral ranges as a result of interference effects. Common lens materials for the infrared are zinc selenide (ZnSe), calcium fluoride (CaF_2), germanium (Ge), and others. Sometimes it is necessary to split a beam into two portions (e.g., to create a reference beam that does not pass over the sample) using a *beam splitter*. Beam splitters are made of the same material as lenses,

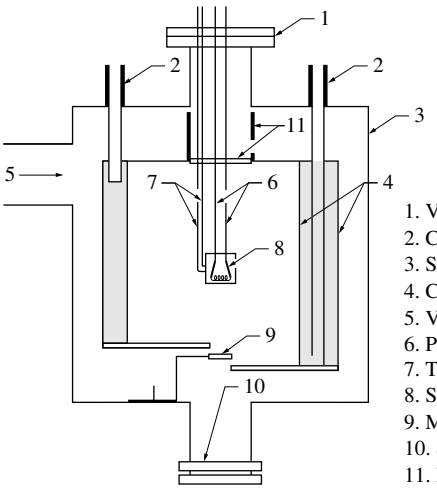

1. Vacuum feed-through flange
2. Coolant fill and vent tubes
3. Stainless steel vacuum jacket
4. Copper chamber walls
5. Vacuum inlet
6. Power leads
7. Thermocouple leads
8. Sample and heating element
9. Magnet-operated shutter
10. Sample viewing port
11. Radiation shields

FIGURE 3-41
Typical setup for calorimetric emission measurements [110].

exploiting their reflecting *and* transmitting tendencies. It is also common to chop the beam using a *mechanical chopper*, which consists of a rotating blade with one or more holes or slits. Chopping may be done for a variety of reasons, such as to provide an alternating signal for a pyroelectric detector, to separate background radiation from desired radiation, to decrease electronic noise by using a lock-in amplifier tuned into the chopper frequency, and so on.

Calorimetric Emission Measurement Methods

If only knowledge of the total, hemispherical emittance of a surface is required, this is most commonly determined by measuring the net radiative heat loss or gain of an isolated specimen [109–125]. Figure 3-41 shows a typical experimental setup, which was used by Funai [110]. The specimen is suspended inside an evacuated test chamber, the walls of which are coated with a near-black material. The chamber walls are cooled, while the specimen is heated electrically, directly (metallic samples), through a metal substrate (nonconducting samples), or by some other means. Temperatures of the specimen and chamber wall are monitored by thermocouples. The emittance of the sample can be determined from steady-state [109–117] or transient measurements [111, 118–125].

In the steady-state method the sample is heated to, and kept at, a desired temperature by passing the appropriate current through the heating element. The total, hemispherical emittance may then be calculated by equating electric heat input to the specimen with the radiative heat loss from the specimen to the surroundings, or

$$\epsilon(T) = \frac{I^2 R}{A_s \sigma (T_s^4 - T_w^4)}, \tag{3.108}$$

where I^2R is the dissipated electrical power, A_s is the exposed surface area of the specimen, and T_s and T_w are the temperatures of specimen and chamber walls, respectively. As will be discussed in Chapter 5, equation (3.108) assumes that the surface area of the chamber is much larger than A_s and/or that the emittance of the chamber wall is near unity [cf. equation (5.36)].

In the transient calorimetric technique the current is switched off when the desired temperature has been reached, and the rates of loss of internal energy and radiative heat loss are equated, or

$$\epsilon(T) = -\frac{m_s c_s \, dT_s/dt}{A_s \sigma (T_s^4 - T_w^4)}, \tag{3.109}$$

where m_s and c_s are mass and specific heat of the sample, respectively.

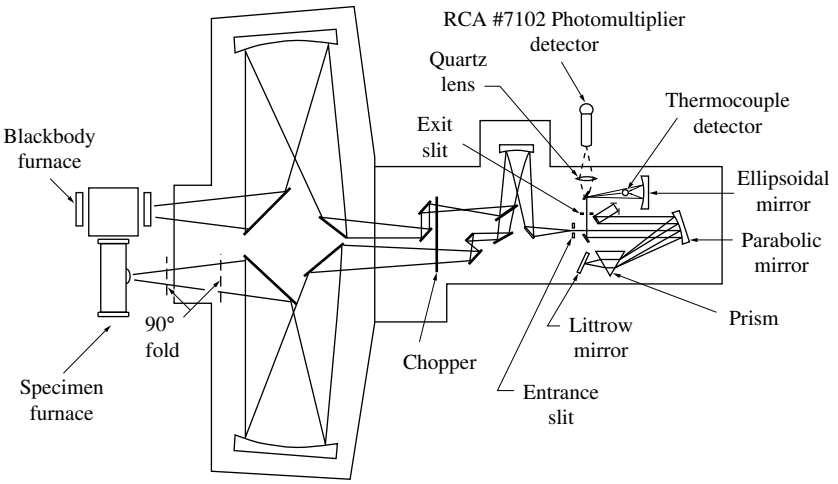

FIGURE 3-42
Emissometer with separate reference blackbody and two optical paths [126].

Radiometric Emission Measurement Methods

High-temperature, spectral, directional surface emittances are most often determined by comparing the emission from a sample with that from a blackbody at the same temperature and wavelength, both viewed by the same detector over an identical or equivalent optical path. Under those conditions the signal from both measurements will be proportional to emitted intensity (with the same proportionality constant), and the spectral, directional emittance is found by taking the ratio of the two signals, or

$$\epsilon'_\lambda(T,\lambda,\theta,\psi) = \frac{I_\lambda(T,\lambda,\theta,\psi)}{I_{b\lambda}(T,\lambda)}. \tag{3.110}$$

The comparison blackbody may be a separate blackbody kept at the same temperature, or it may be an integral part of the sample chamber. The latter is generally preferred at high temperatures, where temperature control is difficult, and for short wavelengths, where small deviations in temperatures can cause large inaccuracies.

Separate reference blackbody. In this method a blackbody, usually a long, cylindrical, isothermal cavity with an L/D-ratio larger than 4, is kept separate from the sample chamber, while both are heated to the same temperature. Radiation coming from this *Hohlraum* is essentially black (cf. Table 5.1). The control system keeps the sample and blackbody at the same temperature by monitoring temperature differences with a differential thermocouple and taking corrective action whenever necessary. To monitor sample and blackbody emission via an identical optical path, either two identical paths have to be constructed, or sample and blackbody must be alternately placed into the single optical path. In the former method, identical paths are formed either through two sets of optics [126], or by moving optical components back and forth [39]. Figure 3-42 shows an example of a system with two different optical paths [126], while Fig. 3-43 is an example of a linearly actuated blackbody/sample arrangement [127]. It is also possible to combine blackbody and sample, and the device is rotated or moved back-and-forth inside a single furnace [128]. Markham and coworkers [129] mounted sample/reference blackbody individually on a turntable, heated them with a torch, and measured the directional, spectral emittance of sandblasted aluminum (up to 750 K), alumina (1300 to 2200 K), fused quartz (900 K), and sapphire (1000 K) with an FTIR spectrometer. Other materials measured with the separate reference blackbody technique include the normal, spectral emittance of solid and liquid silicon just below and above the melting point [130], and of a collection of 30 metals and alloys at temperatures up to 1200°C [131, 132].

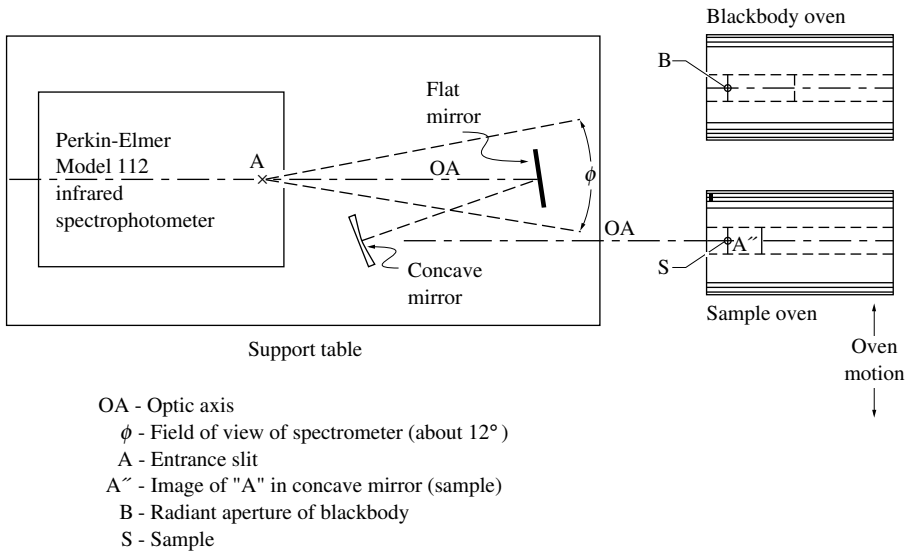

FIGURE 3-43
Emissometer with separate reference blackbody and linearly actuated sample/blackbody arrangement [127].

Integrated reference blackbody. At high temperatures it is preferable to incorporate the reference blackbody into the design of the sample furnace. If the sample rests at the bottom of a deep isothermal, cylindrical cavity, the radiation leaving the sample (by emission and reflection) corresponds to that of a black surface. If the hot side wall is removed or replaced by a cold one, radiation leaving the sample is due to emission only. Taking the ratio of the two signals then allows the determination of the spectral, directional emittance from equation (3.110). Removing the reflection component from the signal may be achieved in one of two ways. Several researchers have used a tubular furnace with the sample mounted on a movable rod [133–135]. When the sample is deep inside the furnace the signal corresponds to a blackbody. The sample is then rapidly moved to the exit of the furnace and the signal is due to emission alone. Disadvantages of the method are *(i)* maintaining isothermal conditions up to close to the end of the tube, *(ii)* keeping the sample at the same temperature after displacement, and *(iii)* stress on the high-temperature sample due to the rapid movement. In the approach of Vader and coworkers [136] and Postlethwait *et al.* [137], reflection from the sample is suppressed by freely dropping a cold tube into the blackbody cavity. A schematic of the apparatus of Postlethwait *et al.* is shown in Fig. 3-44. Once the cold tube has been dropped, measurements must be taken rapidly (in a few seconds' time), before substantial heating of the drop tube (and cooling of the sample). Vader and coworkers obtained spectral measurements by placing various filters in front of their detector, performing a number of drops for each sample temperature. Postlethwait employed an FTIR spectrometer, allowing them to measure the entire spectral range from 1 μm to 9 μm in a single drop. In a method more akin to the separate blackbody technique, Havstad and colleagues [128] incorporated a small blackbody cavity into a tungsten crucible (holding liquid metal samples). The entire assembly is then moved to have the optics focus on sample or blackbody, respectively.

Reflection Measurements

Reflection measurements are carried out to determine the bidirectional reflection function, the directional–hemispherical reflectance, and the hemispherical–directional reflectance. The latter two provide indirect means to determine the directional absorptance and emittance of opaque specimens, in particular, if sample temperatures are too low for emission measurements.

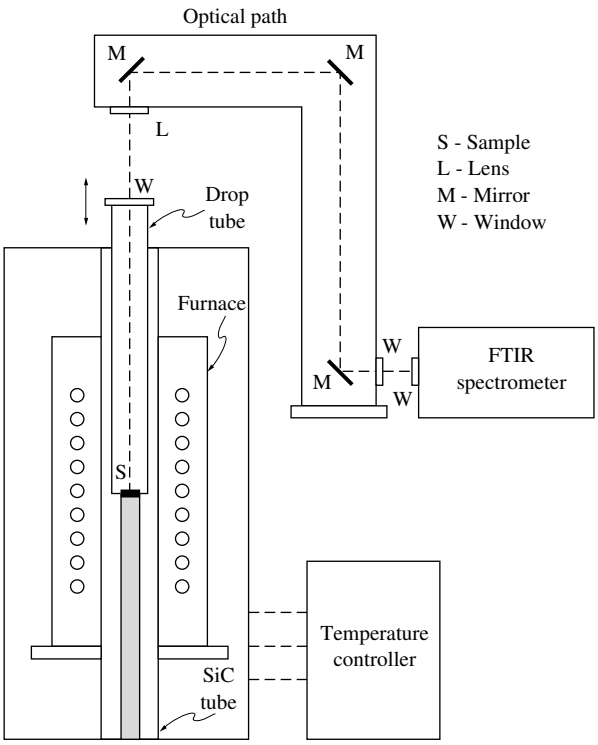

FIGURE 3-44
Schematic of a drop-tube emissometer [137].

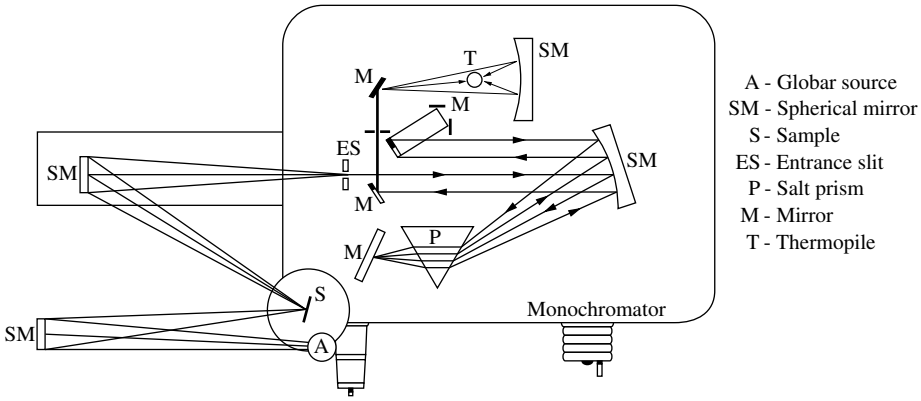

FIGURE 3-45
Schematic of the bidirectional reflection measurement apparatus of Birkebak and Eckert [138].

BIDIRECTIONAL REFLECTION MEASUREMENTS. If the bidirectional reflection behavior of a surface is of interest, the bidirectional reflection function, ρ''_λ, must be measured directly, by irradiating the sample with a collimated beam from one direction and collecting the reflected intensity over various small solid angles. A sketch of an early apparatus used by Birkebak and Eckert [138] and Torrance and Sparrow [139] is shown in Fig. 3-45. Radiation from a globar *A* travels through a diaphragm to a spherical mirror *SM*, which focuses it onto the test sample *S*. A pencil of radiation reflected from the sample into the desired direction is collected by another spherical mirror and focused onto the entrance slit of the monochromator, in which the wavelengths are separated by the rock salt prism *P*, and the signal is recorded by the thermopile *T*. The test sample is mounted on a multiple-yoke apparatus, which allows independent rotation around three perpendicular axes. The resulting measurements are relative (i.e., abso-

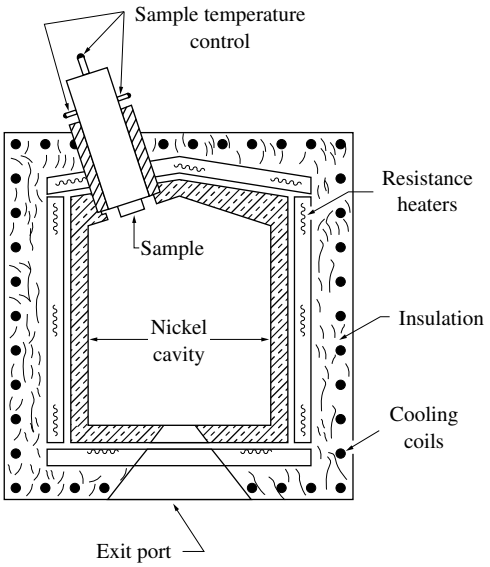

FIGURE 3-46
Schematic of a heated cavity reflectometer [146].

lute values can only be obtained by calibrating the apparatus with a known standard in place of the test sample). Example measurements for magnesium oxide are shown in Fig. 3-5 [12]. More recently built devices use sophisticated, multiple-degree-of-freedom sample mounts as well as FTIR spectrometers, such as the one of Ford and coworkers [140], who measured the bidirectional reflectances of diffuse gold and grooved nickel.

The main problem with bidirectional reflection measurements is the low level of reflected radiation that must be detected (particularly in off-specular directions), even with the advent of FTIR spectrometers and highly sensitive detectors. Consequently, a number of designs have employed strong monochromatic laser sources to overcome this problem, for example, [141–145].

An overview of the different methods to determine directional–hemispherical and hemispherical–directional reflectances has been given by Touloukian and DeWitt [6]. The different types of experiments may be grouped into three categories, *heated cavity reflectometers, integrating sphere reflectometers,* and *integrating mirror reflectometers,* each having their own ranges of applicability, advantages, and shortcomings.

HEATED CAVITY REFLECTOMETERS. The *heated cavity reflectometer* [6, 146–148] (sometimes known as the *Gier–Dunkle reflectometer* after its inventors [148]) consists of a uniformly heated enclosure fitted with a water-cooled sample holder and a viewport, as schematically shown in Fig. 3-46. Since the sample is situated within a more or less closed isothermal enclosure, the intensity striking it from any direction is essentially equal to the blackbody intensity $I_{b\lambda}(T_w)$ (evaluated at the cavity-wall temperature, T_w). Images of the sample and a spot on the cavity wall are alternately focused onto the entrance slit of a monochromator. The signal from the specimen corresponds to emission (at the sample's temperature, T_s) plus reflection of the cavity-wall's blackbody intensity, $I_{b\lambda}(T_w)$. Since the signal from the cavity wall is proportional to $I_{b\lambda}(T_w)$, the ratio of the two signals corresponds to

$$\frac{I_s}{I_w} = \frac{\rho'^{\frown}_{\lambda}(\hat{\mathbf{s}})\, I_{b\lambda}(T_w) + \epsilon'_{\lambda}(\hat{\mathbf{s}})\, I_{b\lambda}(T_s)}{I_{b\lambda}(T_w)}. \tag{3.111}$$

If the sample is relatively cold ($T_s \ll T_w$), emission may be neglected and the device simply measures the hemispherical–directional reflectance. For higher specimen temperatures, and for

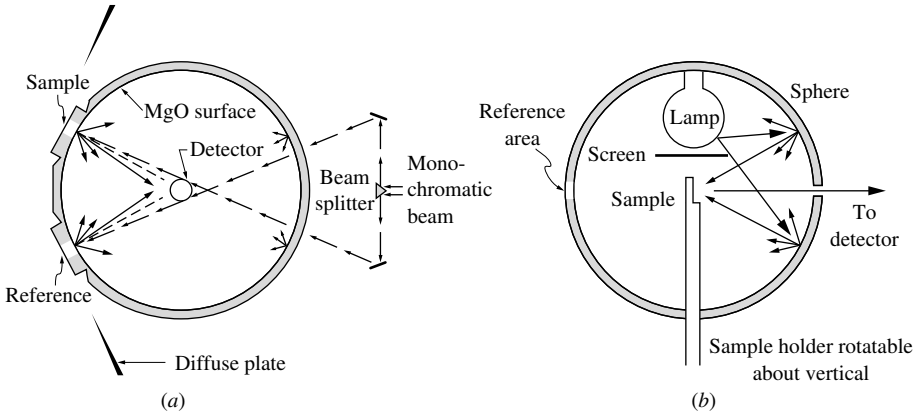

FIGURE 3-47
Typical integrating sphere reflectometers: *(a)* direct mode, *(b)* indirect mode.

an opaque surface with diffuse irradiation, from equations (3.42), (3.39) and (3.44),

$$\rho'^{\frown}_{\lambda}(\hat{\mathbf{s}}) \;=\; \rho'^{\frown}_{\lambda}(\hat{\mathbf{s}}) = 1 - \alpha'_{\lambda}(\hat{\mathbf{s}}) = 1 - \epsilon'_{\lambda}(\hat{\mathbf{s}}), \tag{3.112}$$

and

$$\frac{I_s}{I_w} \;=\; 1 - \epsilon'_{\lambda}(\hat{\mathbf{s}})\left[1 - \frac{I_{b\lambda}(T_s)}{I_{b\lambda}(T_w)}\right]. \tag{3.113}$$

The principal source of error in this method is the difficulty in making the entire cavity reasonably isothermal and (as a consequence) making the reference signal proportional to a blackbody at the cavity-wall temperature. To make these errors less severe the method is generally only used for low sample temperatures.

INTEGRATING SPHERE REFLECTOMETERS. These devices are most commonly employed for reflectance measurements [147,149–159] and are available commercially in a variety of forms, either as separate instruments or already incorporated into spectrophotometers. A good early discussion of different designs was given by Edwards and coworkers [154]. The integrating sphere may be used to measure hemispherical–directional or directional–hemispherical reflectance, depending on whether it is used in *indirect* or *direct mode*. Schematics of integrating spheres operating in the two modes are shown in Fig. 3-47. The ideal device is coated on its inside with a material of high and perfectly diffuse reflectance. The most common material in use is smoked magnesium oxide, which reflects strongly and very diffusely up to $\lambda \simeq 2.6\,\mu$m (cf. Fig. 3-5). Other materials, such as "diffuse gold" [155–158], have been used to overcome the wavelength limitations. The strong, diffuse reflectance, together with the spherical geometry, assures that any external radiation hitting the surface of the sphere is converted into a perfectly diffuse intensity field due to many diffuse reflections. In the direct method the sample is illuminated directly by an external source, as shown in Fig. 3-47*a*. All of the reflected radiation is collected by the sphere and converted into a diffuse intensity field, which is measured by a detector. Similar readings are then taken on a comparison standard of known reflectance, under the same conditions. The sample may be removed and replaced by the standard (*substitution method*); or there may be separate sample and standard holders, which are alternately irradiated by the external source (*comparison method*), the latter being generally preferred. In the indirect method a spot on the sphere surface is irradiated while the detector measures the intensity reflected by the sample (or the comparison standard) directly.

Errors in integrating sphere measurements are primarily caused by imperfections of the surface coating (imperfectly diffuse reflectance), losses out of apertures, and unwanted irradiation onto the detector (direct reflection from the sample in the direct mode, direct reflection from the externally-irradiated spot on the sphere in the indirect mode). Because of temperature sensitivity of the diffuse coatings, integrating-sphere measurements have mostly been limited

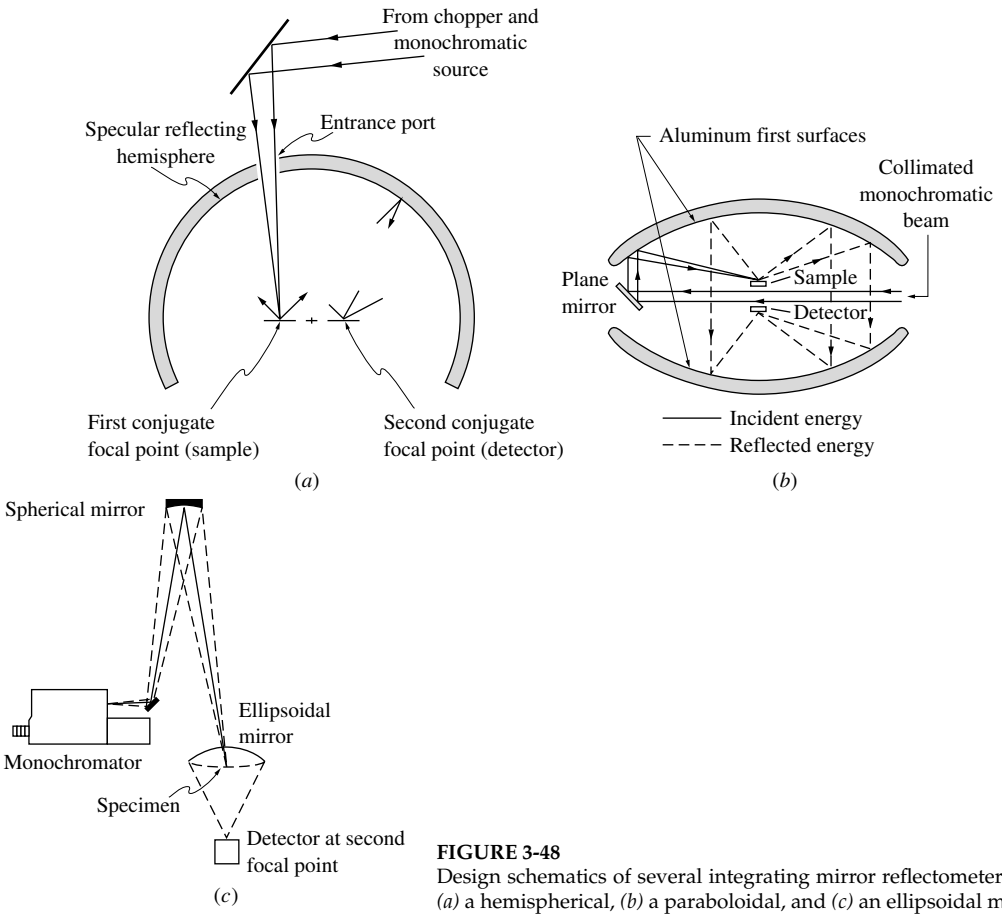

FIGURE 3-48
Design schematics of several integrating mirror reflectometers, using *(a)* a hemispherical, *(b)* a paraboloidal, and *(c)* an ellipsoidal mirror.

to moderate temperature levels. However, for monochromatic and high-speed FTIR measurements it is possible to rapidly heat up only the sample by a high-power source, such as a laser, as was done by Zhang and Modest [160].

INTEGRATING MIRROR REFLECTOMETERS. An alternative to the integrating sphere is a similar design utilizing an integrating mirror. Mirrors in general have high reflectivities in the infrared and are much more efficient than integrating spheres and, hence, are highly desirable in the infrared where the energy of the light source is low. On the other hand, it is difficult to collect the radiant energy, reflected by the sample into the hemisphere above it, into a parallel beam of small cross-section. For this reason, an integrating mirror reflectometer requires a large detector area. There are three types of integrating mirrors: *hemispherical* [161], *paraboloidal* [146, 162] and *ellipsoidal* [163–169]. Schematics of the three different types are shown in Fig. 3-48. The principle of operation of all three is the same, only the shape of the mirror is different. Each of these mirrors has two conjugate focal points, i.e., if a point source of light is placed at one focal point, all radiation will, after reflection off the mirror, fall onto the second focal point. Thus, in the integrating mirror technique an external beam is focused onto the sample, which is located at one of the focal points, through a small opening in the mirror. Radiation reflected from the sample into any direction will be reflected by the integrating mirror and is then collected by the detector located at the other focal point. This technique yields the directional–hemispherical reflectance of the sample, after comparison with a reference signal. Alternatively, one of the focal points can hold a blackbody source, with the ellipsoidal mirror focusing the energy onto the sample at the second focal point. Radiation leaving the sample is then probed through a small hole in the

mirror and spectrally resolved and detected by a monochromator or FTIR spectrometer, yielding the hemispherical–directional reflectance of the sample [169]. Sources for error in the integrating mirror method are absorption by the mirror, energy lost through the entrance port, nonuniform angular response of detectors, and energy missing the detector owing to mirror aberrations. To minimize aberrations, ellipsoids are preferable over hemispheres. The method has generally been limited to relatively large wavelengths, $> 2.5\,\mu$m (because of mirror limitations), and to moderate temperatures. Designs allowing sample temperatures up to about 1000°C have been reported by Battuello and coworkers [167], Ravindra and colleagues [170], and by Freeman *et al.* [171], while the torch-heated sample of Markham and coworkers' design [169] allows sample temperatures up to 2000°C. In general, integrating mirrors are somewhat less popular than integrating spheres because mirrors are more sensitive to flux losses and misalignment errors.

References

1. Goldsmith, A., and T. E. Waterman: "Thermophysical properties of solid materials," Technical Report WADC TR 58-476, Armour Research Foundation, 1959.
2. Gubareff, G. G., J. E. Janssen, and R. H. Torborg: "Thermal radiation properties survey," Honeywell Research Center, Minneapolis, MI, 1960.
3. Wood, W. D., H. W. Deem, and C. F. Lucks: *Thermal Radiative Properties*, Plenum Publishing Company, New York, 1964.
4. Svet, D. I.: *Thermal Radiation: Metals, Semiconductors, Ceramics, Partly Transparent Bodies, and Films*, Plenum Publishing Company, New York, 1965.
5. Edwards, D. K., and I. Catton: "Radiation characteristics of rough and oxidized metals," in *Adv. Thermophys. Properties Extreme Temp. Pressures*, ed. S. Gratch, ASME, pp. 189–199, 1965.
6. Touloukian, Y. S., and D. P. DeWitt (eds.): *Thermal Radiative Properties: Metallic Elements and Alloys*, vol. 7 of *Thermophysical Properties of Matter*, Plenum Press, New York, 1970.
7. Touloukian, Y. S., and D. P. DeWitt (eds.): *Thermal Radiative Properties: Nonmetallic Solids*, vol. 8 of *Thermophysical Properties of Matter*, Plenum Press, New York, 1972.
8. Touloukian, Y. S., D. P. DeWitt, and R. S. Hernicz (eds.): *Thermal Radiative Properties: Coatings*, vol. 9 of *Thermophysical Properties of Matter*, Plenum Press, New York, 1973.
9. Schmidt, E., and E. R. G. Eckert: "Über die Richtungsverteilung der Wärmestrahlung von Oberflächen," *Forschung auf dem Gebiete des Ingenieurwesens*, vol. 7, p. 175, 1935.
10. McNicholas, H. J.: "Absolute methods of reflectometry," *J. Res. Natl. Bur. Std*, vol. 1, pp. 29–72, 1928.
11. Siegel, R., and J. R. Howell: *Thermal Radiation Heat Transfer*, 3rd ed., Hemisphere, New York, 1992.
12. Torrance, K. E., and E. M. Sparrow: "Biangular reflectance of an electric nonconductor as a function of wavelength and surface roughness," *ASME Journal of Heat Transfer*, vol. 87, pp. 283–292, 1965.
13. Drude, P.: *Annalen der Physik*, vol. 39, p. 530, 1890.
14. Ehrenreich, H., H. R. Phillip, and B. Segall: "Optical properties of aluminum," *Physical Review*, vol. 132, no. 5, pp. 1918–1928, 1963.
15. Ehrenreich, H., and H. R. Phillip: "Optical properties of Ag and Cu," *Physical Review*, vol. 128, no. 1, pp. 1622–1629, 1962.
16. Shiles, E., T. Sasaki, M. Inokuti, and D. Y. Smith: "Self-consistency and sum-rule tests in the Kramers–Kronig analysis of optical data: Applications to aluminum," *Physical Review B*, vol. 22, pp. 1612–1628, 1980.
17. Hagemann, H. J., W. Gudat, and C. Kunz: "Optical constants from the far infrared to the x-ray region: Mg, Al, Cu, Ag, Au, Bi, C and Al_2O_3," *Journal of the Optical Society of America*, vol. 65, pp. 742–744, 1975.
18. Parker, W. J., and G. L. Abbott: "Theoretical and experimental studies of the total emittance of metals," in *Symposium on Thermal Radiation of Solids*, ed. S. Katzoff, NASA SP-55, pp. 11–28, 1965.
19. Ordal, M. A., L. L. Long, R. J. Bell, S. E. Bell, R. W. Alexander, and C. A. Ward: "Optical properties of the metals Al, Co, Cu, Au, Fe, Pb, Ni, Pd, Pt, Ag, Ti, and W in the infrared and far infrared," *Applied Optics*, vol. 22, no. 7, pp. 1099–1119, 1983.
20. Gray, D. E. (ed.): *American Institute of Physics Handbook*, 3d ed., ch. 6, McGraw-Hill, New York, 1972.
21. Palik, E. D. (ed.): *Handbook of Optical Constants of Solids*, vol. I, Academic Press, 1985.
22. Palik, E. D. (ed.): *Handbook of Optical Constants of Solids*, vol. II, Academic Press, 1991.
23. Lide, D. R. (ed.): *CRC Handbook of Chemistry and Physics*, 78th ed., Chemical Rubber Company, Cleveland, OH, 1998.
24. Hagen, E., and H. Rubens: "Metallic reflection," *Annalen der Physik*, vol. 1, no. 2, pp. 352–375, 1900.
25. Reuter, G. E. H., and E. H. Sondheimer: "The theory of the anomalous skin effect in metals," *Proceedings of the Royal Society (London) A*, vol. 195, no. 1042, pp. 336–364, 1948.
26. Brandenberg, W. M.: "The reflectivity of solids at grazing angles," in *Measurement of Thermal Radiation Properties of Solids*, ed. J. C. Richmond, NASA SP-31, pp. 75–82, 1963.

27. Brandenberg, W. M., and O. W. Clausen: "The directional spectral emittance of surfaces between 200 and 600 °C," in *Symposium on Thermal Radiation of Solids*, ed. S. Katzoff, NASA SP-55, pp. 313–319, 1965.
28. Price, D. J.: "The emissivity of hot metals in the infrared," *Proceedings of the Physical Society*, vol. 59, no. 331, pp. 118–131, 1947.
29. Dunkle, R. V.: "Thermal radiation characteristics of surfaces," in *Theory and Fundamental Research in Heat Transfer*, ed. J. A. Clark, Pergamon Press, New York, pp. 1–31, 1963.
30. Dunkle, R. V.: "Emissivity and inter-reflection relationships for infinite parallel specular surfaces," in *Symposium on Thermal Radiation of Solids*, ed. S. Katzoff, NASA SP-55, pp. 39–44, 1965.
31. Hering, R. G., and T. F. Smith: "Surface radiation properties from electromagnetic theory," *International Journal of Heat and Mass Transfer*, vol. 11, pp. 1567–1571, 1968.
32. Davisson, C., and J. R. Weeks: "The relation between the total thermal emissive power of a metal and its electrical resistivity," *Journal of the Optical Society of America*, vol. 8, no. 5, pp. 581–605, 1924.
33. Weast, R. C. (ed.): *CRC Handbook of Chemistry and Physics*, 68th ed., Chemical Rubber Company, Cleveland, OH, 1988.
34. Spitzer, W. G., D. A. Kleinman, C. J. Frosch, and D. J. Walsh: "Optical properties of silicon carbide," in *Silicon Carbide — A High Temperature Semiconductor*, eds. J. R. O'Connor and J. Smiltens, Proceedings of the 1959 Conference on Silicon Carbide, Boston, Massachusetts, Pergamon Press, pp. 347–365, 1960.
35. Bao, H., and X. Ruan: "Ab initio calculations of thermal radiative properties: The semiconductor GaAs," *International Journal of Heat and Mass Transfer*, vol. 53, pp. 1308–1312, 2010.
36. Jasperse, J. R., A. Kahan, J. N. Plendl, and S. S. Mitra: "Temperature dependence of infrared dispersion in ionic crystals LiF and MgO," *Physical Review*, vol. 140, no. 2, pp. 526–542, 1966.
37. Bohren, C. F., and D. R. Huffman: *Absorption and Scattering of Light by Small Particles*, John Wiley & Sons, New York, 1983.
38. Roy, S., S. Y. Bang, M. F. Modest, and V. S. Stubican: "Measurement of spectral, directional reflectivities of solids at high temperatures between 9 and 11 μm," *Applied Optics*, vol. 32, no. 19, pp. 3550–3558, 1993.
39. Riethof, T. R., and V. J. DeSantis: "Techniques of measuring normal spectral emissivity of conductive refractory compounds at high temperatures," in *Measurement of Thermal Radiation Properties of Solids*, ed. J. C. Richmond, NASA SP-31, pp. 565–584, 1963.
40. Mitra, S. S., and S. Nudelman: *Far-Infrared Properties of Solids*, Plenum Press, New York, 1970.
41. Beckmann, P., and A. Spizzichino: *The Scattering of Electromagnetic Waves from Rough Surfaces*, Macmillan, New York, 1963.
42. Bass, F. G., and I. M. Fuks: *Wave Scattering from Statistically Rough Surfaces*, Pergamon Press, Oxford, 1979.
43. Ogilvy, J. A.: "Wave scattering from rough surfaces," *Reports on Progress in Physics*, vol. 50, pp. 1553–1608, 1987.
44. Davies, H.: "The reflection of electromagnetic waves from a rough surface," *Proceedings of IEEE*, vol. 101, part IV, pp. 209–214, 1954.
45. Bennett, H. E.: "Specular reflection of aluminized ground glass and the height distribution of surface irregularities," *Journal of the Optical Society of America*, vol. 53, pp. 1389–1394, 1963.
46. Beckmann, P.: "Shadowing of random rough surfaces," *IEEE Transactions on Antennas and Propagation*, vol. AP-13, pp. 384–388, 1965.
47. Torrance, K. E., and E. M. Sparrow: "Theory for off-specular reflection from roughened surfaces," *Journal of the Optical Society of America*, vol. 57, no. 9, pp. 1105–1114, 1967.
48. Berry, M. V.: "Diffractals," *Journal of Physics A: Mathematical and General*, vol. 12, pp. 781–797, 1979.
49. Berry, M. V., and T. M. Blackwell: "Diffractal echoes," *Journal of Physics A: Mathematical and General*, vol. 14, pp. 3101–3110, 1981.
50. Majumdar, A., and C. L. Tien: "Reflection of radiation by rough fractal surfaces," in *Radiation Heat Transfer: Fundamentals and Applications*, vol. HTD-137, ASME, pp. 27–35, June 1990.
51. Majumdar, A., and B. Bhushan: "Role of fractal geometry in roughness characterization and contact mechanics of surfaces," *ASME Journal of Tribology*, vol. 112, pp. 205–216, 1990.
52. Majumdar, A., and C. L. Tien: "Fractal characterization and simulation of rough surfaces," in *Wear*, vol. 136, pp. 313–327, 1990.
53. Houchens, A. F., and R. G. Hering: "Bidirectional reflectance of rough metal surfaces," in *Thermophysics of Spacecrafts and Planetary Bodies*, ed. G. B. Heller, vol. 20, AIAA, Progress in Astronautics and Aeronautics, MIT Press, pp. 65–89, 1967.
54. Smith, T. F., and R. G. Hering: "Comparison of bidirectional reflectance measurements and model for rough metallic surfaces," in *Proceedings of the Fifth Symposium on Thermophysical Properties*, ASME, Boston, pp. 429–435, 1970.
55. Dimenna, R. A., and R. O. Buckius: "Electromagnetic theory predictions of the directional scattering from triangular surfaces," *ASME Journal of Heat Transfer*, vol. 116, no. 3, pp. 639–645, 1994.
56. Dimenna, R. A., and R. O. Buckius: "Quantifying specular approximations for angular scattering from perfectly conducting random rough surfaces," *Journal of Thermophysics and Heat Transfer*, vol. 8, no. 3, pp. 393–399, 1994.
57. Yang, Y., and R. O. Buckius: "Surface length scale contributions to the directional and hemispherical emissivity and reflectivity," *Journal of Thermophysics and Heat Transfer*, vol. 9, no. 4, pp. 653–659, 1995.
58. Tang, K., R. A. Dimenna, and R. O. Buckius: "Regions of validity of the geometric optics approximation for angular scattering from very rough surfaces," *International Journal of Heat and Mass Transfer*, vol. 40, no. 1, pp. 49–59, 1997.

59. Thorsos, E.: "The validity of the Kirchhoff approximation for rough surface scattering using Gaussian roughness spectrum," *Journal of the Acoustical Society of America*, vol. 83, pp. 78–92, 1988.
60. Chen, M. F., and A. K. Fung: "A numerical study of the regions of validity of the Kirchhoff and small-perturbation rough surface scattering models," *Radio Science*, vol. 23, pp. 163–170, 1988.
61. Nieto-Vesperinas, M., and J. A. Sanchez-Gil: "Light transmission from a randomly rough dieletric diffuser: Theoretical and experimental results," *Optics Letters*, vol. 15, pp. 1261–1263, 1990.
62. Tang, K., and R. O. Buckius: "The geometric optics approximation for reflection from two-dimensional random rough surfaces," *International Journal of Heat and Mass Transfer*, vol. 41, no. 13, pp. 2037–2047, 1998.
63. Tang, K., Y. Yang, and R. O. Buckius: "Theory and experiments on scattering from rough interfaces," in *Annual Review of Heat Transfer*, ed. C. L. Tien, vol. X, Begell House, pp. 101–140, 1999.
64. Tang, K., P. Kawka, and R. O. Buckius: "Geometric optics applied to rough surfaces coated with an absorbing thin film," *Journal of Thermophysics and Heat Transfer*, vol. 13, no. 2, pp. 169–176, 1999.
65. Zhou, Y., and Z. M. Zhang: "Radiative properties of semitransparent silicon wafers with rough surfaces," *ASME Journal of Heat Transfer*, vol. 125, no. 3, pp. 462–470, 2003.
66. Zhu, Q. Z., and Z. M. Zhang: "Anisotropic slope distribution and bidirectional reflectance of a rough silicon surface," *ASME Journal of Heat Transfer*, vol. 126, no. 6, pp. 985–993, 2004.
67. Lee, H. J., Y. B. Chen, and Z. M. Zhang: "Directional radiative properties of anisotropic rough silicon and gold surfaces," *International Journal of Heat and Mass Transfer*, vol. 49, pp. 4482–4495, 2006.
68. Tang, K., and R. O. Buckius: "A statistical model of wave scattering from random rough surfaces," *International Journal of Heat and Mass Transfer*, vol. 44, no. 21, pp. 4059–4073, 2001.
69. Fu, K., and P.-F. Hsu: "New regime map of the geometric optics approximation for scattering from random rough surfaces," *Journal of Quantitative Spectroscopy and Radiative Transfer*, vol. 109, no. 2, pp. 180–188, 2008.
70. Carminati, R., and J.-J. Greffet: "A model for the radiative properties of opaque rough surfaces," in *Proceedings of the 11th International Heat Transfer Conference*, vol. 7, Kyongju, Korea, pp. 427–432, 1998.
71. Ishimaru, A., and J. S. Chen: "Scattering from very rough surfaces based on the modified second-order Kirchhoff approximation with angular and propagation shadowing," *Journal of the Acoustical Society of America*, vol. 88, no. 4, pp. 1877–1883, 1990.
72. Bennett, H. E., M. Silver, and E. J. Ashley: "Infrared reflectance of aluminum evaporated in ultra-high vacuum," *Journal of the Optical Society of America*, vol. 53, no. 9, pp. 1089–1095, 1963.
73. Schulz, L. G.: "The experimental studies of the optical properties of metals and the relation of the results to the Drude free electron theory," *Suppl. Phil. Mag.*, vol. 6, pp. 102–144, 1957.
74. Dunkle, R. V., and J. T. Gier: "Snow characteristics project progress report," Technical report, University of California at Berkeley, June 1953.
75. Bennett, H. E., J. M. Bennett, and E. J. Ashley: "Infrared reflectance of evaporated aluminum films," *Journal of the Optical Society of America*, vol. 52, pp. 1245–1250, 1962.
76. Spitzer, W. G., D. A. Kleinman, and D. J. Walsh: "Infrared properties of hexagonal silicon carbide," *Physical Review*, vol. 113, no. 1, pp. 127–132, January 1959.
77. Gaumer, R. E., E. R. Streed, and T. F. Vajta: "Methods for experimental determination of the extra-terrestrial solar absorptance of spacecraft materials," in *Measurement of Thermal Radiation Properties of Solids*, ed. J. C. Richmond, NASA SP-31, pp. 135–146, 1963.
78. Pezdirtz, G. F., and R. A. Jewell: "A study of the photodegradation of selected thermal control surfaces," in *Symposium on Thermal Radiation of Solids*, ed. S. Katzoff, NASA SP-55, pp. 433–441, 1965.
79. Hottel, H. C.: "Radiant heat transmission," in *Heat Transmission*, ed. W. H. McAdams, 3rd ed., ch. 4, McGraw-Hill, New York, 1954.
80. Edwards, D. K., A. F. Mills, and V. E. Denny: *Transfer Processes*, 2nd ed., Hemisphere/McGraw-Hill, New York, 1979.
81. Wylie, C. R.: *Advanced Engineering Mathematics*, 5th ed., McGraw-Hill, New York, 1982.
82. Hsieh, C. K., and K. C. Su: "Thermal radiative properties of glass from 0.32 to 206 μm," *Solar Energy*, vol. 22, pp. 37–43, 1979.
83. Gardon, R.: "The emissivity of transparent materials," *Journal of The American Ceramic Society*, vol. 39, no. 8, pp. 278–287, 1956.
84. Neuroth, N.: "Der Einfluss der Temperatur auf die spektrale Absorption von Gläsern im Ultraroten, I (Effect of temperature on spectral absorption of glasses in the infrared, I)," *Glastechnische Berichte*, vol. 25, pp. 242–249, 1952.
85. Yoldas, B. E., and D. P. Partlow: "Wide spectrum antireflective coating for fused silica and other glasses," *Applied Optics*, vol. 23, no. 9, pp. 1418–1424, 1984.
86. Fan, J. C. C., and F. J. Bachner: "Transparent heat mirrors for solar-energy applications," *Applied Optics*, vol. 15, no. 4, pp. 1012–1017, 1976.
87. Yoldas, B. E., and T. O'Keefe: "Deposition of optically transparent IR reflective coatings on glass," *Applied Optics*, vol. 23, no. 20, pp. 3638–43, 1984.
88. Smith, G. B., S. Dligatch, and R. Sullivan: "Thin film angular selective glazing," *Solar Energy*, vol. 62, no. 3, pp. 229–244, 1998.
89. Edwards, D. K.: "Solar absorption by each element in an absorber-coverglass array," *Solar Energy*, vol. 19, pp. 401–402, 1977.

90. Edwards, D. K.: "Finite element embedding with optical interference," *Presentation of the Twentieth Joint ASME/AIChE National Heat Transfer Conference*, vol. 81-HT-65, 1981.
91. Mitts, S. J., and T. F. Smith: "Solar energy transfer through semitransparent systems," *Journal of Thermophysics and Heat Transfer*, vol. 1, no. 4, pp. 307–312, 1987.
92. Shurcliff, W. A.: "Transmittance and reflection loss of multi-plate planar window of a solar-radiation collector: Formulas and tabulations of results for the case of n = 1.5," *Solar Energy*, vol. 16, pp. 149–154, 1974.
93. Duffie, J. A., and W. A. Beckman: *Solar Energy Thermal Processes*, John Wiley & Sons, New York, 1974.
94. Martin, D. C., and R. J. Bell: "The use of optical interference to obtain selective energy absorption," in *Proceedings of the Conference on Coatings for the Aerospace Environment*, vol. WADD-TR-60-TB, 1960.
95. Hottel, H. C., and B. B. Woertz: "The performance of flat-plate solar-heat collectors," *Transactions of ASME, Journal of Heat Transfer*, vol. 64, pp. 91–104, 1942.
96. Gier, J. T., and R. V. Dunkle: "Selective spectral characteristics as an important factor in the efficiency of solar collectors," in *Transactions of the Conference on the Use of Solar Energy*, vol. 2, University of Arizona Press, Tucson, AZ, p. 41, 1958.
97. Tabor, H., J. A. Harris, H. Weinberger, and B. Doron: "Further studies on selective black coatings," *Proceedings of the UN Conference on New Sources of Energy*, vol. 4, p. 618, 1964.
98. Tabor, H.: "Selective surfaces for solar collectors," in *Low Temperature Engineering Applications of Solar Energy*, ASHRAE, 1967.
99. Edwards, D. K., K. E. Nelson, R. D. Roddick, and J. T. Gier: "Basic studies on the use and control of solar energy," Technical Report 60-93, The University of California, Los Angeles, CA, 1960.
100. Thekaekara, M. P.: "Solar energy outside the earth's atmosphere," *Solar Energy*, vol. 14, pp. 109–127, 1973.
101. Trombe, F., M. Foex, and V. LePhat: "Research on selective surfaces for air conditioning dwellings," *Proceedings of the UN Conference on New Sources of Energy*, vol. 4, pp. 625–638, 1964.
102. Hollands, K. G. T.: "Directional selectivity, emittance, and absorptance properties of vee corrugated specular surfaces," *Solar Energy*, vol. 7, no. 3, pp. 108–116, 1963.
103. Perlmutter, M., and J. R. Howell: "A strongly directional emitting and absorbing surface," *ASME Journal of Heat Transfer*, vol. 85, no. 3, pp. 282–283, 1963.
104. Richmond, J. C. (ed.): *Measurement of Thermal Radiation Properties of Solids*, NASA SP-31, 1963.
105. Katzoff, S. (ed.): *Symposium on Thermal Radiation Properties of Solids*, NASA SP-55, 1964.
106. Sacadura, J.-F.: "Measurement techniques for thermal radiation properties," in *Proceedings of the Ninth International Heat Transfer Conference*, Hemisphere, Washington, D.C., pp. 207–222, 1990.
107. Hutley, M. C.: *Diffraction Gratings*, Academic Press, New York, 1982.
108. Griffiths, P. R., and J. A. de Haseth: *Fourier Transform Infrared Spectrometry*, vol. 83 of *Chemical Analysis*, John Wiley & Sons, New York, 1986.
109. Sadler, R., L. Hemmerdinger, and I. Rando: "A device for measuring total hemispherical emittance," in *Measurement of Thermal Radiation Properties of Solids*, ed. J. C. Richmond, NASA SP-31, pp. 217–223, 1963.
110. Funai, A. I.: "A multichamber calorimeter for high-temperature emittance studies," in *Measurement of Thermal Radiation Properties of Solids*, ed. J. C. Richmond, NASA SP-31, pp. 317–327, 1963.
111. McElroy, D. L., and T. G. Kollie: "The total hemispherical emittance of platinum, columbium-1%, zirconium, and polished and oxidized iron-8 in the range 100°C to 1200°C," in *Measurement of Thermal Radiation Properties of Solids*, ed. J. C. Richmond, NASA SP-31, pp. 365–379, 1963.
112. Moore, V. S., A. R. Stetson, and A. G. Metcalfe: "Emittance measurements of refractory oxide coatings up to 2900°C," in *Measurement of Thermal Radiation Properties of Solids*, ed. J. C. Richmond, NASA SP-31, pp. 527–533, 1963.
113. Nyland, T. W.: "Apparatus for the measurement of hemispherical emittance and solar absorptance from 270°C to 650°C," in *Measurement of Thermal Radiation Properties of Solids*, ed. J. C. Richmond, NASA SP-31, pp. 393–401, 1963.
114. Zerlaut, G. A.: "An apparatus for the measurement of the total normal emittance of surfaces at satellite temperatures," in *Measurement of Thermal Radiation Properties of Solids*, ed. J. C. Richmond, NASA SP-31, pp. 275–285, 1963.
115. Chen, S. H. P., and S. C. Saxena: "Experimental determination of hemispherical total emittance of metals as a function of temperature," *Ind. Eng. Chem. Fundam.*, vol. 12, no. 2, pp. 220–224, 1973.
116. Jody, B. J., and S. C. Saxena: "Radiative heat transfer from metal wires: Hemispherical total emittance of platinum," *Journal of Physics E: Scientific Instruments*, vol. 9, pp. 359–362, 1976.
117. Taylor, R. E.: "Determination of thermophysical properties by direct electrical heating," *High Temperatures - High Pressures*, vol. 13, pp. 9–22, 1981.
118. Gordon, G. D., and A. London: "Emittance measurements at satellite temperatures," in *Measurement of Thermal Radiation Properties of Solids*, ed. J. C. Richmond, NASA SP-31, pp. 147–151, 1963.
119. Rudkin, R. L.: "Measurement of thermal properties of metals at elevated temperatures," in *Temperature, Its Measurement and Control in Science and Industry*, vol. 3, part 2, Reinhold Publishing Corp., New York, pp. 523–534, 1962.
120. Gaumer, R. E., and J. V. Stewart: "Calorimetric determination of infrared emittance and the α/ϵ ratio," in *Measurement of Thermal Radiation Properties of Solids*, ed. J. C. Richmond, NASA SP-31, pp. 127–133, 1963.
121. Butler, C. P., and R. J. Jenkins: "Space chamber emittance measurements," in *Measurement of Thermal Radiation Properties of Solids*, ed. J. C. Richmond, NASA SP-31, pp. 39–43, 1963.

122. Butler, C. P., and E. C. Y. Inn: "A method for measuring total hemispherical and emissivity of metals," in *First Symposium - Surface Effects on Spacecraft Materials*, John Wiley & Sons, New York, pp. 117–137, 1960.
123. Smalley, R., and A. J. Sievers: "The total hemispherical emissivity of copper," *Journal of the Optical Society of America*, vol. 68, pp. 1516–1518, 1978.
124. Ramanathan, K. G., and S. H. Yen: "High-temperature emissivities of copper, aluminum and silver," *Journal of the Optical Society of America*, vol. 67, pp. 32–38, 1977.
125. Masuda, H., and M. Higano: "Measurement of total, hemispherical emissivities of metal wires by using transient calorimetric techniques," *ASME Journal of Heat Transfer*, vol. 110, pp. 166–172, 1988.
126. Limperis, T., D. M. Szeles, and W. L. Wolfe: "The measurement of total normal emittance of three nuclear reactor materials," in *Measurement of Thermal Radiation Properties of Solids*, ed. J. C. Richmond, NASA SP-31, pp. 357–364, 1963.
127. Fussell, W. B., and F. Stair: "Preliminary studies toward the determination of spectral absorption coefficients of homogeneous dielectric material in the infrared at elevated temperatures," in *Symposium on Thermal Radiation of Solids*, ed. S. Katzoff, NASA SP-55, pp. 287–292, 1965.
128. Havstad, M. A., W. I. McLean, and S. A. Self: "Apparatus for the measurement of the optical constants and thermal radiative properties of pure liquid metals from 0.4 to 10 μm," *Review of Scientific Instruments*, vol. 64, pp. 1971–1978, 1993.
129. Markham, J. R., P. R. Solomon, and P. E. Best: "An FT-IR based instrument for measuring spectral emittance of material at high temperature," *Review of Scientific Instruments*, vol. 61, no. 12, pp. 3700–3708, 1990.
130. Takasuka, E., E. Tokizaki, K. Terashima, and S. O. Kazutaka: "Emissivity of liquid silicon in visible and infrared regions," *Journal of Applied Physics*, vol. 81, pp. 6384–6389, 1997.
131. Kobayashi, M., M. Otsuki, H. Sakate, F. Sakuma, and A. Ono: "System for measuring the spectral distribution of normal emissivity of metals with direct current heating," *International Journal of Thermophysics*, vol. 20, no. 1, 1999.
132. Kobayashi, M., A. Ono, M. Otsuki, H. Sakate, and F. Sakuma: "Database of normal spectral emissivities of metals at high temperatures," *International Journal of Thermophysics*, vol. 20, no. 1, pp. 299–308, 1999.
133. Knopken, S., and R. Klemm: "Evaluation of thermal radiation at high temperatures," in *Measurement of Thermal Radiation Properties of Solids*, ed. J. C. Richmond, NASA SP-31, pp. 505–514, 1963.
134. Bennethum, W. H.: "Thin film sensors and radiation sensing techniques for measurement of surface temperature of ceramic components," in *HITEMP Review, Advanced High Temperature Engine Materials Technology Program*, NASA CP-10039, 1989.
135. Atkinson, W. H., and M. A. Cyr: "Sensors for temperature measurement for ceramic materials," in *HITEMP Review, Advanced High Temperature Engine Materials Technology Program*, NASA CP-10039, pp. 287–292, 1989.
136. Vader, D. T., R. Viskanta, and F. P. Incropera: "Design and testing of a high-temperature emissometer for porous and particulate dielectrics," *Review of Scientific Instruments*, vol. 57, no. 1, pp. 87–93, 1986.
137. Postlethwait, M. A., K. K. Sikka, M. F. Modest, and J. R. Hellmann: "High temperature normal spectral emittance of silicon carbide based materials," *Journal of Thermophysics and Heat Transfer*, vol. 8, no. 3, pp. 412–418, 1994.
138. Birkebak, R. C., and E. R. G. Eckert: "Effect of roughness of metal surfaces on angular distribution of monochromatic reflected radiation," *ASME Journal of Heat Transfer*, vol. 87, pp. 85–94, 1965.
139. Torrance, K. E., and E. M. Sparrow: "Off-specular peaks in the directional distribution of reflected thermal radiation," *ASME Journal of Heat Transfer*, vol. 88, pp. 223–230, 1966.
140. Ford, J. N., K. Tang, and R. O. Buckius: "Fourier transform infrared system measurement of the bidirectional reflectivity of diffuse and grooved surfaces," *ASME Journal of Heat Transfer*, vol. 117, no. 4, pp. 955–962, 1995.
141. Hsia, J. J., and J. C. Richmond: "A high resolution laser bidirectional reflectometer," *Journal Research of N.B.S.*, vol. 80A, no. 2, pp. 189–220, 1976.
142. De Silva, A. A., and B. W. Jones: "Bidirectional spectral reflectance and directional-hemispherical spectral reflectance of six materials used as absorbers of solar energy," *Solar Energy Materials*, vol. 15, pp. 391–401, 1987.
143. Greffet, J.-J.: "Design of a fully automated bidirectional laser reflectometer; applications to emissivity measurement," in *Proceedings of SPIE on Stray Light and Contamination in Optical Systems*, ed. R. P. Breault, vol. 967, pp. 184–191, 1989.
144. Al Hamwi, M., and J.-F. Sacadura: "Méthode de détermination des propriétes radiatives spectrales et directionnelles, dans le proche et moyen i.r., de surfaces opaques métalliques et non-métalliques," *Proceedings of JITH '89*, pp. 126–136, November 1989.
145. Zaworski, J. R., J. R. Welty, and M. K. Drost: "Measurement and use of bi-directional reflectance," *International Journal of Heat and Mass Transfer*, vol. 39, pp. 1149–1156, 1996.
146. Dunkle, R. V.: "Spectral reflection measurements," in *First Symposium - Surface Effects on Spacecraft Materials*, John Wiley & Sons, New York, pp. 117–137, 1960.
147. Hembach, R. J., L. Hemmerdinger, and A. J. Katz: "Heated cavity reflectometer modifications," in *Measurement of Thermal Radiation Properties of Solids*, ed. J. C. Richmond, NASA SP-31, pp. 153–167, 1963.
148. Gier, J. T., R. V. Dunkle, and J. T. Bevans: "Measurement of absolute spectral reflectivity from 1.0 to 15 microns," *Journal of the Optical Society of America*, vol. 44, pp. 558–562, 1954.
149. Fussell, W. B., J. J. Triolo, and F. A. Jerozal: "Portable integrating sphere for monitoring reflectance of spacecraft coatings," in *Measurement of Thermal Radiation Properties of Solids*, ed. J. C. Richmond, NASA SP-31, pp. 103–116, 1963.

150. Drummeter, L. F., and E. Goldstein: "Vanguard emittance studies at NRL," in *First Symposium - Surface Effects on Spacecraft Materials*, John Wiley & Sons, New York, pp. 152–163, 1960.
151. Snail, K. A., and L. M. Hangsen: "Integrating sphere designs with isotropic throughput," *Applied Optics*, vol. 28, pp. 1793–1799, May 1989.
152. Egan, W. G., and T. Hilgeman: "Integrating spheres for measurements between 0.185 μm and 12 μm," *Applied Optics*, vol. 14, pp. 1137–1142, May 1975.
153. Kneissl, G. J., and J. C. Richmond: "A laser source integrating sphere reflectometer," Technical Report NBS-TN-439, National Bureau of Standards, 1968.
154. Edwards, D. K., J. T. Gier, K. E. Nelson, and R. D. Roddick: "Integrating sphere for imperfectly diffuse samples," *Journal of the Optical Society of America*, vol. 51, pp. 1279–1288, 1961.
155. Willey, R. R.: "Fourier transform infrared spectrophotometer for transmittance and diffuse reflectance measurements," *Applied Spectroscopy*, vol. 30, pp. 593–601, 1976.
156. Richter, W.: "Fourier transform reflectance spectrometry between 8000 cm^{-1} (1.25 μm) and 800 cm^{-1} (12.5 μm) using an integrating sphere," *Applied Spectroscopy*, vol. 37, pp. 32–38, 1983.
157. Gindele, K., M. Köhl, and M. Mast: "Spectral reflectance measurements using an integrating sphere in the infrared," *Applied Optics*, vol. 24, pp. 1757–1760, 1985.
158. Richter, W., and W. Erb: "Accurate diffuse reflection measurements in the infrared spectral range," *Applied Optics*, vol. 26, no. 21, pp. 4620–4624, November 1987.
159. Sheffer, D., U. P. Oppenheim, D. Clement, and A. D. Devir: "Absolute reflectometer for the 0.8–2.5 μm region," *Applied Optics*, vol. 26, no. 3, pp. 583–586, 1987.
160. Zhang, Z., and M. F. Modest: "Temperature-dependent absorptances of ceramics for Nd:YAG and CO_2 laser processing applications," *ASME Journal of Heat Transfer*, vol. 120, no. 2, pp. 322–327, 1998.
161. Janssen, J. E., and R. H. Torborg: "Measurement of spectral reflectance using an integrating hemisphere," in *Measurement of Thermal Radiation Properties of Solids*, ed. J. C. Richmond, NASA SP-31, pp. 169–182, 1963.
162. Neher, R. T., and D. K. Edwards: "Far infrared reflectometer for imperfectly diffuse specimens," *Applied Optics*, vol. 4, pp. 775–780, 1965.
163. Neu, J. T.: "Design, fabrication and performance of an ellipsoidal spectroreflectometer," *NASA CR 73193*, 1968.
164. Dunn, S. T., J. C. Richmond, and J. F. Panner: "Survey of infrared measurement techniques and computational methods in radiant heat transfer," *Journal of Spacecraft and Rockets*, vol. 3, pp. 961–975, July 1966.
165. Heinisch, R. P., F. J. Bradar, and D. B. Perlick: "On the fabrication and evaluation of an integrating hemi-ellipsoid," *Applied Optics*, vol. 9, no. 2, pp. 483–489, 1970.
166. Wood, B. E., P. G. Pipes, A. M. Smith, and J. A. Roux: "Hemi-ellipsoidal mirror infrared reflectometer: Development and operation," *Applied Optics*, vol. 15, no. 4, pp. 940–950, 1976.
167. Battuello, M., F. Lanza, and T. Ricolfi: "Infrared ellipsoidal mirror reflectometer for measurements between room temperature and 1000°C," *High Temperature*, vol. 18, pp. 683–688, 1986.
168. Snail, K. A.: "Reflectometer design using nonimaging optics," *Applied Optics*, vol. 26, no. 24, pp. 5326–5332, 1987.
169. Markham, J. R., K. Kinsella, R. M. Carangelo, C. R. Brouillette, M. D. Carangelo, P. E. Best, and P. R. Solomon: "Bench top Fourier transform infrared based instrument for simultaneously measuring surface spectral emittance and temperature," *Review of Scientific Instruments*, vol. 64, no. 9, pp. 2515–2522, 1993.
170. Ravindra, N. M., S. Abedrabbo, W. Chen, F. M. Tong, A. K. Nanda, and A. C. Speranza: "Temperature-dependent emissivity of silicon-related materials and structures," *IEEE Transactions on Semiconductor Manufacturing*, vol. 11, no. 1, pp. 30–39, 1998.
171. Freeman, R. K., F. A. Rigby, and N. Morley: "Temperature-dependent reflectance of plated metals and composite materials under laser irradiation," *Journal of Thermophysics and Heat Transfer*, vol. 14, no. 3, pp. 305–312, 2000.
172. Hale, G. M., and M. R. Querry: "Optical constants of water in the 200 nm to 200 μm wavelength region," *Applied Optics*, vol. 12, pp. 555–563, 1973.

Problems

3.1 A diffusely emitting surface at 500 K has a spectral, directional emittance that can be approximated by 0.5 in the range $0 < \lambda < 5\,\mu$m and 0.3 for $\lambda > 5\,\mu$m. What is the total, hemispherical emittance of this surface surrounded by *(a)* air and *(b)* a dielectric medium of refractive index $n = 2$?

3.2 A certain material at 600 K has the following spectral, directional emittance:

$$\epsilon'_\lambda = \begin{cases} 0.9\cos\theta, & \lambda < 1\,\mu\text{m}, \\ 0.2, & \lambda > 1\,\mu\text{m}. \end{cases}$$

(a) What is the total, hemispherical emittance of the material?

(b) If the sun irradiates this surface at an angle of $\theta = 60°$ off-normal, what is the relevant total absorptance?

(c) What is the net radiative energy gain or loss of this surface (per unit time and area)?

3.3 For optimum performance a solar collector surface has been treated so that, for the spectral, directional emittance

$$\epsilon'_\lambda = \left\{ \begin{array}{ll} 0.9\cos 2\theta, & \theta < 45^\circ \\ 0.0 & \theta > 45^\circ \end{array} \right\}, \qquad \lambda < 2\,\mu\text{m},$$

$$= \quad 0.1, \qquad \text{all } \theta, \qquad \lambda > 2\,\mu\text{m}.$$

For solar incidence of 15° off-normal and a collector temperature of 400 K, what is the relevant ratio of absorptance to emittance?

3.4 A long, cylindrical antenna of 1 cm radius on an Earth-orbiting satellite is coated with a material whose emittance is

$$\epsilon'_\lambda = \begin{cases} 0, & \lambda < 1\,\mu\text{m}, \\ \cos\theta, & \lambda \geq 1\,\mu\text{m}. \end{cases}$$

Find the absorbed energy per meter length. (Assume irradiation is from the sun only, and in a direction normal to the antenna's axis; neglect the Earth and stars.)

3.5 The spectral, hemispherical emittance of a (hypothetical) metal may be approximated by the relationship

$$\epsilon_\lambda = \begin{cases} 0.5, & \lambda < \lambda_c = 0.5\,\mu\text{m}, \\ 0.5\lambda_c/\lambda, & \lambda > \lambda_c \end{cases}$$

(independent of temperature). Determine the total, hemispherical emittance of this material using *(a)* Planck's law, and *(b)* Wien's distribution, for a surface temperature of *(i)* 300 K, and (*ii*) 1000 K. How accurate is the prediction using Wien's distribution?

3.6 A treated metallic surface is used as a solar collector material; its spectral, directional emittance may be approximated by

$$\epsilon'_\lambda = \begin{cases} 0.5\,\mu\text{m}/\lambda, & \theta < 45^\circ, \\ 0, & \theta > 45^\circ. \end{cases}$$

What is the relevant α/ϵ-ratio for near normal solar incidence if $T_{\text{coll}} \simeq 600$ K?

3.7 A surface sample with

$$\epsilon'_\lambda = \begin{cases} 0.9\cos\theta, & \lambda < 2\,\mu\text{m}, \\ 0.2, & \lambda > 2\,\mu\text{m}, \end{cases}$$

is irradiated by three tungsten lights as shown. The tungsten lights may be approximated by black spheres at $T = 2000$ K fitted with mirrors to produce parallel light beams aimed at the sample. Neglecting background radiation, determine the absorptance of the sample.

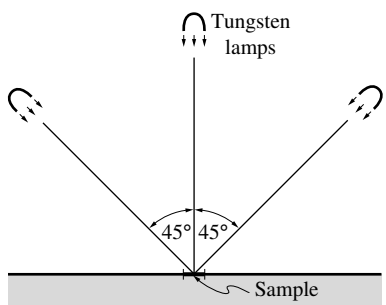

3.8 An antenna of a satellite may be approximated by a long half cylinder, which is exposed to sunshine as shown in the sketch. The antenna has a high conductivity (i.e., is isothermal), and is coated with the material of Fig. 3-36, i.e., the material may be assumed to be gray with the following directional characteristics:

$$\epsilon'_\lambda = \begin{cases} 0.9, & 0 \leq \theta < 40^\circ, \\ 0, & \theta > 40^\circ. \end{cases}$$

Determine the equilibrium temperature of the antenna, assuming it exchanges heat only with the sun (and cold outer space).

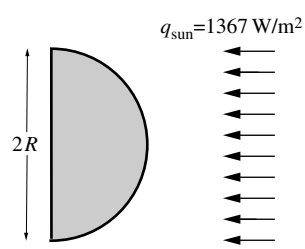

3.9 A large isothermal plate (temperature $T = 400\,\text{K}$) is exposed to a long monochromatic ($\lambda = 1\,\mu\text{m}$) line source as shown. The strength of the line source is Q' (W/m length of source) $= h\sigma T^4$, spreading equally into all directions. The plate has a spectral, directional emittance of

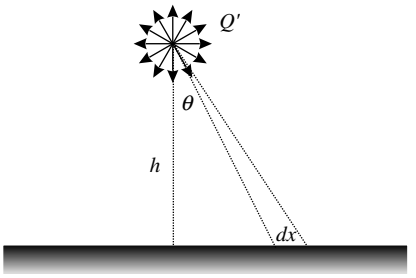

$$\epsilon'_\lambda = \begin{cases} 0.9\cos^2\theta, & \lambda < 2.5\,\mu\text{m}, \\ 0.1, & \lambda > 2.5\,\mu\text{m}, \end{cases} \quad 0 \le \theta < \frac{\pi}{2}.$$

For a general location, x, determine relevant absorptance, emittance, and the net local heat flux $q_{\text{net}}(x)$, which must be supplied to/removed from the plate to keep it isothermal at T.

3.10 A large isothermal plate (temperature $T = 400\,\text{K}$) is exposed to a long tungsten–halogen line source as shown in the sketch next to Problem 3.9. The strength of the line source is $Q' = 1000$ W/m length of source, spreading equally into all directions, and it has the spectral distribution of a blackbody at 4000K. The plate has a spectral, directional emittance of

$$\epsilon'_\lambda = \begin{cases} 0.8\cos\theta, & \lambda < 3\mu\text{m}, \\ 0.2, & \lambda > 3\mu\text{m}. \end{cases} \quad 0 \le \theta < \frac{\pi}{2}$$

For a general location, x, give an expression for local irradiation H, determine the relevant absorptance and emittance, and give an expression for the net local heat flux $q_{\text{net}}(x)$ that must be supplied to/removed from the plate to keep it isothermal at T.

3.11 An isothermal disk (temperature $T = 400\,\text{K}$) is exposed to a small black spherical source (temperature $T_s = 4000\,\text{K}$) as shown. The strength of the source is Q (W), spreading equally into all directions. The plate has a spectral, directional emittance of

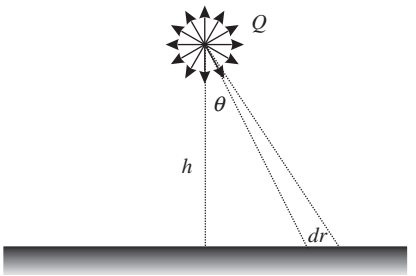

$$\epsilon'_\lambda = \begin{cases} 0.9\cos\theta, & \lambda < 4\mu\text{m}, \\ 0.3, & \lambda > 4\mu\text{m}. \end{cases} \quad 0 \le \theta < \frac{\pi}{2}$$

For a general location, r, determine relevant absorptance, relevant emittance, and the net local heat flux $q_{\text{net}}(r)$ that must be supplied to/removed from the plate to keep it isothermal at T.

3.12 A conical cavity is irradiated by a defocused CO_2 laser (wavelength = $10.6\,\mu\text{m}$) as shown. The conical surface is maintained at 500 K. For cavity coating with a spectral, directional emittance

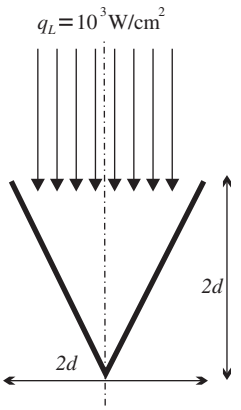

$$\epsilon'_\lambda(\lambda,\theta) = \begin{cases} 0.15\cos\theta, & \lambda < 6\,\mu\text{m}, \\ 0.8\cos^2\theta, & \lambda > 6\,\mu\text{m}, \end{cases}$$

determine the relevant total absorptance and emittance.

3.13 A metal ($m_2 = 50 - 50\,i$) is coated with a dielectric ($m_1 = 2 - 0\,i$), which is exposed to vacuum.

(a) What is the range of possible directions from which radiation can impinge on the metal?

(b) What is the normal reflectance of the dielectric–metal interface?

(c) What is the (approximate) relevant hemispherical reflectance for the dielectric–metal interface?

3.14 For a certain material, temperature, and wavelength the spectral, hemispherical emittance has been measured as ϵ_λ. Estimate the refractive index of the material under these conditions, assuming the material to be *(a)* a dielectric with $\epsilon_\lambda = 0.8$, *(b)* a metal in the infrared with $\epsilon_\lambda = 0.2$ (the Hagen–Rubens relation being valid).

3.15 It can be derived from electromagnetic wave theory that

$$\frac{\epsilon_\lambda}{\epsilon_{n\lambda}} \simeq \frac{4}{3} - \frac{1}{4}\epsilon_{n\lambda} \quad \text{for} \quad \epsilon_{n\lambda} \ll 1.$$

Determine ϵ_λ for metals with $\epsilon_{n\lambda} \ll 1$ as a function of wavelength and temperature.

3.16 A solar collector surface with emittance

$$\epsilon'_\lambda = \begin{cases} 0.9\cos\theta, & \lambda < 2\,\mu\text{m}, \\ 0.2, & \lambda > 2\,\mu\text{m}, \end{cases}$$

is to be kept at $T_c = 500\,\text{K}$. For $q_{\text{sol}} = 1300\,\text{W/m}^2$, what is the range of possible sun positions with respect to the surface for which at least 50% of the maximum net radiative energy is collected? Neglect conduction and convection losses from the surface.

3.17 On one of those famous clear days in Central Pennsylvania (home of PennState), a solar collector is irradiated by direct sunshine and by a diffuse atmospheric radiative flux. The magnitude of the solar flux is $q_{\text{sun}} = 1000\,\text{W/m}^2$ (incident at $\theta_{\text{sun}} = 45°$), and the effective blackbody temperature for the sky is $T_{\text{sky}} = 244\,\text{K}$. The absorber plate is isothermal at 320 K and is covered with a nongray, nondiffuse material whose spectral, directional emittance may be approximated by

$$\epsilon'_\lambda(\lambda,\theta) = \epsilon_{n\lambda}\cos\theta, \qquad \epsilon_{n\lambda} = \begin{cases} 0.9, & \lambda < 2.2\,\mu\text{m}, \\ 0.1, & \lambda > 2.2\,\mu\text{m}, \end{cases}$$

where $\epsilon_{n\lambda}$ is the normal, spectral emittance. Determine the net radiative flux on the collector.

3.18 A small plate, insulated at the bottom, is heated by irradiation from a defocused CO_2 laser beam (wavelength 10.6 μm) with an incidence angle of 30° off-normal. The radiative properties of the surface are

$$\epsilon'_\lambda = \begin{cases} 0.2\cos^2\theta, & \lambda < 3\,\mu\text{m}, \\ 0.8\cos\theta, & \lambda > 3\,\mu\text{m}. \end{cases}$$

The strength of the laser beam is $1300\,\text{W/m}^2$. Neglecting losses due to natural convection, determine the temperature of the plate.
Note: For such weak laser irradiation levels the heating effect is relatively small.

3.19 A thin disk, insulated at the bottom, is irradiated by a CO_2 laser ($\lambda = 10.6\,\mu$m) as shown. The top surface is exposed to a low temperature (300K) environment. Assume that the entire disk surface is uniformly irradiated with $q_L = 5\,\text{MW/m}^2$ and that the specific heat/area of the disk is $\rho c_p \delta = 2\,\text{kJ/m}^2\text{K}$. The disk is at ambient temperature when the laser is turned on. The emittance of the disk surface is

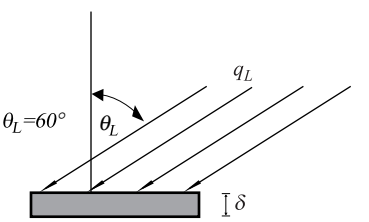

$$\epsilon'_\lambda = \begin{cases} 0.2, & \lambda < 6\,\mu\text{m}, \\ 0.9\cos\theta, & \lambda > 6\,\mu\text{m}. \end{cases}$$

(a) Indicate how to calculate the temperature history of the disk.
(b) Determine the initial heating rate (in K/s) at $t = 0$.
(c) What is the steady state temperature of the disk? (This is expected to be very high, say > 3000 K.)

3.20 Determine the total, normal emittance of copper, silver, and gold for a temperature of 1500 K. Check your results by comparing with Fig. 3-8.

3.21 Determine the total, hemispherical emittance of copper, silver, and gold for a temperature of 1500 K. Check your results by comparing with Fig. 3-11.

3.22 A polished platinum sphere is heated until it is glowing red. An observer is stationed a distance away, from where the sphere appears as a red disk. Using the various aspects of electromagnetic wave theory and/or Fig. 3-9 and Table 3.3, explain how the brightness of emitted radiation would vary across the disk, if observed with *(a)* the human eye, *(b)* an infrared camera.

3.23 Two aluminum plates, one covered with a layer of white enamel paint, the other polished, are directly facing the sun, which is irradiating the plates with 1000 W/m^2. Assuming that convection/conduction losses of the plates to the environment at 300 K can be calculated by using a heat transfer coefficient of 10 W/m^2 K, and that the back sides of the plates are insulated, estimate the equilibrium temperature of each plate.

3.24 Consider a metallic surface coated with a dielectric layer.

(a) Show that the fraction of energy reflected at the vacuum–dielectric interface is negligible ($n_1 = 1.2$; $k_1 = 0$).

(b) Develop an expression for the normal, spectral emittance for the metal substrate, similar to the Hagen–Rubens relationship.

(c) Develop an approximate relation for the directional, spectral emittance of the metal substrate for large wavelengths and moderate incidence angles, say $\theta < 75°$.

3.25 A plate of metal with $n_2 = k_2 = 100$ is covered with a dielectric as shown. The dielectric has an absorption band such that $n_1 = 2$, and $k_1 = 1$ for $0.2\,\mu\text{m} < \lambda < 2\,\mu\text{m}$ and $k_1 = 0$ elsewhere. The dielectric is thick enough, such that any light traveling through it of wavelengths $0.2\,\mu\text{m} < \lambda < 2\,\mu\text{m}$ is entirely absorbed before it reaches the metal.

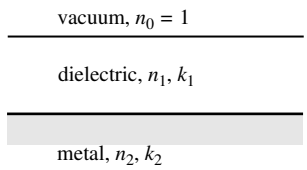

(*a*) What is the total, normal emittance of the composite if its temperature is 400 K?

(*b*) What is the total, normal absorptance if the sun shines perpendicularly onto the composite?

3.26 Estimate the total, normal emittance of α-SiC for a temperature of *(i)* 300 K, *(ii)* 1000 K. You may assume the spectral, normal emittance to be independent of temperature.

3.27 Estimate the total, hemispherical emittance of a thick slab of pure silicon at room temperature.

3.28 Estimate and compare the total, normal emittance of room temperature aluminum for the surface finishes given in Fig. 3-25.

3.29 A satellite orbiting Earth has part of its (flat) surface coated with spectrally selective "black nickel," which is a diffuse emitter and whose spectral emittance may be approximated by

$$\epsilon_\lambda = \begin{cases} 0.9, & \lambda < 2\,\mu\text{m}, \\ 0.25, & \lambda > 2\,\mu\text{m}. \end{cases}$$

Assuming the back of the surface to be insulated, and the front exposed to solar irradiation of $q_{\text{sol}} = 1367\,\text{W/m}^2$ (normal to the surface), determine the relevant α/ϵ-ratio for the surface. What is its equilibrium temperature? What would be its equilibrium temperature if the surface is turned away from the sun, such that the sun's rays strike it at a polar angle of $\theta = 60°$?

3.30 Repeat Problem 3.29 for white paint on aluminum, whose diffuse emittance may be approximated by

$$\epsilon_\lambda = \begin{cases} 0.1, & \lambda < 2\,\mu\text{m}, \\ 0.9, & \lambda > 2\,\mu\text{m}. \end{cases}$$

3.31 Estimate the spectral, hemispherical emittance of the grooved materials shown in Fig. 3-36. Repeat Problem 3.29 for these materials, assuming them to be gray.

3.32 Repeat Problem 1.7 for a sphere covered with the grooved material of Fig. 3-36, whose directional, spectral emittance may be approximated by

$$\epsilon'_\lambda = \begin{cases} 0.9, & 0 \le \theta < 40^\circ, \\ 0.0, & 40^\circ < \theta < 90^\circ. \end{cases}$$

Assume the material to be gray.

3.33 A solar collector consists of a metal plate coated with "black nickel." The collector is irradiated by the sun with a strength of $q_{\text{sol}} = 1000\,\text{W/m}^2$ from a direction that is $\theta = 30^\circ$ from the surface normal. On its top the surface loses heat by radiation and by free convection (heat transfer coefficient $h_1 = 10\,\text{W/m}^2\,\text{K}$), both to an atmosphere at $T_{\text{amb}} = 20^\circ\text{C}$. The bottom surface delivers heat to the collector fluid ($h_2 = 50\,\text{W/m}^2\,\text{K}$), which flows past the surface at $T_{\text{fluid}} = 20^\circ\text{C}$. What is the equilibrium temperature of the collector plate? How much energy (per unit area) is collected (i.e., carried away by the fluid)? Discuss the performance of this collector. Assume black nickel to be a diffuse emitter.

3.34 Make a qualitative plot of temperature *vs.* the total hemispherical emittance of:

(a) a 3 mm thick sheet of window glass,

(b) polished aluminum, and

(c) an ideal metal that obeys the Hagen–Rubens relation.

3.35 A horizontal sheet of 5 mm thick glass is covered with a 2 mm thick layer of water. If solar radiation is incident normal to the sheet, what are the transmissivity and reflectivity of the water/glass layer at $\lambda_1 = 0.6\,\mu\text{m}$ and $\lambda_2 = 2\,\mu\text{m}$? For water $m_{\text{H}_2\text{O}}(0.6\,\mu\text{m}) = 1.332 - 1.09 \times 10^{-8}\,i$, $m_{\text{H}_2\text{O}}(2\,\mu\text{m}) = 1.306 - 1.1 \times 10^{-3}\,i$ [172]; for glass $m_{\text{glass}}(0.6\,\mu\text{m}) = 1.517 - 6.04 \times 10^{-7}\,i$, $m_{\text{glass}}(2\,\mu\text{m}) = 1.497 - 5.89 \times 10^{-5}\,i$ [82].

3.36 A solar collector plate of spectral absorptivity $\alpha_{\text{coll}} = 0.90$ is fitted with two sheets of 5 mm thick glass as shown in the adjacent sketch. What fraction of normally incident solar radiation is absorbed by the collector plate at a wavelength of 0.6 μm? At 0.6 μm $m_{\text{glass}} = 1.517 - 6.04 \times 10^{-7}\,i$ [82].